

Delft University of Technology  
Faculty of Applied Sciences  
Erasmus Medical Center  
Department of Radiation Oncology

---

## Back to the Future

Towards Ridge Filters in Clinical FLASH Proton Therapy  
Treatment Planning for Neuro-Oncological Targets

---

A.E. Meijer  
Student nr.: 4555651

Master Thesis  
MSc Applied Physics  
Delft, the Netherlands

Supervisors:  
Dr. S.J.M. Habraken - Erasmus MC  
Dr.ir. D. Lathouwers - TU Delft

June 18, 2021



## Abstract

FLASH proton therapy is a growing field of research, especially due to its biological benefits in radiation oncology: sparing healthy tissue while delivering the treatment within a millisecond. However, instead of sparing healthy tissue, the conventional FLASH approach, using transmission beams, damages the tissue behind the distal edge of a tumour. Therefore, this approach is less attractive in the clinical application of FLASH proton therapy. To solve this problem, the use of a ridge filter and patient-specific range compensator, to shift the spread-out Bragg peak (SOBP) of the proton beam to the tumour, is proposed.

In this research, the clinical feasibility and acceptability of FLASH-compatible treatment plans, optimized with multiple, Monte Carlo-simulated ridge filter beams, is analysed. An SOBP-database is generated using energy spectrum approximations and interpolations of energy spectra retrieved from Monte Carlo simulations in TOPAS. To obtain optimized FLASH-compatible treatment plans for neuro-oncological targets, this database is implemented in the in-house treatment planning software of the Erasmus Medical Center, iCycle.

The resulting treatment plans show that it is possible to generate FLASH-compatible treatment plans using a ridge filter. A FLASH enhancement ratio between 1.4 and 2.1 would potentially give clinically acceptable plans for the three patients considered. In some optimized plans, the homogeneity of the tumour dose is also increased.

A limitation of this research is that configuration of a stable ridge filter beam treatment plan optimizer appears to be challenging. Besides this, the FLASH enhancement ratio and the dose rate are not taken into account to find the regions in the patient where the FLASH conditions (dose  $> 8$  Gy, dose rate  $> 40$  Gy/s and treatment time  $< 0.1$  s) are met.

Recommendations for future research include: implementing the FLASH enhancement ratio and the dose rate optimization in treatment plan optimization; investigating the influence of fractionation of a FLASH treatment plan on the tumour control and the healthy tissue irradiated; study the relative biological effectiveness (RBE) and the biological character of FLASH radiotherapy, and investigate the clinical potential of a combination of FLASH and non-FLASH treatment.

## Preface

‘Science begins with curiosity’. It is a statement that not only (partially) explains why research is done, it also shows that science is conducted by human beings. Human beings with each their own interests, their own skills and motivation, their own strengths and flaws. About a year ago, I started looking for a Master Thesis project that would fit my interests: health care and radiation; and that would help me develop my skills in writing, communicating, collaborating, planning and other academic dexterities. Eureka! I’ve found exactly that and the result lies before you, the report: ‘Towards Ridge Filters in Clinical FLASH Proton Therapy Treatment Planning for Neuro-Oncological Targets’. It is written to fulfill the requirements of the Master of Science Applied Physics at the Delft University of Technology.

I have a lot to be thankful for and I am grateful for all people I have met during this past year of doing research.

First of all, I sincerely want to thank both my supervisors. Steven Habraken and Danny Lathouwers, without supervisors like you, my project would have gone much less smoothly. Both of you have loads of professional knowledge in your field and are willing to share these insights. I have learnt a lot from that. Steven, I have not only appreciated your pragmatics and your clinical expertise, but also your kindness and empathy. Danny, although you initially were my second supervisor, I think I can safely say that in supervising you have done as much as a first supervisor. Your dry-wit humour, quick feedback and down-to-earth manner often boosted me. Over the past year, I have often thought about how thankful I am for both of you and I couldn’t have imagined more suitable supervisors. You have been true blessings.

Besides this, there are a lot of other people to thank. Thank you, Marta Rovituso, for providing me with the measurements needed for the validation of my simulations. All credits for the measurement results go to you, Atia and Henar. GSI produced the ridge filter and sent the 3D CAD-file of the ridge filter; without these, the Monte Carlo simulations would not have turned out so well as they did now. Michelle Oud, thank you for sharing your knowledge about iCycle. Mischa Hoogeman and Sebastiaan Breedveld, thank you for your constructive comments and thoughts on my project during the weekly FLASH progress meetings. I also would like to thank the entire Radiation Oncology Department in the Erasmus MC and the Medical Physics & Technology Department of the TU Delft for welcoming me in their teams. It really was a pity that I was not able to work and speak with you as much as I would have liked due to the COVID situation. I had a wonderful time with you, gaining new knowledge and relaxing during breaks back in September and October. In the beginning of the project, the TOPAS community helped me familiarize myself with TOPAS, the Monte Carlo simulation software. I valued this a lot.

Finally, I want to thank the people dearest to me: my family and friends. Willem-Jan, thank you for encouraging me, believing in me, helping me wherever you can, and listening to my stories. You know me very well. Pappie en mammië, dank jullie wel dat jullie mij een stabiel, veilig en liefdevol thuis hebben geboden, dat jullie me altijd weer thuis verwelkomden en me van de bus (of zelfs vanuit Delft) wilden komen ophalen als ik naar huis kwam. Marleen, over this past year you have become a good friend and it was always nice having you as my thesis buddy, to study, talk, Duolingo and make music together in the time that we could not go to the office. All my other family and friends, thank you very much for standing next to me this past year.

There is a lot I am very grateful for, especially the opportunities I have received, to study, to do this project, to meet the people I have met, to use the talents that are given to me, to learn how to live the life that is given to me and there is only One to thank for all of these blessings. So, I thank the One who is most important to me in life for everything He has given me. The One who teaches me that everything I do in my life only has true value if it is done for Him, if it seeks the good of people, and if it is done in love.

*Angeline Meijer  
Delft, June 2021*

## List of abbreviations

BP	Bragg peak
CTV	Clinical target volume
Erasmus MC	Erasmus Medical Center
FER	FLASH enhancement ratio
GTV	Gross tumour volume
HI	Homogeneity index
HollandPTC	Holland Proton Therapy Center
IAEA	International Atomic Energy Agency
ICRU	International Commission on Radiation Units and Measurements
IMPT	Intensity Modulated Proton Therapy
MC	Monte Carlo
OAR	Organ at risk
PIXE	Particle induced X-ray emission
PTV	Planning target volume
RBE	Relative Biological Effectiveness
R&D	Research & Development
SOBP	Spread-out Bragg peak
TU Delft	Delft University of Technology
VMAT	Volumetric Modulated Arc Therapy
WHO	World Health Organization

# Contents

<b>1</b>	<b>Introduction</b>	<b>1</b>
1.1	Proton therapy . . . . .	1
1.1.1	Proton interactions . . . . .	2
1.1.2	FLASH radiotherapy . . . . .	4
1.1.3	Ridge filters . . . . .	5
1.2	Research goal . . . . .	7
1.3	Structure of report . . . . .	7
<b>2</b>	<b>Theoretical background</b>	<b>9</b>
2.1	Basics of Monte Carlo simulations . . . . .	9
2.1.1	Definitions . . . . .	9
2.1.2	Particle transport . . . . .	9
2.1.3	Phase space . . . . .	10
2.1.4	Monte Carlo compared to other methods . . . . .	11
2.2	Erasmus-iCycle . . . . .	11
2.2.1	The iCycle workflow . . . . .	12
2.2.2	Dose calculation algorithm . . . . .	15
2.2.3	Treatment plan quality assessment . . . . .	16
<b>3</b>	<b>Methodology</b>	<b>19</b>
3.1	TOPAS simulations . . . . .	19
3.1.1	Simulation settings . . . . .	19
3.1.2	Geometrical components . . . . .	20
3.1.3	Scoring elements . . . . .	22
3.1.4	Validation of Bragg peak dose-depth curves . . . . .	23
3.2	SOBP-database generation . . . . .	24
3.2.1	Structure of the database . . . . .	24
3.2.2	Optimization of the energy spectrum . . . . .	24
3.2.3	Additional aspects of the database generation . . . . .	25
3.2.4	Validation of the database . . . . .	26
3.3	Erasmus-iCycle optimizations . . . . .	27
3.3.1	Requirements of FLASH optimization . . . . .	27
3.3.2	Settings iCycle . . . . .	28
3.3.3	Extensions and adjustments of iCycle . . . . .	29
3.3.4	FLASH compatibility assessment . . . . .	38
<b>4</b>	<b>Results</b>	<b>39</b>
4.1	TOPAS simulations . . . . .	39
4.1.1	Validation of the model . . . . .	39
4.1.2	SOBP-simulations . . . . .	42
4.2	Validation of SOBP-database . . . . .	45
4.2.1	Preparation of the database generation . . . . .	45
4.2.2	Validation of simulated data . . . . .	48
4.2.3	Validation of interpolated data . . . . .	49
4.3	Erasmus-iCycle optimizations . . . . .	51
4.3.1	Conventional run . . . . .	51
4.3.2	Initial run . . . . .	54
4.3.3	Final runs . . . . .	57

<b>5</b>	<b>Discussion</b>	<b>60</b>
5.1	Validation of TOPAS simulations . . . . .	60
5.1.1	Particle population . . . . .	60
5.1.2	Bragg peak results . . . . .	60
5.1.3	Ridge filter results . . . . .	61
5.1.4	Simulation setup . . . . .	61
5.1.5	Physics of the simulations . . . . .	62
5.2	SOBP-database generation . . . . .	62
5.2.1	Phase plane properties . . . . .	62
5.2.2	SOBP-database range . . . . .	63
5.2.3	Energy spectrum optimization . . . . .	63
5.2.4	Database generation . . . . .	63
5.3	Erasmus-iCycle optimizations . . . . .	64
5.3.1	Number of pencil beams . . . . .	64
5.3.2	Dose homogeneity . . . . .	65
5.3.3	Dose conformity . . . . .	65
5.3.4	Difference between initial and final runs . . . . .	66
5.3.5	Computation time . . . . .	67
5.4	Clinical implementation . . . . .	67
5.4.1	FLASH proton therapy . . . . .	67
5.5	Future research . . . . .	68
<b>6</b>	<b>Conclusion</b>	<b>70</b>
<b>A</b>	<b>Appendix</b>	<b>75</b>
A.1	TOPAS scripts . . . . .	75
A.1.1	Physics settings . . . . .	75
A.1.2	Beam characteristics . . . . .	75
A.1.3	Pristine Bragg peak simulations . . . . .	76
A.1.4	Spread-out Bragg peak simulations . . . . .	77
A.2	Wishlist . . . . .	80
A.3	Structure iCycle . . . . .	81
A.4	Additional results of the energy spectrum optimization . . . . .	83
A.5	Erasmus-iCycle results - Patient 2 . . . . .	87
A.5.1	Conventional plan . . . . .	87
A.5.2	Initial run . . . . .	89
A.5.3	Final runs . . . . .	92
A.6	Erasmus-iCycle results - Patient 3 . . . . .	95
A.6.1	Conventional run . . . . .	95
A.6.2	Initial run . . . . .	97
A.6.3	Final runs . . . . .	100

# 1 Introduction

In 2018, cancer accounted for about 9.6 million deaths globally, thus making it the second leading cause of death at that time, according to the World Health Organization (WHO) [1]. That is one of the reasons why treating cancer in the most effective and efficient way has become a priority, not only in hospitals and clinics, but in society as a whole. Common treatments are surgery, for operable tumours; systematic cancer therapy, for tumours with metastases, and radiotherapy, for local tumour control or for irradiation of remaining tumour tissue after surgery. These modalities can be used independently or in combination [2].

In radiotherapy high doses of ionizing radiation are used to kill cancer cells and shrink tumours. It can be applied using photons, electrons, protons, or other particles. Each type of radiotherapy has its own advantages and disadvantages, depending on its physical properties [3].

Though photon therapy is most widely used in radiotherapy, there are cases in which proton therapy is more fitting.

## 1.1 Proton therapy

Proton therapy is different from other radiation therapies in a number of respects, one of the most important being the energy transfer, and thus, the dose deposited in tissue [4], see Figure 2.

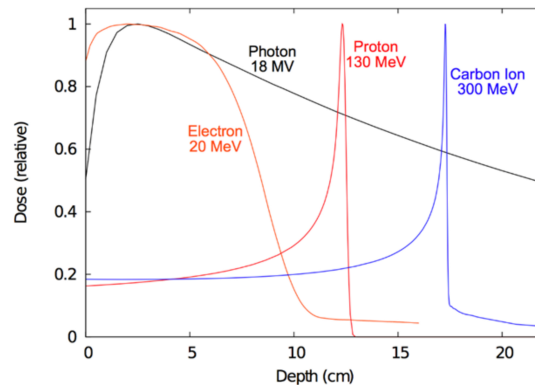


Figure 2: Depth-dose curve of different radiation therapy methods: photons (black), electrons (orange), protons (red) and carbon ions (blue) [4].

It can be seen that protons, in comparison to electrons and photons, have a relatively low entrance dose, while they peak at the end of their range. The term ‘Bragg curve’ is used to refer to this curve. These characteristics make proton therapy suitable for tumours lying deeper in the body. The deposited dose in the healthy tissue before the tumour is low, and the tissue after the tumour does not receive any dose at all (in the ideal case), see Figure 3. Therefore, in some cases, proton therapy can increase the curing probability or decrease the probability of complications or side effects [5].

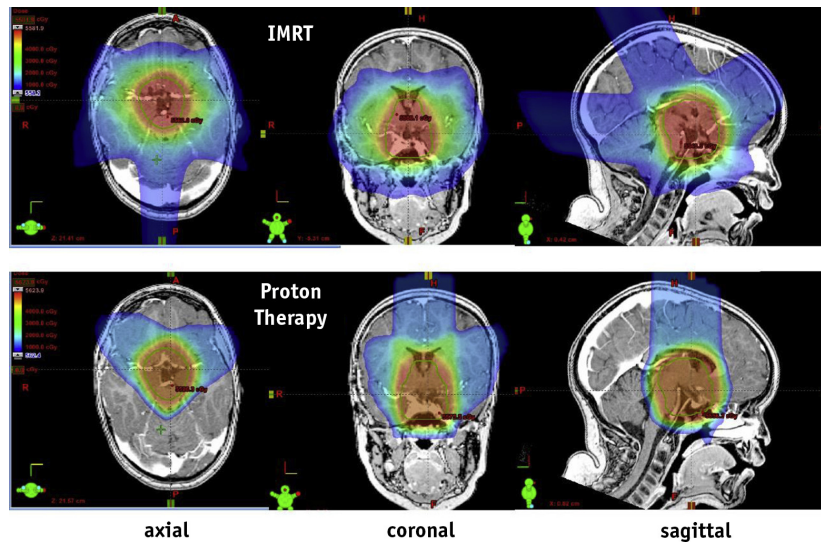


Figure 3: Example of a craniopharyngioma photon (IMRT, top) and proton (bottom) comparison plan in 3 planes [6].

This classical behaviour of protons is caused by the ways in which protons interact with matter.

### 1.1.1 Proton interactions

When talking about radiotherapy in general, it is important to understand that a large part of the physics involved boils down to one explanation: particle interactions. In proton therapy, the energy of the protons is transferred to the medium through which it travels through interactions. These interactions are governed by (quantum) electrodynamics and nuclear physics. The results of these interactions can be classified in three processes: slowing down of the proton (stopping), deflecting of the proton (scattering) and the generation of secondary particles (by nuclear interactions) [7].

#### Stopping and stopping power

The first important possible result of proton interactions is the slowing down of protons. Slowing down occurs when protons interact with atomic electrons. The longer the proton and the electron interact, the more kinetic energy the proton loses. Thus, the stopping power, the rate at which protons lose energy, increases when slowing down. It is to be noted that not all energy that is lost is deposited in the surrounding material, some energy transfers to neutral secondary radiation, such as  $\gamma$ -rays or neutrons.

The stopping power increases with decreasing kinetic energy. This gives rise to the characteristic Bragg peak (BP) in the dose-deposition curve of protons, Figure 2. Beyond the stopping point of the protons, the range, the dose in the material is negligible. This range depends on the initial energy of the proton and the material through which it travels. Thus, in a mono-energetic proton beam the protons stop at approximately the same depth. The slight deviations in range of a mono-energetic beam are called range straggling. This is caused by the interactions being random, and, therefore the central limit theorem says that the (energy) distribution becomes Gaussian. So, there is always some (Gaussian) energy spread around the mean energy. This has influence on the fluence- and dose-depth curves, as can be seen in Figure 4.

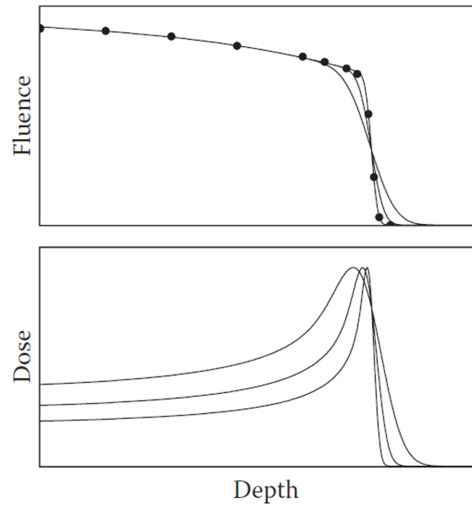


Figure 4: Proton fluence and dose as a function of depth for different energy spreads [7].

### Scattering

Scattering in a proton beam mainly occurs when protons interact with nuclei. After multiple interactions, multiple Coulomb scattering, the direction of the proton gets deflected more and more. Through scattering, a mono-energetic proton beam gets a nearly Gaussian angular distribution. Because of the different length scales between the electronic and the nuclear reactions, a slightly more accurate approximation of the angular distribution would be a double Gaussian. However, often the Gaussian approximation is used in calculations and simulations. In every medium, protons are scattered, but not every medium has the same scattering power. High  $Z$  materials have a higher scattering power than low  $Z$  materials.

### Nuclear interactions

Nuclear interactions occur less often than the electromagnetic interactions of protons, but they are not rare and are of importance in proton therapy. Three reasons for that are: their contribution to the total absorbed dose; the resulting low energy and/or heavy secondaries enhancing the relative biological effectiveness (RBE), and the production of neutrons, which leads to dose deposition outside the target volume [8]. This lowers the peak in the Bragg curve and gives a dose build-up in its entrance region. These secondaries are produced by inelastic or nonelastic nuclear reactions. Nonelastic reactions contain all reactions for which kinetic energy is not conserved. The term inelastic reactions refers to reactions for which kinetic energy is not conserved, but the bombarded nucleus does not lose any particles or undergo break up.

Clinical implementations of proton therapy have been used over the past seventy years. Over this period of time technical developments have improved the therapy, regarding the tumour sites that can be treated as well as the dose delivery precision. While in the first years mainly scattering proton therapy was applied, nowadays the state-of-the-art pencil beam scanning is increasingly practiced [9]. Both modalities are still in use. Although pencil beam scanning is technologically more advanced, in some cases, for example eye tumours, passive scattering is still preferred. In 1954, the first patient treatments were carried out, and since then the interest in proton therapy has only grown [10]. Since the nineties more and more proton centers are built in Europe [11].

### 1.1.2 FLASH radiotherapy

In 2014, researchers in the field of radiotherapy first discovered the FLASH effect: when using extremely high dose rates ( $> 40$  Gy/s), high doses ( $> 8$  Gy) and very short treatment times ( $< 0.1$  s) the normal tissue toxicity in healthy tissue is lower than when using conventional radiation therapy, while the extent of tumour control has not changed [12]. The numerical values of these conditions are not set in stone, but there is general consensus based on biological experiments that under these conditions the FLASH effect occurs.

Another, non-biological, advantage of this ultra-high dose rate irradiation is that it ‘freezes’ the organ motion because the treatment time is so short. Therefore, interplay effects, the interference of the moving target with the pencil beam, do not play a role anymore [13]–[15]. Besides this, when ‘freezing’ organ motions or other anatomical changes and positional variations, such as the bladder filling or bowel movement, the tumour could be irradiated with smaller margins.

Several mechanisms underlying the FLASH effect have been investigated, but no final explanation has been agreed upon. Some simulations suggest that radiolytic oxygen depletion might cause the FLASH effect. When there is less oxygen, overall less free radicals can be generated. Thus, the negative effects of these radicals in damaging DNA is decreased. This is in agreement with in vitro studies done in the ‘60s and the ‘70s, though in that time the differential effect of the FLASH effect had not been shown. But the results of in vivo FLASH experiments can not (fully) be explained by this oxygen depletion. On the contrary, a research group from France found that the oxygen depletion levels in conventional radiotherapy and FLASH radiotherapy are around the same level. They propose yet another hypothesis: the FLASH effect might be caused not only by physical or chemical mechanisms, but also biological effects may play a role [16], [17]. For example, in FLASH radiotherapy the liberation of electrons in tissue is higher than in conventional radiotherapy. Thus, the amount of ionizations and redox reactions is increased. These redox reactions would propagate in *biological* tissues and eventually decay in a series of *biochemical* and *biophysical* reactions. The path of this decaying is expected to be different in FLASH radiotherapy than in conventional radiotherapy [14]. Such a change in redox metabolism can reduce cell damage. Another effect of ultra-high dose rate irradiation is that less circulating blood cells are irradiated. This might still spare the immune system even though the ones that are irradiated receive a higher dose [18]. Besides this, it is suggested that chromatin remodelling is also involved in the FLASH effect. Other studies suggest that less inflammation in the tissue could also influence the FLASH effect [12], [19], [20].

The FLASH effect is a hot topic in proton therapy research. Compared to other modern irradiation techniques, such as VMAT, the CyberKnife, or using protons or carbon-ions, using the FLASH effect offers an entirely new and different approach to increase the bandwidth of clinically acceptable treatment plans. In 2019, the first patient was treated with FLASH therapy using electrons [21]. In the same year, the first implementation of FLASH in a proton therapy setting was used in an experiment [22].

The majority of experimental researches into FLASH therapy have been done using electrons in a linear accelerator setup. However, in clinical proton settings, synchrotron and cyclotron accelerators are more common [7]. Synchrotrons have the advantage that they can switch the energy of the beam quickly, but the energy range of the synchrotron often does not allow for FLASH compatible dose rates. FLASH doses and dose rates, however, can be achieved by using pencil beam scanning with a very high energy and current in a cyclotron. A typical cyclotron-based beamline setup is shown in Figure 5.

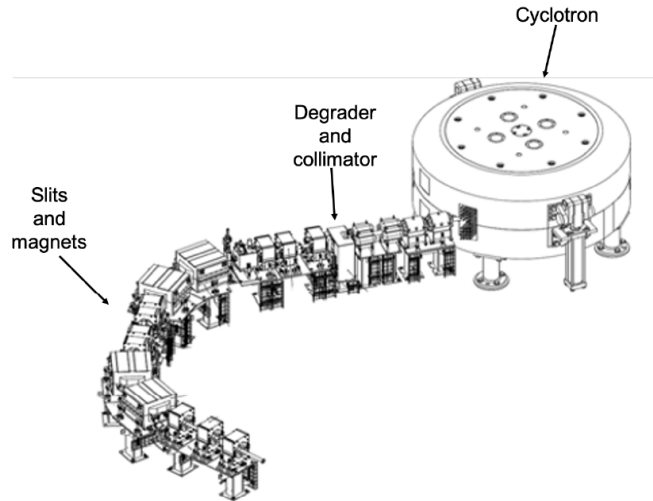


Figure 5: Typical cyclotron-based proton beam transport system. The protons are accelerated in the cyclotron. The energy of the protons leaving the cyclotron is degraded by the standard energy degraders, while the collimator blocks the particles that are too far from the main beam axis. Passing by the slits and magnets with which the particles are steered, the protons enter the treatment room [23].

The proton beam leaving the cyclotron has a high energy and intensity. Studies have been carried out that look into the use of these high energy and high dose rate beams in proton therapy treatment planning [16], [24]. A disadvantage of this approach is that using these beams, the Bragg peak falls behind the patient and thus more healthy tissue is irradiated. These beams, that shoot straight through the patient, are called ‘transmission beams’.

An interesting approach to this problem is to look whether the Bragg peaks can be brought back into the patient by range modulation. In that way, the tissue behind the tumour could still be spared. Using the standard energy degraders in the beginning of the beamline, however, is infeasible since the shifting of the degraders for energy modulation is very time-consuming. Besides this, more particles are lost due to scatter when the energy is modulated in the beginning of the beamline. Thus, these degraders are not suitable for maintaining an ultra-high dose rate. A feasible solution would be an energy modulation technique that is not time-dependent and preferably as close to the patient as possible to limit the negative effect of scattering. Besides, it would be desirable if the Bragg peak of the proton beam was more spread out to cover a larger part of the tumour without energy modulation [13], [25], [26].

### 1.1.3 Ridge filters

To obtain the FLASH compatible dose rates and to spread out the Bragg peak without intermediate energy shifting in pencil beam scanning Patriarca et al [25] suggest to use a ridge filter. Treatment times using a ridge filter are 5-10 times shorter than when using a range modulator wheel or the standard energy degrading system.

A ridge filter is an object that modulates the range of a proton beam. It consists of pins or ridges with a certain profile, see Figure 6. The same figure demonstrates the effect of a ridge filter in carbon-ion therapy. When a mono-energetic beam passes through the filter, it leaves the filter with a spread-out energy distribution. The initial energy of the particles gets shifted with different energy shifts for dif-

ferent thicknesses of the filter. So, the beam at the exit of the filter generates Bragg peaks at different depths. Since it ‘spreads out’ the Bragg peak, this is called a ‘spread-out Bragg peak’ (SOBP). [13].

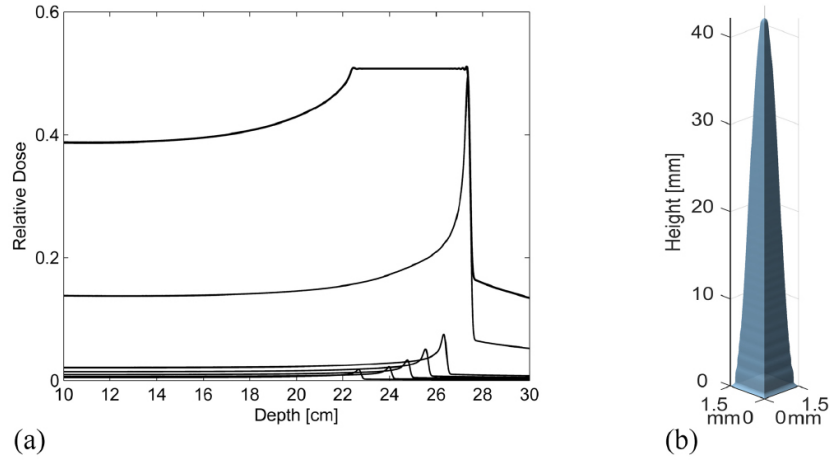


Figure 6: (a) shows an example of a dose-depth profile resulting from the weighted superposition of Bragg peaks with different ranges. The line with the highest dose distribution is the total dose line, all the lower lines are the weighted Bragg peak dose distributions making up this total dose distribution. In (b) an example of a single pyramid-shaped pin optimized for a 5 cm SOBP in water from 12-C 400.41 MeV/u beam is given [13].

It is visible that in carbon-ion therapy the tissue behind the SOBP also receives dose. This is different in proton therapy. Using protons, the resulting dose-depth curve after a ridge filter would look like the one given in Figure 7.

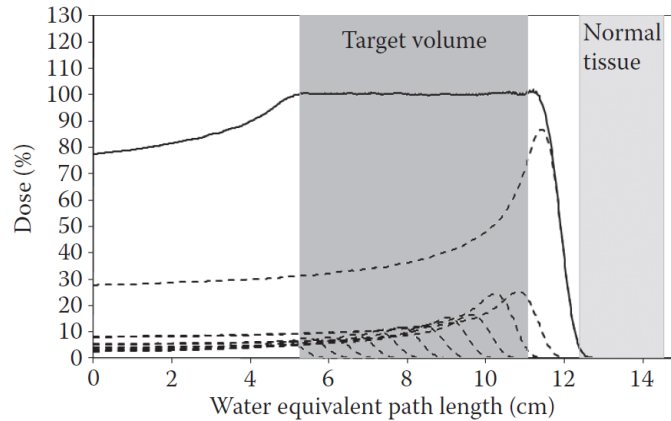


Figure 7: Proton depth-dose diagram showing weighted pristine Bragg peaks (dashed) and their resulting SOBP (continuous) [7]. The dose is given in percentages and the depth as the water equivalent path length in cm.

The amount of particles that end up at a certain depth is determined by the shape of the pins. Furthermore, a ridge filter should be placed as close to the target as possible. In that way, the amount of protons scattered to outside the tumour site is limited.

Ridge filters are mainly used in passive scattering techniques. In some way, going from movable

degraders and range modulator wheels to the static ridge filter may seem like a step back in time, back to the time where only static components could be used. However, since the FLASH effect is bound to such a tight time constraint, static components may not only be the past of proton therapy, but also its future.

One may wonder why passive scattering is not used for FLASH. In that way, the time it takes to scan all the pencil beams could be skipped and another time-consuming element of the therapy would be eliminated. The answer to that is that using passive scattering, where the initial pencil beam is scattered to a larger lateral field, the intensity of the beam is often not large enough to irradiate the target with a high enough dose rate.

## 1.2 Research goal

In this research, the clinical potential of the frequently mentioned solution to the transmission beam ‘problem’, the ridge filter, is explored. Ridge filters have already been used in in vivo mouse experiments using FLASH beams. In these experiments, however, only basic, single beam setups have been used. The goal of this research is to:

- ⇒ **find out to what extent it is possible to generate clinically acceptable, FLASH compatible treatment plans with ridge filter beams.**

To reach that goal, the project is divided into two main parts:

1. generate a SOBP-database by post-processing the effects of a ridge filter in the Holland Proton Therapy Center (HollandPTC) FLASH proton beamline model in TOPAS, a Monte Carlo simulating machine, and
2. optimize treatment plans of patients in Erasmus-iCycle, the in-house treatment planning system of the Erasmus Medical Center (Erasmus MC), using the SOBP-beams from the SOBP-database.

From the clinical point of view, the proton therapy setup of HollandPTC in Delft is taken as a starting point. It consists of a cyclotron particle accelerator, followed by a beam transportation system such as in Figure 5, leading the proton beam to the gantry. With the 800 nA cyclotron current and a dose rate of almost 1000 Gy/s in the entrance region of a 250 MeV beam, the setup at HollandPTC can facilitate extremely high dose rates. IBA cyclotrons do not come close to these dose rates, and many other proton centres using a Varian cyclotron have a more compact variant that is also not suitable for such high dose rates. In this report, it is assumed that in the clinical implementation of a ridge filter a constant beam energy of 244 MeV (the maximum for the clinical proton beam model) is used. For modulating the range and spreading out the Bragg peak the use of a ridge filter and a patient-specific range compensator is proposed.

This investigation has a simulation-based approach. The first step in this approach is to validate the TOPAS implementation of the ridge filter for several beam energies. After that, an optimization is done to approximate the energy spectra of the protons after the ridge filter with energies and weights of individual pencil beams for different nominal beam energies. From this, a database is made and used to optimize treatment plans of brain tumours with ridge filter beams in Erasmus-iCycle.

Ridge filters in proton therapy could open a door to FLASH proton therapy becoming more and more realistic and common. It could lead to an improved treatment of tumours and less side effects after treatments.

## 1.3 Structure of report

The overall structure of this study takes the form of five chapters. Chapter 2 starts with providing the theoretical background on Monte Carlo simulations and the Erasmus MC in-house treatment optimization software, iCycle. Then Chapter 3 describes the methods used to derive the results, which

are given in Chapter 4. A discussion on the validity of the results and their implications can be found in Chapter 5. Finally, the conclusions of this thesis are drawn in Chapter 6.

This report is written to document the results of the Master Thesis Project, done in the second year of the Master of Science Applied Physics of the Delft University of Technology. This project is done in a collaboration of the Delft University of Technology (TU Delft), the Erasmus University Medical Center (Erasmus MC) and the Holland Proton Therapy Center (HollandPTC). HollandPTC has been in operation since 2018. It is one of the three proton centra in the Netherlands [27].

## 2 Theoretical background

This chapter expands on necessary background knowledge for a better understanding of this research. Two key concepts that are touched upon are: the theory of Monte Carlo simulations, and the background behind the treatment planning software Erasmus-iCycle.

### 2.1 Basics of Monte Carlo simulations

Going down to the basis of many particle (transport) simulations, one often finds the Monte Carlo technique. This numerical method simulates the temporal behaviour of random processes, but is also often used in problems without a direct probabilistic interpretation [28], [29]. It attempts to model nature through direct simulation of the essential dynamics of the system in question.

#### 2.1.1 Definitions

The Monte Carlo method has been defined in different ways for different applications, but here it will be seen as: *a numerical method to solve equations or calculate integrals using (weighted) random number sampling* [29]. However, the output of a computer program is, by definition, predictable. To overcome this problem, huge sequences of numbers that should at least *appear* uncorrelated are used. A more correct term for the sampling is then ‘pseudorandom’. It is desired that the outcome of a problem or simulation is the same whatever sequence of ‘random’ numbers is used.

In a radiotherapy simulation three characteristics of the pseudorandomly generated sequence are important:

1. the period in the number sequence after which it repeats should be large enough;
2. the number of particles in the simulation should be high enough, and
3. in an  $n$ -dimensional problem, the numbers should be uniformly distributed in the  $n$ -dimensional space.

If the first two requirements are not met, the result of the experiment will still be correlated and therefore not completely accurate. Furthermore, sometimes the random numbers need to be generated according to some weight distribution function  $p(x)$  instead of uniformly distributed. This can be achieved using  $P(x)$ , the cumulative distribution function on interval  $[a,b]$ :

$$P(x) = \int_a^x dx' p(x'), \quad (1)$$

with  $a \leq x \leq b$  and  $P(a) = 0$ ,  $P(b) = 1$ . Using this function and uniformly generated random numbers  $\eta$ , the non-uniformly generated numbers  $\zeta$  with distribution  $p(x)$  can be calculated using:

$$\zeta = P^{-1}(\eta). \quad (2)$$

#### 2.1.2 Particle transport

Monte Carlo models for particle transport contain a lot of physics settings and processes [30]. The generation of the initial particles in a particle beam is performed by pseudorandomly generating particles according to some distribution function of position and energy. This is done as described in the previous section, Section 2.1.1. After that first step, the particles travel through space and while they travel, they interact with a certain probability (cross-section) or decay with a certain mean-life. Due to interactions secondary particles can also be set in motion.

In a simulation, the particles proceed in steps. In each step the particle can interact and/or decay and at the end of each step, the parameters of the particles are updated. The step size depends on the material the particle is travelling through, the geometry, and many more aspects.

For interaction or decay, first of all the probability  $P$  of ‘surviving’ (travelling) a distance  $l$  is characterised:

$$P(l) = e^{-n_\lambda l}, \quad (3)$$

with  $n_\lambda = \int_0^l \frac{1}{\lambda(l)} dl$  and  $\lambda$  the mean free path. For decay and for interactions there is a different  $\lambda$ .

For decay:

$$\lambda = \gamma v \tau, \quad (4)$$

with  $v$  the velocity,  $\tau$  the mean life and  $\gamma$  the Lorentz-factor,  $\gamma = \frac{1}{\sqrt{1-v^2/c^2}}$  with  $c$  the speed of light. Although protons themselves do not decay, decaying secondary particles are also taken into account in the Monte Carlo simulations.

For interactions:

$$\lambda = \frac{1}{\rho \sum_i x_i \sigma_i / m_i}, \quad (5)$$

with  $\rho$  the density of the current material,  $x_i$  the mass fraction of isotope  $i$  in the material,  $m_i$  the mass of isotope  $i$  and  $\sigma_i$  the cross-section of that isotope.

The probability density function of  $n_\lambda$  is a simple exponential, not depending on the material or energy. So, at the point where a particle is produced,  $n_\lambda$  is given by:

$$n_\lambda = -\ln(\eta). \quad (6)$$

Here,  $\eta$  is a pseudorandom number uniformly generated in the range (0,1).

### 2.1.3 Phase space

For doing calculations based on Monte Carlo simulations, or for consecutive simulations in a Monte Carlo simulation tool, using a phase space file is an accurate way to obtain a lot of information. The file contains desired particle information for all particles in a certain plane in the Monte Carlo simulation space [31]. When doing consecutive simulations in a Monte Carlo tool this is not always the most efficient way. All particles have to be read in again in the simulation. In some cases, the time this takes is comparable to the particle transport time. Since in this research the phase space will only be used for analysis of particle information, this is a very time-efficient way to obtain results from the Monte Carlo simulations, compared to scoring each property separately.

The International Atomic Energy Agency (IAEA) has set a standard format for phase spaces [32]. A phase space generally contains for every particle the position ( $x$ ,  $y$  and  $z$ ), the direction (cosine along  $x$ , cosine along  $y$  and cosine in  $z$ ), the kinetic energy  $E$ , the statistical weight of the particle  $w$ , the particle type and whether the particle is a primary or secondary particle.

When building a simulation setup in a Monte Carlo simulation tool, an already saved phase space can be loaded as a source, or if there is another source, the phase space can be retrieved at a certain distance from the source. A phase space enables one to separate two parts of a simulation or transfer results between different codes [31].

### 2.1.4 Monte Carlo compared to other methods

As with other modelling methods also the Monte Carlo method comes with its advantages and disadvantages. Often the probabilistic Monte Carlo model is compared with analytical methods [29]. On the one hand, analytical models can give more insight in the macroscopic theory and reality. They allow for development of a better intuition on how the involved macroscopic fields work. Monte Carlo is, for that matter, more an approach based on randomness. It relies on repeating randomly sampled simulations to obtain numerical results. On the other hand, Monte Carlo techniques become more advantageous computation-wise when the complexity of the system grows, see Figure 8.

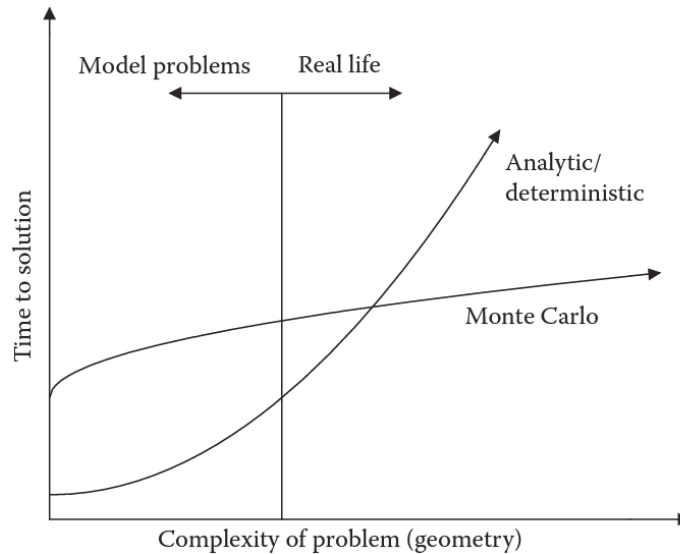


Figure 8: Time to solution of the Monte Carlo method compared with analytic/deterministic methods for varying complexities of the problem [29].

For problems with a dimensionality of five dimensions or higher, the Monte Carlo is more efficient than analytical models [29]. In particle transport problems this is often the case as the particles have a position (three dimensions) and a momentum (three dimensions). Besides this, time dependence or different particles can be taken into account, also adding to the dimensionality of the problem.

## 2.2 Erasmus-iCycle

In radiotherapy, treatment planning softwares (TPSs) are used to construct a personalized treatment plan for a patient. It contains for example the beam directions, positions, energies and intensities of the treatment. The Erasmus MC has an in-house developed prioritized multi-criteria optimizing TPS, Erasmus-iCycle [33].

### 2.2.1 The iCycle workflow

The iCycle workflow consists of three parts, the initialization, the optimization and the finalization, see Figure 9.

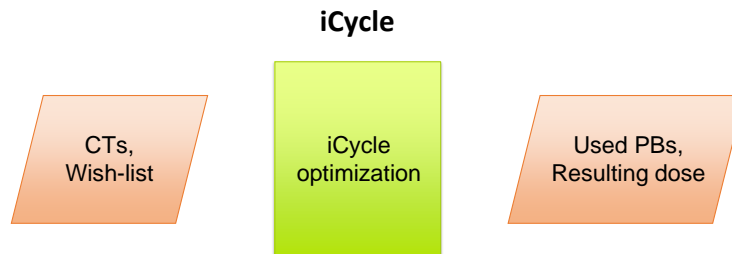


Figure 9: Flowchart of the main structure of iCycle. In the initialization phase, iCycle processes all input data for the optimization: the patient CTs and the wish-list with the defined optimization parameters, objectives and constraints. After the optimization takes place, iCycle returns the output in the finalization: the resulting accurate dose to the tissue and the used pencil beams with their weights.

#### Initialization

As with other treatment planning softwares, iCycle uses an image dataset (i.e. CTs) of a patient with the indicated important anatomical structures. What is different is that iCycle also takes as an input a ‘wish-list’. This is a list of prioritized dose objectives and constraints for every structure, see Figure 10. The constraints have to be met for a plan to be feasible [34]. The objectives are ‘goals’ that the optimization strives to achieve, but they are more flexible. Thus, the priority of the constraints is always higher than those of the objectives.

	Structure	Min/Max	Type	Goal	Limit	Sufficient	Priority	Weight	Parameters	Active	LRPM	Robust
1	GTV	Maximize (minimum) †	linear	$A * 0.95$			Constraint	1		Yes	0	No
2	CTV_5040	Maximize (minimum) †	linear	$A * 0.98$			Constraint	1		Yes	0	No
3	OpticNrv_L	Minimize (maximum) ‡	linear	55			Constraint	1		Yes	0	No
4	OpticNrv_R	Minimize (maximum) ‡	linear	55			Constraint	1		Yes	0	No
5	OpticChiasm	Minimize (maximum) ‡	linear	55			Constraint	1		Yes	0	No
6	GTV	Minimize (maximum) ‡	linear	$A * 1.12$			1	1		Yes	0	No
7	CTV_5040	Minimize (maximum) ‡	linear	$A * 1.07$			1	1		Yes	0	No
8	Hippocampus_L	Minimize (maximum) ‡	mean	1			2	1		Yes	0	No
9	Brainstem	Minimize (maximum) ‡	linear	55			3	1		Yes	0	No
10	Cochlea_R	Minimize (maximum) ‡	mean	45			4	1		Yes	0	No
11	Cochlea_L	Minimize (maximum) ‡	mean	45			4	1		Yes	0	No
12	Retina_L	Minimize (maximum) ‡	linear	20			5	1		Yes	0	No
13	Retina_R	Minimize (maximum) ‡	linear	20			5	1		Yes	0	No
14	GlnD_Lacrimal_R	Minimize (maximum) ‡	mean	26			7	1		Yes	0	No
15	MU	Minimize (maximum) ‡	linear	1			8	1		Yes	0	No

Figure 10: Example of a wish-list for a neuro-oncological tumour, with  $A$  the desired dose at the tumour. In this case,  $A$  is 54 Gy.

The wish-lists are not patient specific and can be used for an entire patient group with the same tumour site. This saves time compared to conventional planning approaches, as there is no time-consuming tweaking per patient required [35].

### Optimization

After reading the CTs, the parameters from the wish-list and the optimization parameters, the optimization starts. At the core of proton therapy treatment optimization there is always the problem of the reduction of spots. Using all the pencil beams with a Bragg peak in the tumour would give far too many pencil beams. So, in some way, it is desired to have as few spots as possible, but still have a clinically acceptable dose distribution. With fewer spots, not only the optimization times for the treatment planning are shorter, also the treatments themselves are faster. In iCycle this problem can be handled in two different ways: using a regular grid, see Figure 11, or using resampling, Figure 12.

#### *Regular grid*

One way is to choose a lateral spacing and an energy spacing and thus obtain a 3D regular grid of pencil beams. Using all the spots that fall within the tumour, the beams in the beamlist, the dose-deposition matrix is calculated. Then the weights for these pencil beams are calculated with inverse optimization. In the end, the pencil beams with a weight smaller than  $x$  are deleted, see Figure 11.

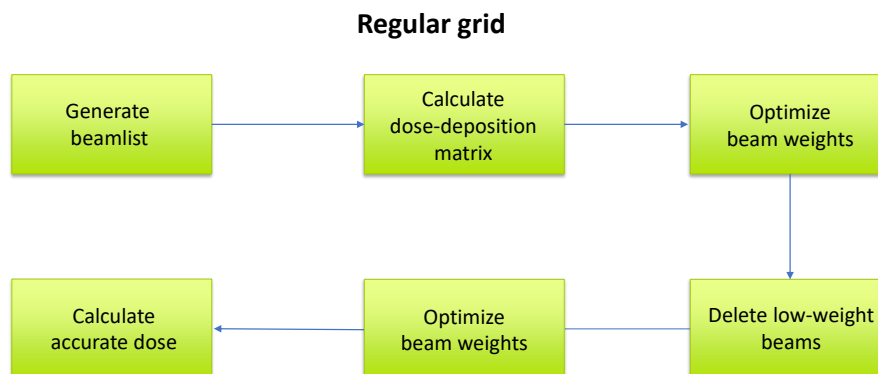


Figure 11: Visual representation of the regular grid optimization.

#### *Resampling*

The other way is to use resampling. In this approach, all pencil beams on a certain fine grid that have their Bragg peaks in the tumour are calculated and put in the beamlist. These are the ‘candidate spots’. From this set of candidate spots a sample with a certain sample size is taken. For this sample the dose-deposition matrix is calculated. With inverse optimization the weights for the individual pencil beams are optimized and the pencil beams with a weight smaller than the weight threshold are deleted. Then other pencil beams are selected from the candidate spots and the same is done. Thus, the plan iterates to a better solution, see Figure 12 on the next page.

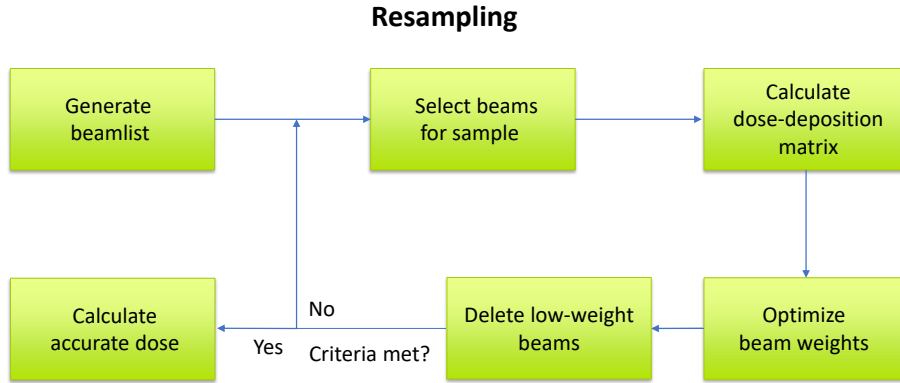


Figure 12: Visual representation of the resampling optimization.

The optimization times for the methods depend on the amount of spots involved and for resampling also on the stopping criterion of the optimization.

In both approaches the dose-deposition matrix is calculated and used for the inverse optimization. A dose-deposition matrix looks like this:

$$\mathbf{D} = \begin{bmatrix} D_{1,1} & D_{1,2} & \cdots & D_{1,n} \\ D_{2,1} & D_{2,2} & \cdots & D_{2,n} \\ \vdots & \vdots & \ddots & \vdots \\ D_{m,1} & D_{m,2} & \cdots & D_{m,n} \end{bmatrix},$$

with  $D_{i,j}$  the dose at voxel  $i$  caused by pencil beam  $j$ ,  $n$  is the number of pencil beams and  $m$  the number of voxels. In general,  $n$  is a lot smaller in resampling than when using a regular grid.

The weights of the pencil beams used in the matrix-vector product in Equation 7 are then determined by inversely optimizing this product. The weights are optimized such that the dose in all structures is Pareto and clinically optimal.

$$\mathbf{D} \cdot \mathbf{w} = \mathbf{d}, \quad (7)$$

here  $D$  is the dose-deposition matrix,  $w$  the weight vector with the weight for each pencil beam and  $d$  the dose in each voxel that is taken into account.

The pencil beams with a weight lower than a certain threshold are deleted.

The optimizer optimizes the weights of the pencil beams in a prioritized multi-criteria optimization, taking into account dose constraints and prioritized dose objectives [36]. In the optimization, a goal,  $b_i$ , is set for each objective,  $f_i(x)$ , with priority,  $i$ , and for the constraints,  $\mathbf{g}(x)$ , the boundary is set to  $\mathbf{0}$ . The functions  $f_i(x)$  and  $\mathbf{g}(x)$  are determined by the wish-list. The wish-list contains information on whether, for an objective or constraint, the minimum dose is maximized or the maximum dose is minimized. The used 2-phase  $\epsilon$ -constraint method optimizes one objective at a time while constraining the others. The dose is optimized such that the goal is met within the boundaries of the hard constraints  $\mathbf{g}(x) \leq \mathbf{0}$ . Often, the optimizer can optimize that certain objective further, but generally it is advantageous to start minimizing the dose for lower priority objectives first. In that way, it is prevented that a really low dose is obtained in one organ at risk (OAR) while another OAR receives a high dose. So, instead of continuing the optimization of that objective, the optimizer starts minimizing a lower

priority objective while setting a bound on the first objective. In more mathematical connotation this is:

$$\begin{aligned} \min \quad & f_1(x) \\ \text{s.t.} \quad & \mathbf{g}(x) \leq \mathbf{0}, \end{aligned}$$

with as a result  $x^*$ . Then, the optimization of the second objective looks like:

$$\begin{aligned} \min \quad & f_2(x) \\ \text{s.t.} \quad & \mathbf{g}(x) \leq \mathbf{0} \\ & f_1(x) \leq \epsilon_1, \end{aligned}$$

with  $\epsilon_i$  is:

$$\epsilon_i = \begin{cases} b_i & f_i(x^*)\delta < b_i \\ f_i(x^*)\delta & f_i(x^*)\delta \geq b_i. \end{cases}$$

$\delta$  is a relaxation constant, often set to 1.03 (giving a relaxation of 3%). This objective optimization is repeated for all objectives. This is the end of the first phase in the 2-phase  $\epsilon$ -constraint optimization.

In the second phase, the objectives that have met their goals are, in order of priority, further minimized up to the hilt, while keeping the other objectives as constraints:

$$\begin{aligned} \min \quad & f_i(x) \\ \text{s.t.} \quad & \mathbf{g}(x) \leq \mathbf{0} \\ & f_k(x) \leq \epsilon_k, \quad k \in \{1, \dots, n\} \setminus i. \end{aligned}$$

Given that the resulting solution of such an optimization is  $x^*$ ,  $\epsilon$  is set to  $f_i(x^*)\delta$ .

### Finalization

When all constraints and the objectives are met, or the number of iterations becomes too large, or there is no significant improvement in dose distribution, the optimization is finished. The optimizer in iCycle returns the final beams and the weights for those beams. With this information, the accurate dose distributed in the patient is calculated.

### 2.2.2 Dose calculation algorithm

The dose calculations in Erasmus-iCycle are done with the pencil beam algorithm used in Astroid [37]. Astroid is the in-house treatment planning system dose developed at Massachusetts General Hospital - Harvard Medical School [38].

In pencil beam algorithms, pencil beams are used to approximate all dose-deposition processes in a patient by local effects [7]. This local model is insensitive to inhomogeneities that are outside the beam envelope. The proton beams used in the treatment are modelled by a composition of narrow beams. In that way, with the set of pencil beams (the narrow beams) all degrees of freedom of the radiation field are modelled; the physical space of the radiation field is filled, and a slab of the patient is approximated as a set of interactions that the pencil beam has in that slab. Here, there is one limitation of the pencil beam algorithm. It only takes into account the interactions within the lateral beam envelope, while interactions are well understood for a laterally infinite slab. In pencil beam algorithms, the energy released in a medium,  $E$ , for a set of pencil beams,  $p$ , is given by:

$$E(\vec{x}, d) = \sum_p \rho(d)K(r, \rho(d))dA. \quad (8)$$

Here  $\vec{x}$  is a point in the lateral plane at depth  $d$ , where  $\rho$  is the radiological depth and  $K$  the lateral energy diffusion kernel.  $dA$  is the lateral area of a pencil beam. Pencil beam models are a good

representation of the physical proton transport through the patient, since the physical proton pencil beam is well approximated by the mathematical pencil beam [7]. The computation time of pencil beam models scales linearly with the number of pencil beams.

The algorithm implemented in Astroid, and thus also implemented in iCycle, has several special features [38]. A first aspect is that the model allows for implementation of an aperture or a range compensator. Another valuable characteristic is that the spatial resolution of the physical pencil beams does not influence the spatial resolution of the dose calculation in the patient. The dose,  $D$ , is calculated by the algorithm using:

$$D(\vec{x}) = \sum_S G_S \tag{9a}$$

$$\times \sum_K \left( \int \frac{1}{2\pi\sigma_O^2(R_S, z)} \exp\left(-\frac{\Delta_{S,K}^2}{2\sigma_O^2(R_S, z)}\right) dA_K \right) \tag{9b}$$

$$\times \frac{D_{R_S}^\infty(\rho)}{2\pi\sigma_P^2(R_S, \rho)} \exp\left(-\frac{\Delta_K^2(\vec{x})}{2\sigma_P^2(R_S, \rho)}\right). \tag{9c}$$

In Equation 9a,  $G_S$  is the number of gigaprotons of the physical pencil beams  $S$ . Equation 9b describes the allocation of the  $G_S$  protons given the intrinsic lateral spread,  $\sigma_O^2(R_S, z)$ , of the set of computational pencil beams  $K$ . The number of pencil beams in  $K$  is the highest resolution essential for accurately representing the dose in the patient.  $\sigma_O^2$  depends on the spot range,  $R_S$ , and the depth,  $z$ , along the pencil beam axis of the physical pencil beams in  $S$ . The distance of a point in the computational pencil beam area  $A_K$  to the spot in the spot coordinate system is denoted by  $\Delta_{S,K}$ . In Equation 9c, the diffusion of the protons is modelled, given the scatter spread,  $\sigma_P(R_S, \rho)$ . This total pencil beam spread is caused by multiple Coulomb scatter in the patient and depends on the range of a spot,  $R_S$ , and the radiologic depth,  $\rho$ . The term  $D_{R_S}^\infty(\rho)$  is the measured depth dose per gigaproton integrated over an infinite plane at depth  $\rho$ . Lastly,  $\Delta_K(\vec{x})$  is the distance from the calculation point to the computational pencil beams ( $K$ ) axis.

The depth doses in Equation 9c are obtained from 19 pristine Bragg peak measurements carried out by Varian in HollandPTC. The 19 nominal proton beam energies that are considered are: every 10 MeV from 70 MeV up to 240 MeV, and 244 MeV.

### 2.2.3 Treatment plan quality assessment

The International Commission on Radiation Units and Measurements (ICRU) has defined standards, reference points and limits for treatment plans [39]. To analyse the treatments plans two measures are often used: the dose-volume histogram and the homogeneity index [40], [41].

The dose-volume histogram of a plan shows how much volume (in % of the total volume of a structure) receives at least a certain dose, see Figure 13.

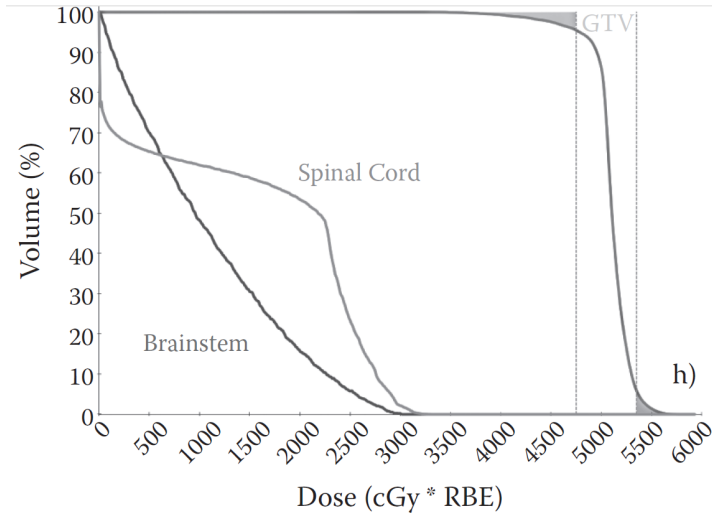


Figure 13: Example dose-volume histogram of the gross tumour volume (GTV) and two organs at risk (OARs): the spinal cord and the brainstem. The vertical lines indicate 95% (lower) and 107% (higher) of the prescribed dose to the tumour. The grey area at the from the 95% line down indicates underdosing of the GTV, while the grey area from the 107% upwards indicates the overdosing [7]. In this dose-volume histogram, the volume is given in percentages and the dose in cGy·RBE.

To set constraints for the target structure: the tumour, three tumour volumes are defined, the gross tumour volume (GTV), the clinical target volume (CTV) and the planning target volume (PTV). In Figure 14, a schematic representation of these volumes are given. The CTV is the GTV with an extra margin to include the microscopic malignant growth of the tumour. When treating the tumour, there can be setup and range errors, and there might be some CTV motion. To take that into account, in photon therapy, the PTV is defined. The PTV is the CTV with an extra margin such that it includes the CTV for all scenarios [42]. Defining the PTV for proton therapy treatments is more difficult, since simply expanding the geometry of the CTV is inadequate [43]. Therefore, generally the CTV is used.

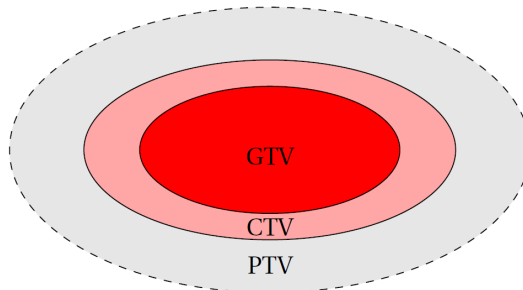


Figure 14: Schematic representation of the GTV, CTV and PTV [42].

In the part of radiotherapy where this research takes place, it is the convention to scale the dose-volume histogram such that the near minimum dose delivered to the tumour is 95% of the prescribed dose [44]. The near minimum dose,  $D_{98}$ , is the dose that is delivered to 98% of the volume of the planning tumour volume (PTV) or, in case of proton plans, the clinical tumour volume (CTV) [39].

The minimum dose in the tumour is not sufficient for qualifying a treatment plan. For a qualification of the plan, also the homogeneity of the dose in the tumour needs to be taken into account. A

measure for the homogeneity of the dose in the tumour is the homogeneity index,  $HI$ , which can be defined as [41], [45]:

$$HI = \frac{D_2 - D_{98}}{D_{Pr}} \times 100\%. \quad (10)$$

Here  $D_2$  is the near maximum, the heighest dose that is delivered to 2% of the volume of the planning tumour volume (PTV) or, when the PTV is not present, the clinical tumour volume (CTV); and  $D_{Pr}$  is the prescribed dose to the tumour. A  $HI$  in the range of 0% to 50% is desired [45].

## 3 Methodology

In this chapter, the methods employed in this research are described in more detail. The chapter is divided in three sections, the first section is about the beam simulations in the Monte Carlo (MC) calculation software, TOPAS; the second deals with the translation from the TOPAS results to Erasmus-iCycle with the spread-out Bragg peak (SOBP) database generation; and the last concerns the implementation of the SOBP-database in Erasmus-iCycle.

### 3.1 TOPAS simulations

The proton beam of the HollandPTC R&D room is simulated in TOPAS. TOPAS is a Monte Carlo platform for research and clinical applications based on Geant4, an MC platform written in C [46]. In order for the simulations to be repeatable, all settings and elements in the TOPAS implementations are given in this section. The scripts that are used can be found in Appendix A.1.

#### 3.1.1 Simulation settings

The settings used in the simulations are divided in two groups: physics settings, with the physical processes and parameters that are set for the simulation, and beam characteristics, with the settings that modulate the HollandPTC R&D beamline.

##### Physics settings

Physics settings in TOPAS are set in the same way as is done in Geant4: using ‘physics lists’. A physics list specifies the energy range, the physical processes, the types of particles and their range cuts (the particle stops, or is absorbed, after traveling the range cut distance [47]) that are taken into account in the simulation. Which physics lists should be implemented depends on the accuracy required for the results and the desired calculation speed [31]. Here, the default Geant4\_Modular physics list is used. This list contains the following default modules [48]:

Table 1: Modules implemented in the default physics list in TOPAS.

Modules	Content
g4em-standard_opt4	Electromagnetic interactions
g4h-phy_QGSP_BIC_HP	Nuclear interactions using binary cascade model
g4decay	Decay of excited residual nuclei
g4ion-binarycascade	Nuclear interactions of light ions using binary cascade model
g4h-elastic_HP	Elastic scattering
g4stopping	Capture of charged particles at rest

Furthermore, particle induced x-ray emission (PIXE), fluorescence and Auger cascades are also taken into account. These default settings have been shown to give good results for proton therapy research [31], [46]. In the simulation, the maximum length that a particle travels before a new calculation is done, the maximum step size, was varied depending on the scorer to be at least one-fifth of the smallest feature of the voxel grid used for the scorer [48].

##### Beam characteristics

The characteristics for the simulated proton beam are derived from earlier research on modelling the HollandPTC R&D beamline in TOPAS [48]. For integral dose-depth curves and energy spectra the characteristics of influence are the energy distribution, and, in case of a Gaussian distribution, the mean energy of the beam and the energy spread. In Table 2, the beam characteristics for a nominal energy of 70, 150, 200 and 240 MeV are given. In TOPAS, the proton beam has a Gaussian energy distribution with mean energy,  $E_{simulation}$  and standard deviation,  $\sigma_{E_{simulation}}$ .

Table 2: The mean simulation energies,  $\bar{E}_{simulation}$  in MeV, and energy spreads,  $\sigma_{E_{simulation}}$  in (%), are given for four nominal measurement energies,  $E_{measurement}$  in MeV, for the HollandPTC R&D beamline.

$E_{measurement}$ (MeV)	$\bar{E}_{simulation}$ (MeV)	$\sigma_{E_{simulation}}$ (%)
70.0	69.87	1.2
150	149.9	0.80
200	199.4	0.62
240	239.4	0.25

For all intermediate energies, the corresponding energy spreads are linearly interpolated.

The lateral and angular spreads of the beam only have a small effect on the dose-depth curves and energy spectra. The differences between these spreads for different energies is therefore neglected. The remaining beam settings, which are independent of the simulation energy, are given in Table 3.

Table 3: General beam settings for beam simulations in TOPAS.

Beam characteristics	Value
Position distribution	Gaussian
Position cut-off shape	Ellipse
Position cut off (x)	10.0 cm
Position cut off (y)	10.0 cm
Position spread (x)	0.33 cm
Position spread (y)	0.25 cm
Angular distribution	Gaussian
Angular cut-off (x)	90.0
Angular cut-off (y)	90.0
Angular spread (x)	0.0038 rad
Angular spread (y)	0.0042 rad

In choosing the number of particles per simulation, there is a trade-off between accuracy and computation time. The number of primary protons in these simulations is set to  $10^5$ . The accuracy and statistical error for these simulations can be found in Section 4.1.1.

### 3.1.2 Geometrical components

In this research, the proton beam leaving the exit window will be simulated. Thus, the beam transportation system and the scanning of the beam with the magnets is not taken into account. The setup of the geometrical components is derived from the measurement setup described in [48] and [49].

#### Pristine Bragg peak simulations

For pristine Bragg peak simulations, the geometrical components included are the exit window of the nozzle, the water tank and some detectors, see Figure 15.

- As is done in [48], the **exit window** is simulated as a kapton cylinder with a radius of 50.0 mm and a thickness of 0.25 mm.  
Position: At the beginning of the beamline.
- The **water tank** is a water cube of 30 cm in each lateral direction and 60 cm in the beam direction. In an experimental setup the water phantom would have plastic or glass sides. Here the water ‘tank’ is merely represented by a cube of water with a scoring element in it as detector,

see Section 3.1.3.

Position: At isocenter, 91.1 cm away from the exit window [49].

- The exact geometry of the **detectors**, the TM34070 Bragg Peak Chamber and the TM7862 X-ray Therapy Monitor Chamber, are not implemented in the simulations. Rather, their water equivalent thicknesses are taken into account in the data analysis, see Section 3.1.4.

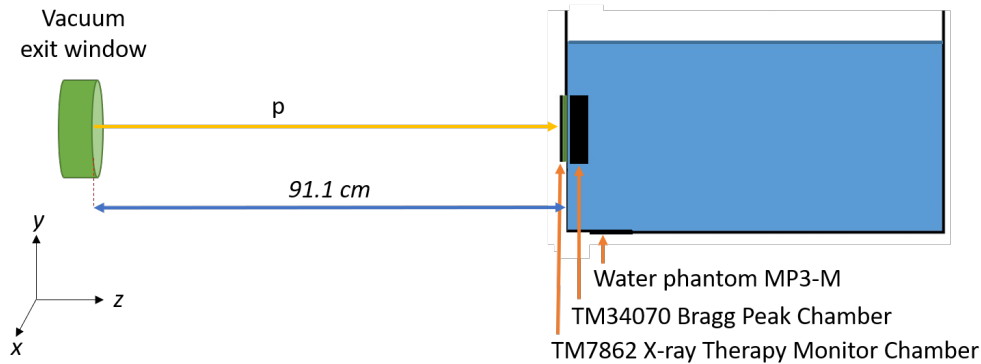


Figure 15: Schematic representation of the pristine Bragg peak measurement setup (not to scale). The proton beam leaves the exit window on the left and travels to the water phantom at isocenter, 91.1 cm from the exit window [50].

### Spread-out Bragg peak simulations

The setup for the SOBP-simulations is somewhat different from that of the Bragg peak simulations. Although the same exit window and positions for a detector are used, a different detector is used and a ridge filter is added to generate the spread-out region, see Figure 16. Ibrahimi [49] has used the Giraffe detector instead of the water phantom to measure the dose-depth curves. In the simulations, however, the same water phantom as for the Bragg peak measurements is used.

- The **ridge filter** is a static plastic square object with pins on it, Figure 17. It is implemented in the MC code by inputting the 3D CAD-file with the 3D printing file of the ridge filter. This file is obtained from the manufacturers [51].  
Position: 74.7 cm from the exit window, more on this in Section 4.1.2.

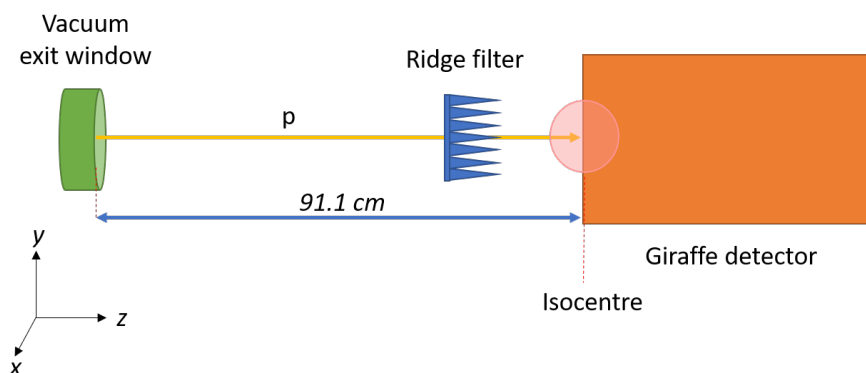


Figure 16: Schematic representation of the SOBP measurement setup (not to scale). The proton beam leaves the exit window on the left and travels through the ridge filter to the Giraffe detector on the right.

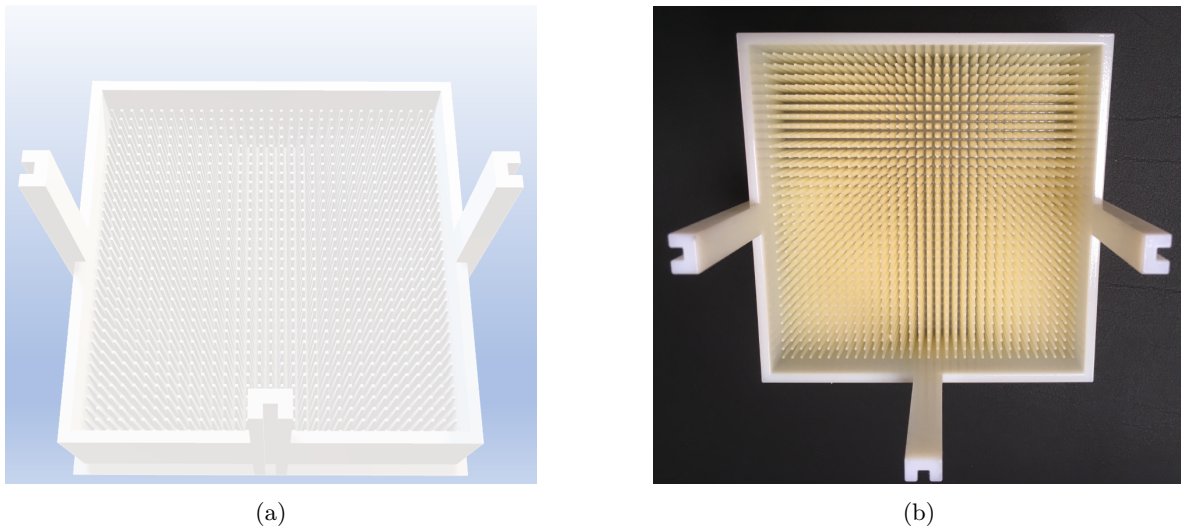


Figure 17: Ridge filter used to generate the simulation and measurement data. In (a) the 3D model of the filter manufactured by GSI [51] is shown and in (b) a picture of the ridge filter used in the measurements [49].

### 3.1.3 Scoring elements

In TOPAS different so called ‘scorers’ can be used to ‘measure’ various quantities of interest in the simulation. In this section two different scoring elements, one for the dose-depth curves and one for the energy spectrum, are discussed. Scoring elements evaluate physical quantities without having an impact on the physics of the simulation. Therefore, the scoring elements are so to speak ‘virtual’.

#### Dose-depth curves

To obtain the Bragg dose-depth curves of the proton beam a scorer is placed in the water tank. This scoring element resembles the detector that is used in the Varian measurements, the TM34070. It scores the dose in a cylinder with a radius of 4.08 cm and a length of 60 cm placed within the water phantom. There is only a discretization grid in the  $z$ -direction of the cylinder: 1200 bins with a width of 0.5 mm. The scorer scores the integral dose for each of the 1200 bins.

Position: At the isocenter, 91.1 cm away from the exit window.

The scoring element used for the SOBPD-dose-depth curve is similar to the one that is used for the BP dose-depth curves, but with a different radius. The radius of the electrode of the Giraffe detector is 6.0 cm [52], and thus, the radius of the scorer has also been chosen to be 6.0 cm.

#### Energy spectrum

The energy spectrum of protons passing through a plane perpendicular to the beam axis, a lateral plane, is scored only for the ridge filter simulations. This is done by scoring the phase space of that plane. In the simulations of a proton beam directed on a ridge filter, a phase space before and after the filter is scored.

Position 1: 9.7 cm from the exit window.

Position 2: 90.7 cm from the exit window, in front of the water phantom.

A schematic representation of the simulation setup can be seen in Figure 18.

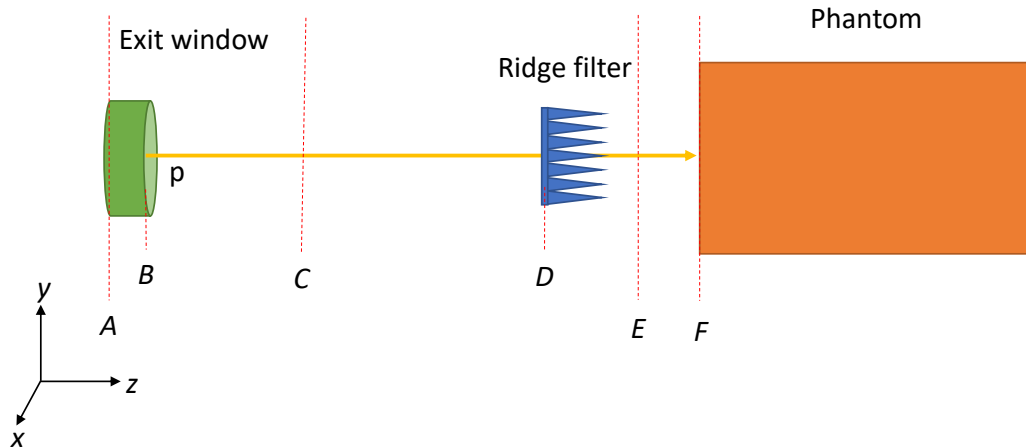


Figure 18: Schematic representation of the simulation setup (not to scale). The simulated proton beam starts on the left in the nominal plane (A), with a nominal energy and energy spread. First, it travels through the exit window with a thickness (distance A-B) of 0.25 mm. Then the beam goes through the first phase space scorer at a distance of 9.7 cm from the exit window (distance B-C), and the ridge filter at distance of 74.7 cm from the exit window (distance B-D). Following is the second phase space scorer, at the so called ‘phase plane’: the plane perpendicular to the beam axis where the second phase space is scored, at a distance of 90.7 cm from the exit window (distance B-E). Finally, the beam enters the phantom placed at 91.1 cm from the exit window (distance B-F).

The nominal energy is the mean energy of the proton beam at the exit window. Likewise, the nominal energy spread is the energy spread of the beam at the exit window. In contrast, the phase plane energy and phase plane energy spread are the energy and energy spread of the proton beam scored in the phase plane: the plane perpendicular to the beam axis where the second phase space is scored, at a distance of 90.7 cm from the exit window.

### 3.1.4 Validation of Bragg peak dose-depth curves

To validate the simulation settings, the integral dose-depth curves of the pristine Bragg peak simulations are compared to measurements.

Measurements performed by Varian are used for validation of the TOPAS simulations. The measurement setup used is shown in Figure 15. A water tank of 30 by 30 cm in the lateral direction and 60 cm in the beam direction is placed at the isocenter, 91.1 cm from the exit window. The detector, the TM34070 Bragg Peak Chamber, is placed in the water tank and moved backwards to detect the dose at all depths with a resolution of 1 mm. The TM34070 is a detector with an electrode diameter of 8.16 cm [53]. The TM7862 X-ray Therapy Monitor Chamber is used for reference measurements. To compare the simulations with the measurements of the TM34070, the water equivalent thicknesses (WETs) of the objects used in the measurements need to be taken into account. These values are given in Table 4.

Table 4: Water equivalent thicknesses (WETs) of objects used in the Varian Bragg peak measurements in HollandPTC [50].

Object	WET (mm)
PTW 34070	4.0
PTW 7862	0.26
Water phantom MP3-M	5.79

The total WET of the measurement setup is the sum of the individual parts: 10.1 mm. This is added to the depth of the measured dose depth curves.

### 3.2 SOBP-database generation

The SOBP-results from the MC simulations of the ridge filter (the energy spectra and dose-depth curves) are generated for implementation of SOBP-beams in iCycle. To allow that, the SOBP-beams have to be approximated by a series of pristine pencil beams, since the proton optimization algorithm of iCycle is based on pencil beams, see Section 2.2. The idea that is exploited here is that a SOBP can be viewed as a weighted superposition of individual Bragg peaks. So, a SOBP-database is generated. The database contains information on how to convert pristine Bragg peak beam optimizations in iCycle to SOBP-beam optimizations based on energy spectrum optimizations. A more graphical explanation of the SOBP-database generation and validation can be found in Figure 21.

#### 3.2.1 Structure of the database

The database generated is a nested MATLAB structure. The structure contains for every possible proton beam energy in iCycle a substructure. These substructures contain the nominal energies (that are allowed in iCycle) and weights of proton pencil beams that make up that SOBPs, see Figure 19.

SOBP

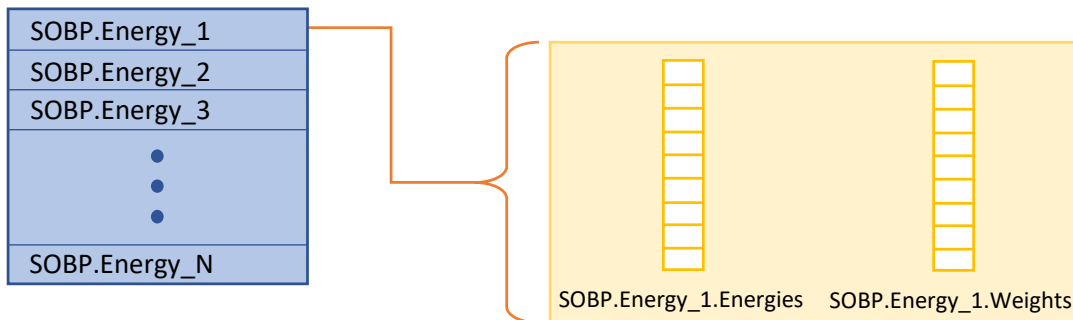


Figure 19: Structure of the SOBP-database with N energies implemented in the database. Every initial energy (blue element) is a substructure with two arrays with the energies and weights of the pristine Bragg peaks that make up the SOBP for that initial energy.

The database should contain the nominal energies of the proton beams, since iCycle uses the nominal energies in the treatment plan optimization.

#### 3.2.2 Optimization of the energy spectrum

A straightforward way to rewrite the simulated SOBP-beams, with nominal energy  $E_{nom}$ , in terms of Bragg peak beams is by approximating the scored energy spectrum after the ridge filter. Using this

method the result is still closely related to the ridge filter simulations and ridge filter design. The estimator is given by:

$$\tilde{E}(\mathcal{E}_j) = \sum_{i=1}^N w_i \cdot G_{E_i, \sigma_i}(\mathcal{E}_j), \quad (11)$$

where  $w_i$  is the weight for a pencil beam with Gaussian energy spectrum,  $N$  the number of pencil beams,  $G_{E_i, \sigma_i}$ , a Gaussian with mean energy,  $E_i$ , in MeV and energy spread,  $\sigma_i$  in MeV.  $\mathcal{E}_j$  is the  $j$ -th energy in MeV for which the approximated energy spectrum is evaluated. The energies  $E_i$  are taken from the HollandPTC-database with all energies that are implemented in iCycle. Between  $E_i$  and  $E_{i+1}$  is approx. 3 MeV for  $E_{nom} < 200$  MeV and for  $E_{nom} > 200$  MeV, the discretization between  $E_i$  and  $E_{i+1}$  is approx. 2 MeV. This corresponds to an energy spacing in water of approx. 3 mm.  $M$  is the total amount of discretization grid points where the approximation is evaluated, so the total amount of energies  $\mathcal{E}_j$ .

To minimize the error of this estimator, a non-negative linear least squares optimization is done, using MATLAB's *lsqnonneg*-function, to obtain the  $w_i$ :

$$\mathbf{w} = \text{lsqnonneg}(\mathbf{C}, \mathbf{d}). \quad (12)$$

Here,  $w$  is a vector with the optimal weights  $w_i$  for all pencil beams with energies  $E_i$ , these weights are of course non-negative.  $C$  is the matrix with the heights of the Gaussian energy spectra for the pencil beams with energies  $E_i$  and standard deviations  $\sigma_i$  at energies  $\mathcal{E}_j$ ,  $G_{E_i, \sigma_i}(\mathcal{E}_j)$ , and  $d$  is a vector with the 'measurement data',  $d_j$ , these are the heights of the scored ridge filter energy spectrum for energies  $\mathcal{E}_j$ .

$$\mathbf{w} = \begin{bmatrix} w_1 \\ w_2 \\ \vdots \\ w_N \end{bmatrix}, \quad \mathbf{C} = \begin{bmatrix} G_{E_1, \sigma_1}(\mathcal{E}_1) & G_{E_2, \sigma_2}(\mathcal{E}_1) & \cdots & G_{E_N, \sigma_N}(\mathcal{E}_1) \\ G_{E_1, \sigma_1}(\mathcal{E}_2) & G_{E_2, \sigma_2}(\mathcal{E}_2) & \cdots & G_{E_N, \sigma_N}(\mathcal{E}_2) \\ \vdots & \vdots & \ddots & \vdots \\ G_{E_1, \sigma_1}(\mathcal{E}_M) & G_{E_2, \sigma_2}(\mathcal{E}_M) & \cdots & G_{E_N, \sigma_N}(\mathcal{E}_M) \end{bmatrix} \mathbf{d} = \begin{bmatrix} d_1 \\ d_2 \\ \vdots \\ d_M \end{bmatrix}. \quad (13)$$

The function *lsqnonneg*, in the right hand side of Equation 12, does a linear least squares optimization by minimizing the following fitness function:

$$\min_{w \geq 0} \frac{1}{2} \sqrt{\left( (\mathbf{C}\mathbf{w} - \mathbf{d})^T (\mathbf{C}\mathbf{w} - \mathbf{d}) \right)^2}. \quad (14)$$

In non-matrix representation, that is:

$$\min_{w \geq 0} \frac{1}{2} \sqrt{\left( \left( \sum_{j=1}^M \left( \sum_{i=1}^N w_i \cdot G_{E_i, \sigma_i}(\mathcal{E}_j) \right) - d_j \right)^2 \right)}. \quad (15)$$

The optimal weight vector and the residual of the optimization are determined for different sets of 3 or 2 MeV spaced  $E_i$  and  $\sigma_i$ . In the SOBP-database, the set that gives the lowest residual is implemented.

### 3.2.3 Additional aspects of the database generation

Two parts of the SOBP-database generation will be discussed in more detail here. First of all, scored simulation data is used in the fitness function of the optimization. However, doing a TOPAS simulation for every energy in the HollandPTC-database would take too much time. Therefore, the results of a few simulations should be manipulated for use for all energies. Furthermore, as mentioned in Section 3.2.1, the energies in the SOBP-database should be nominal energies, while, in the optimizations, phase space energies are used. Thus, it should be possible to convert phase space energies to nominal

energies and phase space energy spreads to nominal energy spreads and vice versa.

### Simulations

Instead of numerous simulations, simulations are done for 19 base nominal energies (every 10 MeV from 70 MeV up to 250 MeV). For these energies, the energy spectrum after the ridge filter and a reference energy spectrum (scored at the same depth, but without implementing a ridge filter) are scored.

### Energies and spreads in the optimization

From the reference results, the mean energy degradation and the energy spread change between the nominal and the phase plane can be derived for the 19 energies. The energy degradation and energy spread changes for the HollandPTC-energies are then obtained by interpolating these results. Thus, the  $E_i$  and  $\sigma_i$  used in the optimizations are the phase plane energies and spreads determined using these energy degradations and energy spread changes, while in the SOBP-database, the corresponding nominal energies are saved.

### Interpolating the SOBP-database

The energy spectrum optimizations can only be done for the 19 energies. To obtain a database with all the HollandPTC-energies, the results from the 19 energies are interpolated. Since not all 19 energies have the same number of resulting Bragg peak pencil beam energies in the database, this is done as follows (Figure 20):

If SOBP nominal energy  $E_n$  can be simulated by  $q$  Bragg peak beams and  $E_{n+1}$  by  $p$  Bragg peak beams, then, if an intermediate energy  $E_{n,m}$  is closer to  $E_n$ , its SOBP is simulated by  $q$  Bragg peaks. The energies of these Bragg peaks are HollandPTC-energies with the same spacing as the ones of  $E_n$  but shifted by  $E_{n,m} - E_n$ . Furthermore, the weights for the beams are the same as the weights for the beams in  $E_n$ .

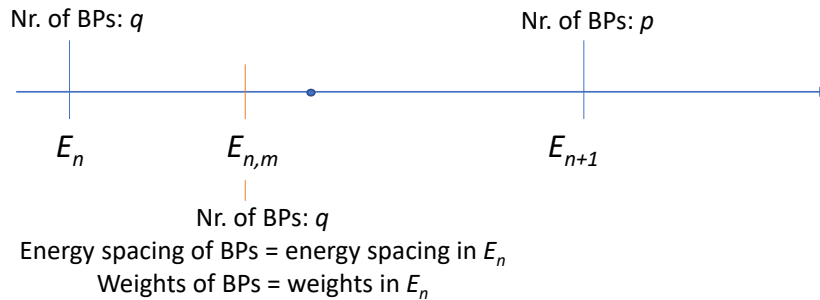


Figure 20: More graphical visualization of the method of interpolation of the SOBP-database described above. In this case,  $E_{n,m}$  is closer to  $E_n$  than to  $E_{n+1}$ .

### 3.2.4 Validation of the database

The resulting SOBP-database is verified for two situations. First, for one of the base energies, the scored ridge filter dose-depth curve and the weighted superposition of the simulated Bragg peak dose-depth curves are compared. Secondly, to validate the interpolation of the base energy database, this is also done for one of the interpolated energies. Finally, for one of the energies not the phase plane energies and spreads are implemented in TOPAS, but also the nominal energies and spreads are implemented. Then, again the scored ridge filter dose-depth curve and the weighted superposition of the simulated Bragg peak dose-depth curves are compared.

In Figure 21, the steps in the SOBP-database generation and validation are shown in a more graphical

way.

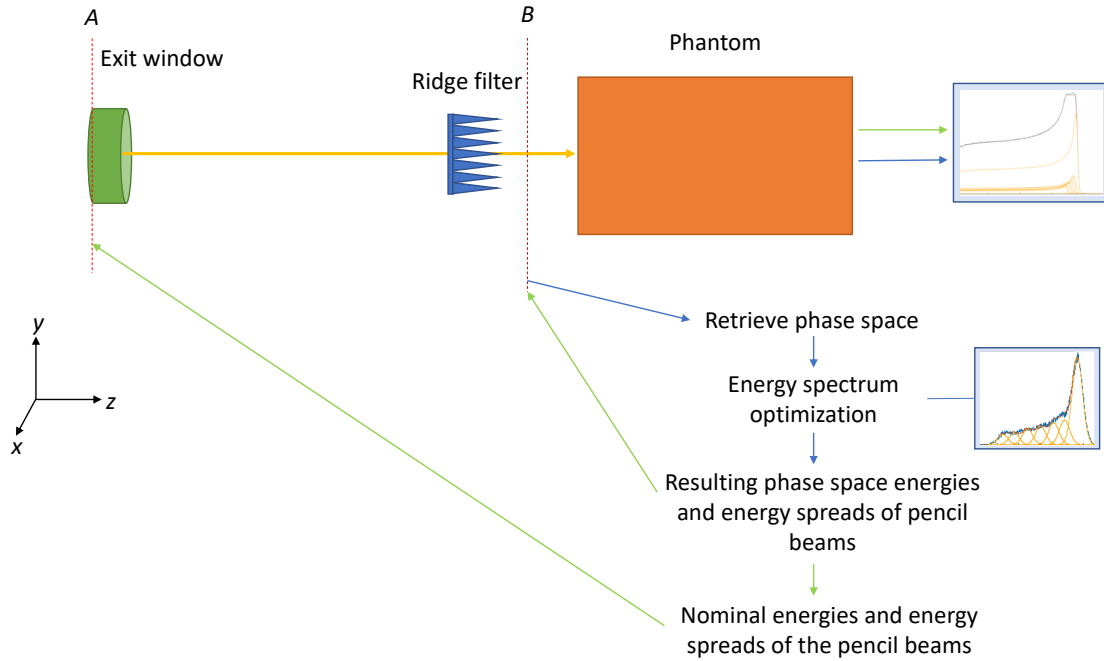


Figure 21: Graphical representation of the steps in the SOBP-database generation (blue arrows) and the validation (green arrows). The proton beam (yellow) starts at the nominal plane (A) with a certain initial, nominal energy,  $E_{nom}$ , and travels through the exit window and the ridge filter. At the phase plane (B), the phase space is scored and in the phantom the dose-depth curve is scored. With the energy information of the phase space, the energy spectrum of the simulation is found. This spectrum is approximated by a weighted sum of Gaussian energy distributions, see Section 3.2.2. The mean energies and energy spreads for the optimal approximation are phase plane HollandPTC energies and energy spreads. These are saved in the SOBP-database structure for the initial energy  $E_{nom}$ . This is done for all HollandPTC nominal energies as initial energies. For some initial energies, the validation is done by simulating beams with the phase plane energies and spreads in the database, scoring the dose-depth curve for those energies, calculating the superposition with the optimal weights and comparing the resulting dose-depth curve to the initially scored dose-depth curve. For one initial nominal energy, the phase plane energies and spreads are converted to nominal energies and spreads, implemented in TOPAS, and also the weighted superposed dose-depth curve is calculated and compared to the initially scored dose-depth curve.

### 3.3 Erasmus-iCycle optimizations

The SOBP-database is implemented in iCycle to pave the way to FLASH proton therapy treatment planning. In this first step towards FLASH treatment planning code is written to enable optimizing treatment plans with SOBP-beams instead of pristine Bragg peak beams.

#### 3.3.1 Requirements of FLASH optimization

The FLASH effect has some requirements that also translate into requirements on the treatment plan optimization. As mentioned before, time sequential energy modulation is time consuming. Therefore, in this research a clinical setup is proposed with a combination of a ridge filter and a range compensator to degrade the energy. Since these are both static objects, it is clear that pencil beams resulting from

the iCycle optimization all need to have a unique lateral position. If two pencil beams do have the same lateral position but a different energy, energy modulation within the irradiation fraction would be needed. In that case, the time constraint cannot be met.

Besides this, in clinical practice a single treatment fraction should, generally speaking, cover the entire tumour with a part of the total dose. Otherwise the detrimental effect of the irradiation on the tumour is less. It is assumed that this is no different in FLASH proton therapy. Because of the time and dose-rate constraints of FLASH, one fraction should be delivered from one beam direction. The repositioning of the patient for irradiating with multiple beam directions would take too much time for a FLASH fraction. So, the dose delivered by one beam should also cover the entire tumour with part of the total dose.

### 3.3.2 Settings iCycle

The settings used by iCycle are mainly given in an XML-file that contains the beam parameters, the structure dose constraints, information on the patient data file, the volumes in the patient and the optimization specifications.

#### Beam parameters

In this research beam angle optimization is not considered, therefore the same beam angles are chosen for all runs: 2 beams with gantry angles of  $240^\circ$  and  $300^\circ$  and  $0^\circ$  for the couch angle, see Figure 22.



Figure 22: Axial plane of a CT of a head with both beam directions used [54]. The  $240^\circ$  direction is the lower arrow and the  $300^\circ$  direction is the upper arrow.

For the optimization a pencil beam algorithm without taking a multileaf collimator into account is used, the Pencil Beam No MultiLeaf Collimator (PB No MLC) algorithm.

#### Dose constraints

Some constraints and objectives are set to maximize the minimum of the dose in a structure, while others are set to minimize the maximum. In the target structures, the overall minimum dose in the structure is maximized with as a constraint in the GTV 95% and in the CTV 98% of the prescribed dose (54 Gy for the skull base glioma). The dose in the tumour should also have an upper limit. Therefore, objectives are set to minimize the maximum in the target structures in the GTV to 112% and in the CTV to 107% of the prescribed dose. For all other structures the linear or mean maximum dose in the tumour is minimized with an objective for the maximal dose. All objectives and constraints can be found in Appendix A.2.

All constraints and objectives are optimized non-robustly.

### Optimization specifications

The optimization modality is Intensity-Modulated Proton Therapy (IMPT) with a regular grid with a lateral spacing between the pencil beams of 5 mm and an energy spacing between the deepest parts of consecutive SOBP-‘spots’ of 10 mm. The used beam model uses the pencil beam scanning data measured at HollandPTC. These data are measured at nominal beam energies of 244 MeV, the maximum energy available in the HollandPTC database in iCycle, and at every 10 MeV from 70 MeV up to 240 MeV.

### 3.3.3 Extensions and adjustments of iCycle

In conventional iCycle optimizations, pristine pencil beams are used to irradiate tumours. In the adjusted version of iCycle, the Bragg peak spots will be converted to SOBP-spots. The relevant part of the iCycle structure with the implemented changes is given in Appendix A.3. In this section the main extensions are explained and given in pseudocode. Besides these extensions, some minor adjustments are done in iCycle. These have to do with the indexation of the beamlist. In some already existing functions instead of using the short SOBP beamlist for indexing, the extended SOBP beamlist is used.

There are four main extensions to the conventional iCycle code:

First, the initial Bragg peak beamlist is converted to the extended Bragg peak beamlist, `extended_SOBP_beamlist`, Function 1. This extended beamlist is used to build up SOBP-beams from individual Bragg peak beams.

---

#### Function 1: `extend_beamlist`

Pseudocode for the function `extend_beamlist`. This function extends the initial BP-beamlist to allow for optimization using SOBP-beams instead of BP-beams.

---

**Input:** `initial_beamlist`, `HollandPTC_EnergyRangeList`, `SOBP-database`

**Output:** `extended_SOBP_beamlist`, `short_SOBP_beamlist`, `initial_beamlist`

---

#### Begin;

- (1) **add** beam indexing column to `initial_beamlist`;
- (2) `threshold_E` = lowest base energy in `SOBP-database`;
- (3) `short_SOBP_beamlist` = `initial_beamlist(E>threshold_E)`;  
`K` = number of beams in `short_SOBP_beamlist`;  
**initialize** `extended_SOBP_beamlist`;
- for**  $i = 1$  to  $K$  **do**
  - find** number of Bragg peaks, their energies and weights in `SOBP-database` corresponding to beam  $i$  in `short_SOBP_beamlist`;
  - ensure** energies are interpolated to the nearest `HollandPTC` energy;
  - (4) **add** Bragg peak beams with weights to `extend_SOBP_beamlist`;
- end**
- (5) **add** column to `short_SOBP_beamlist` with for every beam in `short_SOBP_beamlist` the number of Bragg peaks making up the SOBP-beam for that nominal energy;

#### End

---

A graphical explanation of Function 1 can be found in Figure 23.

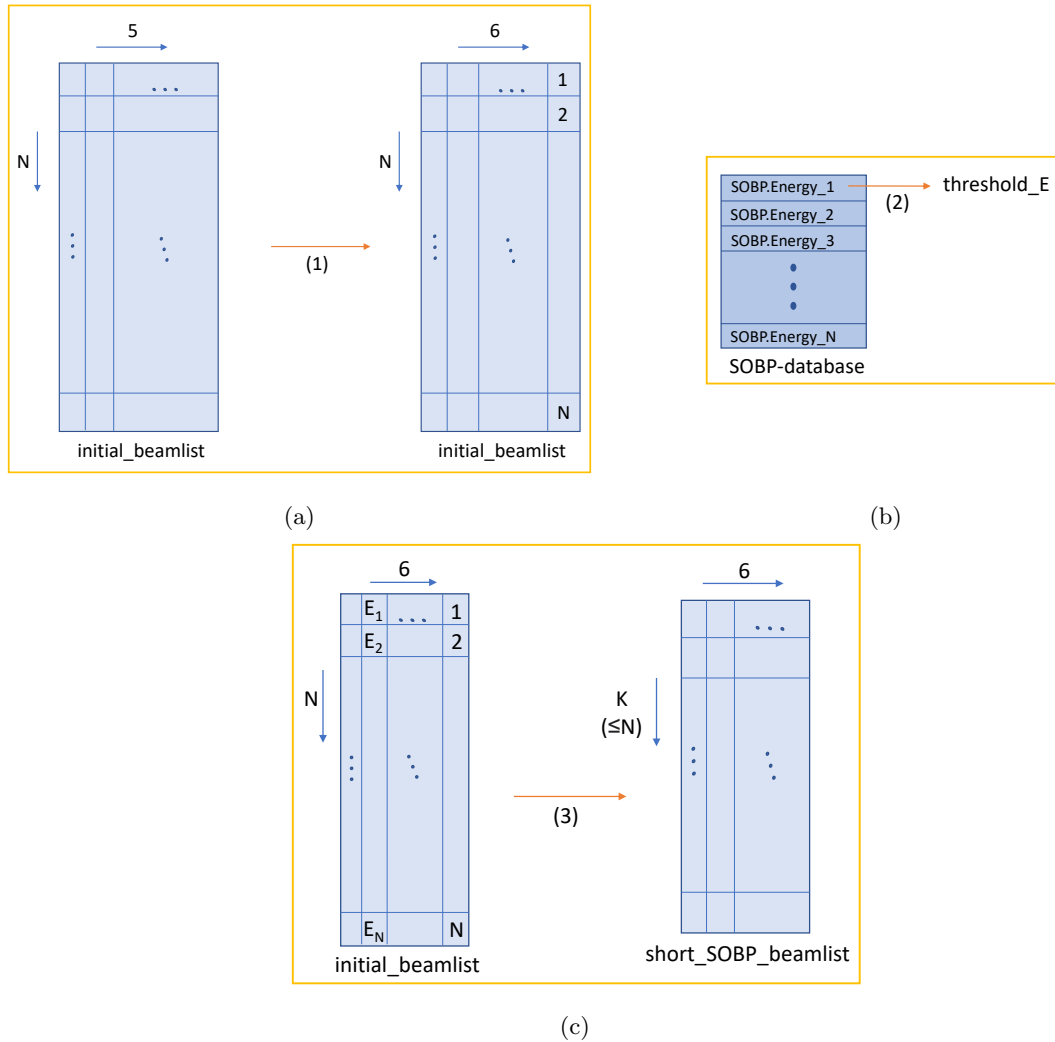
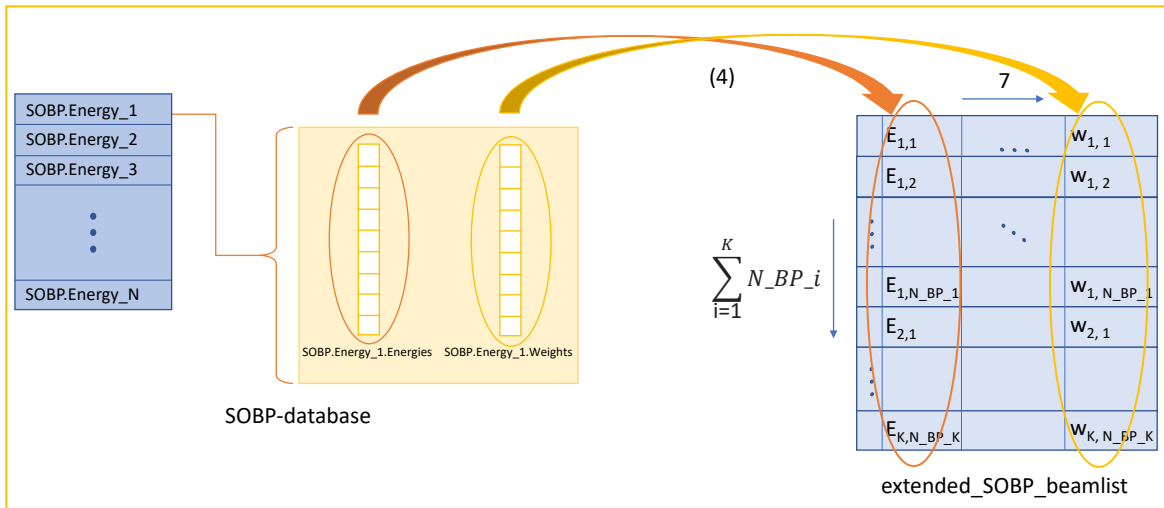
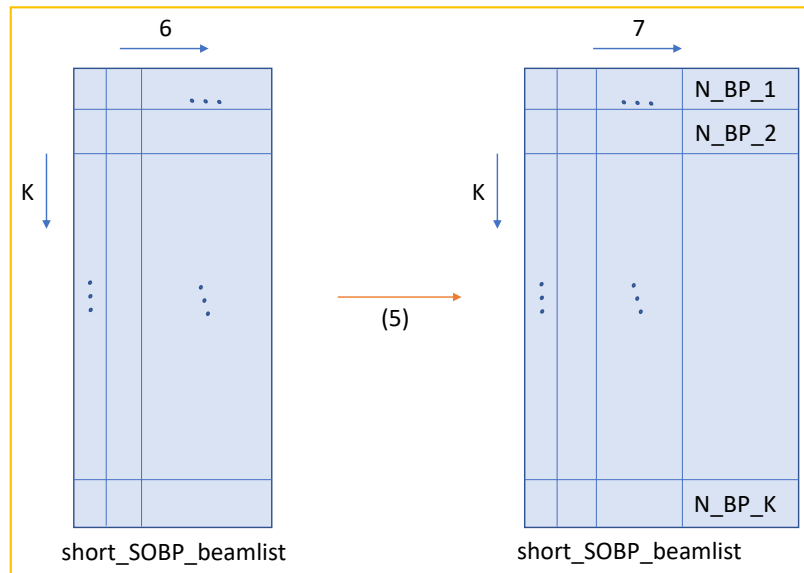


Figure 23: Graphical explanation of Function 1: `extend_beamlist`. This function constructs an extended beamlist from the initial Bragg peak beamlist to allow for optimization using SOBP-beams. The numbers in brackets indicate the numbered lines in Function 1.  $N$  is the number of Bragg peak pencil beams in the initial beamlist. The initial beamlist initially has 5 columns: the first with the number of the beam direction; the second with the energy; the third and fourth with respectively the  $x$ - and  $y$ -position of the pencil beam, and the fifth with a potential degrader value. (a) shows the extension of the initial beamlist (Function 1-(1)), (b) shows which energy in the SOBP-database is the threshold energy (Function 1-(2)), and (c) shows that `short_SOBP_beamlist` is a shorter version of `initial_beamlist`, where the beams with energy lower than 110 MeV are deleted (Function 1-(3)).



(d)



(e)

Figure 23: Continuation of the graphical explanation of Function 1.  $N_{BP_i}$  is the number of pristine Bragg peaks used to approximate SOBP-beam  $i$ . (d) shows how `extended_SOBP_beamlist` is constructed (Function 1-(4)) and (e) shows the extension of `short_SOBP_beamlist` (Function 1-(5)).

The energies in the SOBP-database are rounded HollandPTC energies. Therefore, they need to be interpolated to the nearest full HollandPTC energy. Erasmus-iCycle can only handle unrounded energies in the dose calculations.

Secondly, the SOBP-beam doses are calculated for all SOBP-beams. This is done by adding the doses for the individual Bragg peaks that make up the SOBP with a certain weight, Function 2.

---

**Function 2:** combine\_SOBP\_dose\_matrix

Pseudocode for the function combine\_SOBP\_dose\_matrix that calculates the weighted combination of the pristine Bragg peak columns in the dose-deposition matrix to convert the dose-deposition matrix to the SOBP-beam dose-deposition matrix.

---

**Input:** DoseDepositionMatrix, extended\_SOBP\_beamlist, short\_SOBP\_beamlist, SOBP-database

**Output:** SOBP\_DoseDepositionMatrix

**Begin;**

    K = number of SOBP-beams (length of short\_SOBP\_beamlist);

**for**  $i = 1$  to  $K$  **do**

- |     |   |
|-----|---|
| (1) | SOBP_DoseDepositionMatrix(:,i) = <b>weighted sum</b> of             |
| (2) | the columns of DoseDepositionMatrix belonging to SOBP-beam $i$ with |
|     | the weights given in extended_SOBP_beamlist;                        |

**end**

**End**

---

A visualization of this code can be found in Figure 24 on the next page.

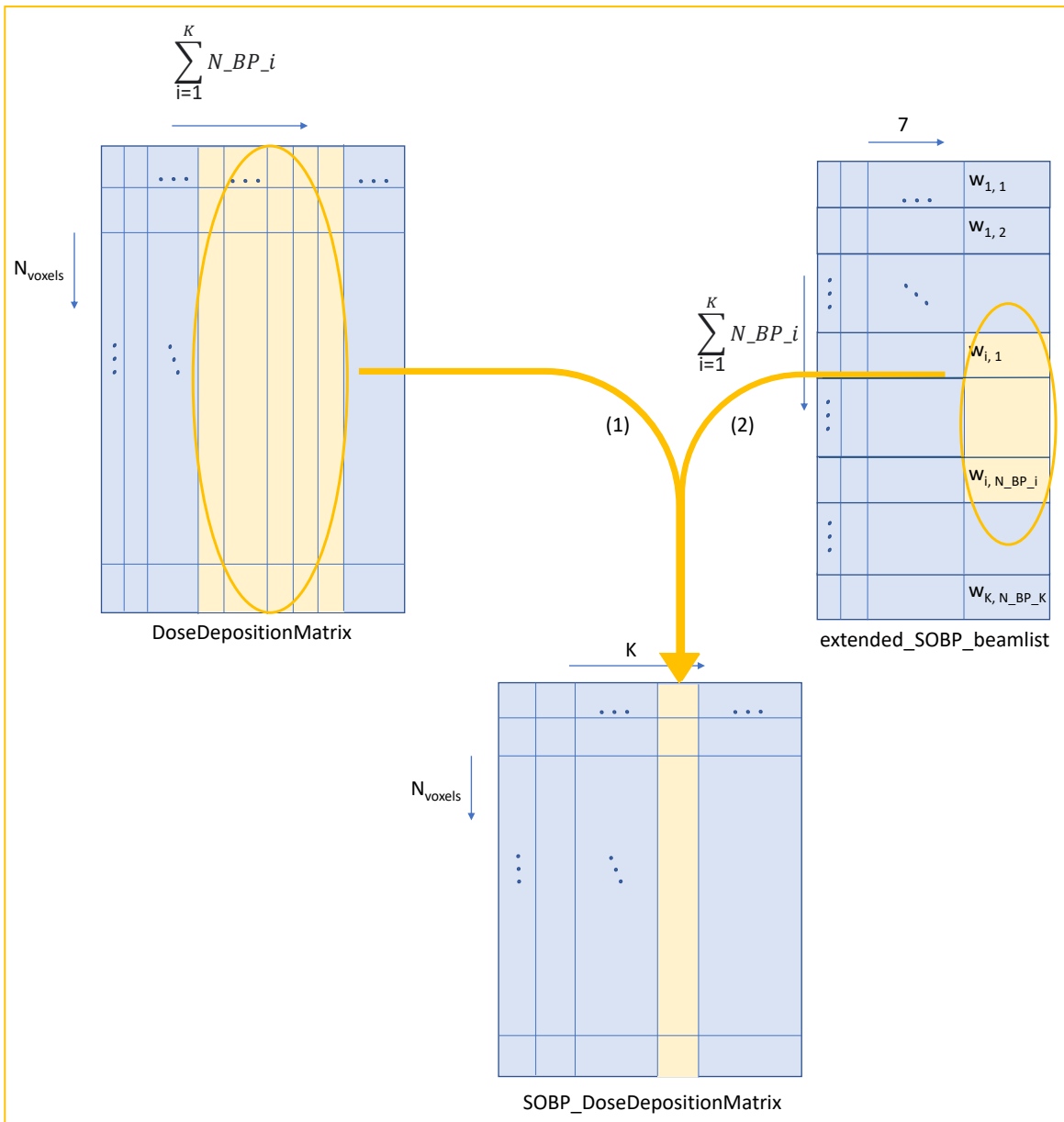


Figure 24: Graphical explanation of Function 2: `combine_SOBP_dose_matrix`. The columns of the `DoseDepositionMatrix` making up one SOBP-beam dose-deposition column are combined with a certain weight. The numbers in brackets indicate the numbered lines in Function 2.  $N_{\text{voxels}}$  is the number of voxels taken into account in the optimization,  $N_{BP\_i}$  is the number of pristine Bragg peaks used to approximate SOBP-beam  $i$ , and  $K$  is the number of beams in `short_SOBP_beamlist`.

The columns of the `DoseDepositionMatrix` belonging to the SOBP-beams are found using the SOBP-database. The columns of the matrices correspond to the beams.

Thirdly, Function 3 finds in the optimal short SOBP-beamlist the SOBP-beams that have the same lateral position and a different nominal energy. As explained in Section 3.3.1, this is not allowed. Therefore, the double-positioned beams with the lowest weight in the optimal solution are deleted.

**Function 3:** double\_position\_deletion

Pseudocode for the function double\_position\_deletion deletes lower weight SOBPs-beams with the same lateral position and keeps the SOBPs-beam with the highest weight for that lateral position.

**Input:** short\_SOBP\_beamlist\_opt, extended\_SOBP\_beamlist\_opt, x\_opt,  
SOBP\_DoseDepthMatrices\_opt

**Output:** short\_SOBP\_beamlist\_opt, extended\_SOBP\_beamlist\_opt, x\_opt,  
SOBP\_DoseDepthMatrices\_opt

**Begin;**

- (1) positions = **find** all used lateral positions in short\_SOBP\_beamlist\_opt;  
Q = number of lateral positions used (length of positions);  
delete\_short = [];
- for**  $i = 1$  to  $Q$  **do**
- (2) index\_del\_beams = **find** all beams that have lateral position  $i$  in  
short\_SOBP\_beamlist\_opt;
- (3) max\_beam = beam from index\_del\_beams that has the maximal weight;  
**delete** max\_beam from index\_del\_beams;  
P = number of beams in short\_SOBP\_beamlist with lateral position  $i$  that need to be  
deleted (length of index\_del\_beams);  
delete\_extended = [];
- for**  $j = 1$  to  $P$  **do**
- to\_delete\_extended = **find** the beams in extended\_SOBP\_beamlist\_opt that  
make up beam  $j$  in index\_del\_beams;
- add** to\_delete\_extended to delete\_extended;
- end**
- add** index\_del\_beams to delete\_short;
- end**
- (4) **delete** matrix columns given in delete\_short from SOBP\_DoseDepthMatrices\_opt;
- (5) **delete** beams given in delete\_short from short\_SOBP\_beamlist\_opt;
- (6) **delete** weights of beams given in delete\_short from x\_opt;
- (7) **delete** beams given in delete\_extended from extended\_SOBP\_beamlist\_opt;

**End**

A graphical explanation of the code can be found in Figure 25. The lines code between line (3) and line (4) in Function 3 are not visualized, these lines describe the indexation of the beams that are deleted.

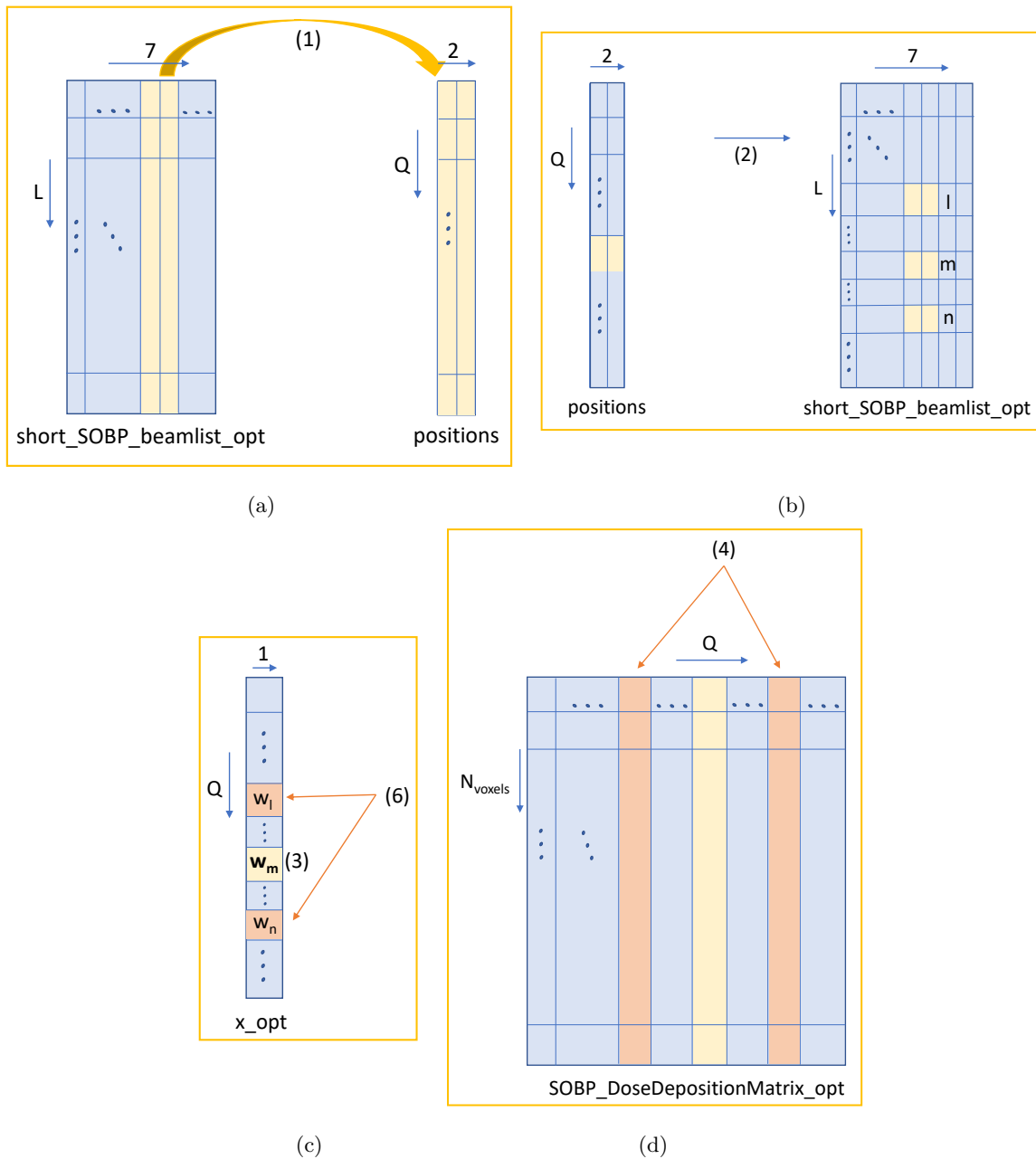


Figure 25: Graphical explanation of Function 3: `double_position_deletion`. This function deletes lower weight SOBP-beams with the same lateral position and keeps the SOBP-beam with the highest weight for that lateral position. The numbers in brackets indicate the numbered lines in Function 3.  $L$  is here the number of beams in `short_SOBP_beamlist_opt`,  $N_{voxels}$  is the number of voxels taken into account in the optimization,  $Q$  is the number of lateral positions used and thus the number of beams in `short_SOBP_beamlist_opt` after deleting all double beams with lower weights. (a) shows how the pencil beam positions are found (Function 3-(1)), (b) shows that the beams in `short_SOBP_beamlist_opt` that have the same position are found (Function 3-(2)), (c) shows that the maximum weight is found (bold) (Function 3-(3)), and that the lower weight SOBP-beams with that position are deleted (red) (Function 3-(6)), and (d) shows the columns that are deleted in `SOBP_DoseDepositionMatrix_opt` (Function 3-(4)).

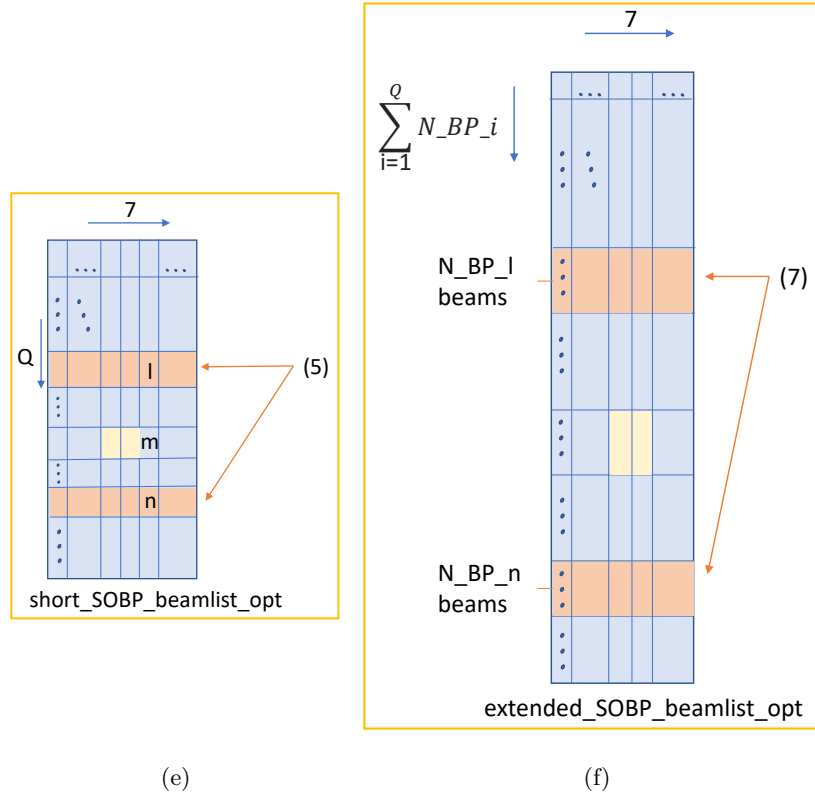


Figure 25: Continuation of the graphical explanation of Function 3.  $N_{BP_i}$  is the number of pristine Bragg peaks used to approximate SOBP-beam  $i$ . (e) shows the beams (rows) that are deleted from `short_SOBP_beamlist_opt` (Function 3-(5)), and (f) shows the beams (rows) that are deleted from `extended_SOBP_beamlist_opt` (Function 3-(6)).

Finally, the conversion from the optimal SOBP-weights to the optimal weights for each individual pencil beam making up the SOBPs is implemented, Function 4 and Figure 26.

---

**Function 4:** `xopt_conversion`

Pseudocode for the function `xopt_conversion` that converts the optimal SOBP-weight vector, `x_opt`, to a vector with the optimal weights for each individual BP making up the SOBP.

---

**Input:** `short_SOBP_beamlist`, `extended_SOBP_beamlist`, `x_opt`

**Output:** `x_opt_extended`

---

**Begin;**

$X$  = number of combined SOBP-beams (length of `x_opt`);

$Y$  = number of individual beams (length of `extended_SOBP_beamlist`);

`extending_matrix` = zero matrix of size  $Y \times X$ ;

**for**  $i = 1$  to  $X$  **do**

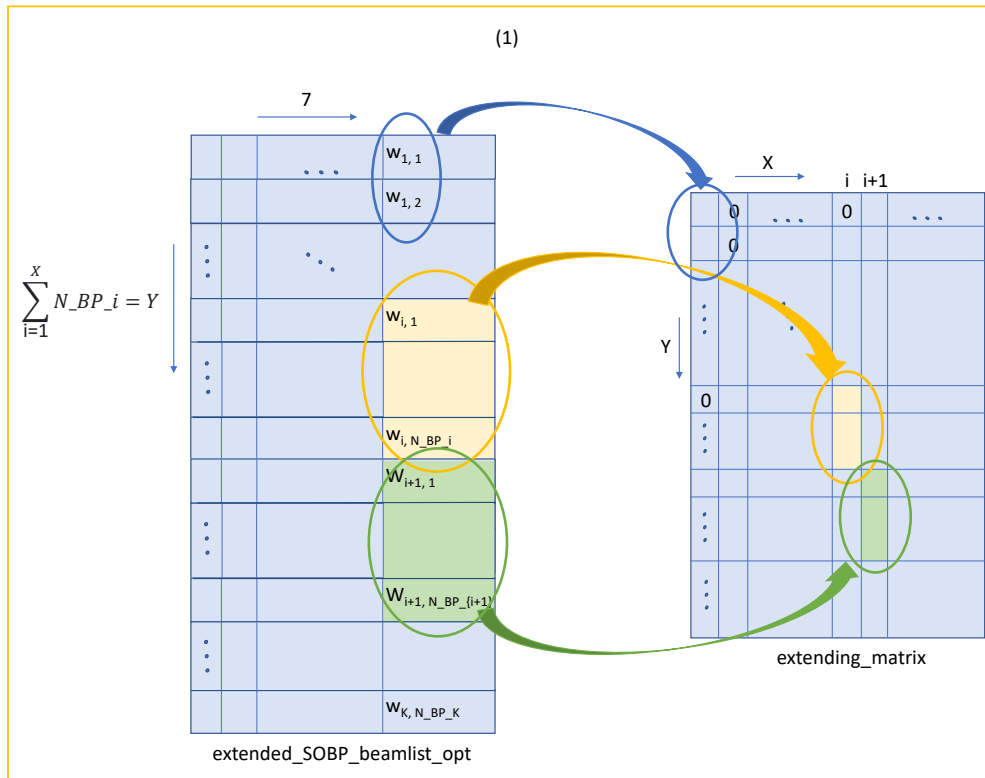
- (1) `corresp_beams` = **find** the indices of the individual beams making up SOBP-beam  $i$ ;  
`extending_matrix`(`corresp_beams`, $i$ ) = weights of individual beams in the weighted superposition;

**end**

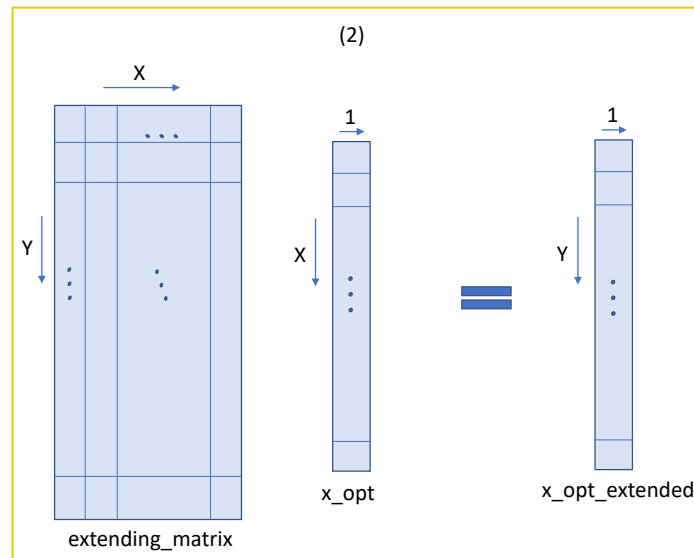
- (2) `x_opt_extended` = **multiply** `extending_matrix` by `x_opt`;

**End**

---



(a)



(b)

Figure 26: Graphical explanation of Function 4: `xopt_conversion`. This function converts the optimal SOBP-weight vector, `x_opt`, to a vector with the optimal weights for each individual BP making up the SOBP. The numbers in brackets indicate the numbered lines in Function 4.  $N\_BP\_i$  is the number of pristine Bragg peaks used to approximate SOBP-beam  $i$ ,  $Y$  are all pencil beams in `extended_SOBP_beamlist_opt`,  $X$  are all SOBP-beams in `short_SOBP_beamlist_opt`. (a) shows how `extending_matrix` is constructed (Function 4-(1)) and (b) shows the matrix-vector product converting `x_opt` to `x_opt_extended` (Function 4-(2)).

### 3.3.4 FLASH compatibility assessment

To evaluate the optimized SOBP-beam treatment plans, two metrics are taken into account. First of all, the homogeneity of the dose in the tumour. The homogeneity index (Equation 10) of the plans should be lower or around the same value as the index for the conventional treatment plan. Besides this, the required ‘FLASH enhancement ratio’ (FER) is considered. The FER is a metric for the FLASH effect. It is the ratio by which FLASH-delivered dose in healthy tissue needs to be divided to obtain an IMPT-delivered dose that would give similar normal tissue toxicities. So, healthy tissue can be FLASH irradiated with higher doses and result in the same damage in healthy tissue as a lower dose in conventional treatment.

The FER is determined by calculating the ratio between the mean dose to healthy tissue in the SOBP-plans and the mean dose to healthy tissue in the conventional treatment plan.

## 4 Results

In this chapter the results of the research are presented. First, the validations of and simulations with the TOPAS model are provided. Furthermore, some energy spectrum optimization results are obtained and given to validate the generated SOBP-database. The SOBP-database is used in Erasmus-iCycle optimizations for several patients. In the end, results of these optimizations are displayed.

### 4.1 TOPAS simulations

The simulations that are done in TOPAS can be categorized in different groups: the pristine Bragg peak validation simulations and the SOBP-simulations.

#### 4.1.1 Validation of the model

To validate the model, Bragg peak curves for 150 and 240 MeV beams are simulated and compared to the measurements. This is done with the simulation setup discussed in Section 3.1 and the script in Appendix A.1.3.

One of the factors influencing the accuracy of the simulations is the amount of particles in the optimization. To validate that a sufficiently high amount of particles is used, Bragg peak simulations are done for  $10^5$  and  $10^6$  particles. Two energies are considered, a 150 MeV nominal beam and a 240 MeV nominal beam. The dose-depth diagrams and difference curves are shown in the Figures 27 and 28.

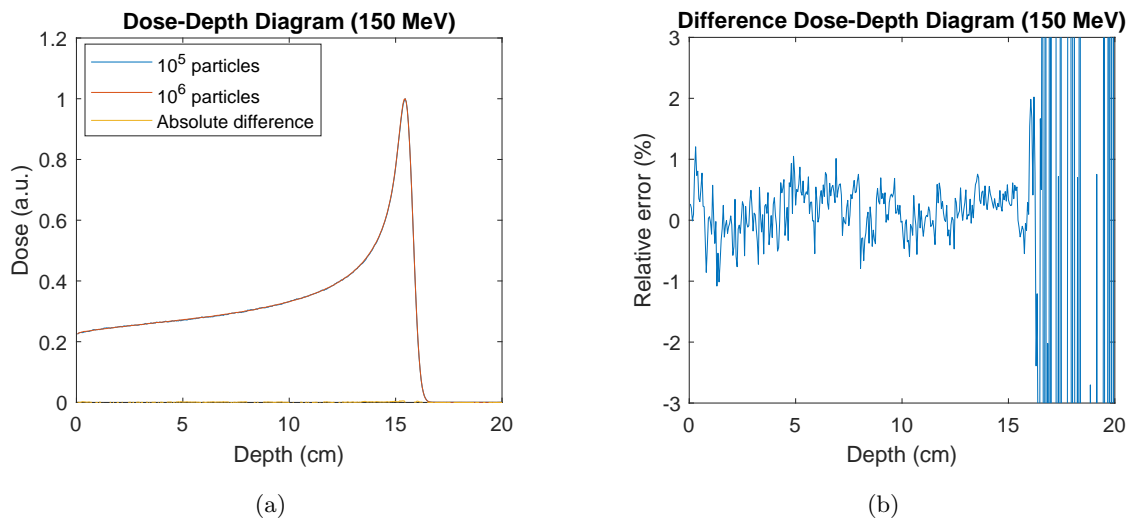


Figure 27: Comparison of a measured and simulated proton beam dose-depth distribution with a nominal energy of 150 MeV. In (a) the measured dose (red) and the simulated dose (blue) are given with the absolute error (yellow) over the depth of the phantom in cm. In (b) the relative error in % between the two dose-depth curves is shown over the depth of the phantom in cm. TOPAS simulation of the beam is done with an initial Gaussian energy distribution with a mean energy of 149.9 MeV and an energy spread of 0.75% of this value.

The absolute mean relative error for a depth smaller than 16.16 cm is 0.34%. At a depth of 16.16 cm, the simulated dose-depth curve for  $10^5$  particles is at 10% of its maximum value.

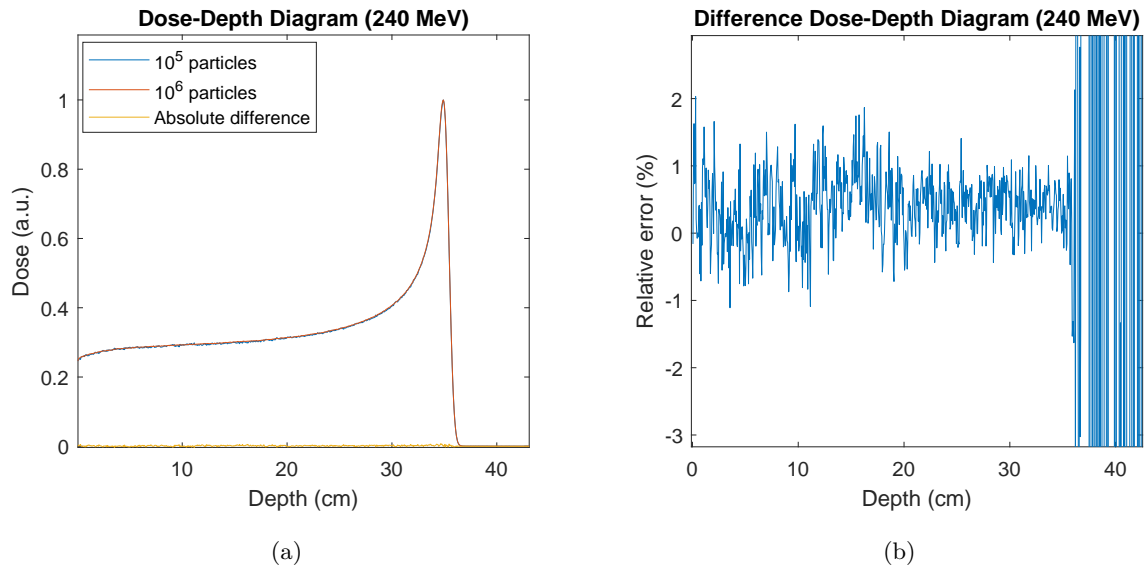


Figure 28: Comparison of a measured and simulated proton beam dose-depth distribution with a nominal energy of 240 MeV. In (a) the measured dose (red) and the simulated dose (blue) are given with the absolute error (yellow) over the depth of the phantom in cm. In (b) the relative error in % between the two dose-depth curves is shown over the depth of the phantom in cm. TOPAS simulation of the beam is done with an initial Gaussian energy distribution with a mean energy of 239.4 MeV and an energy spread of 0.25% of this value.

The absolute mean relative error for a depth smaller than 35.94 cm is 0.51%. At a depth of 35.94 cm, the simulated dose-depth curve for  $10^5$  particles is at 10% of its maximum value.

In Figure 29, the measured and simulated dose-depth distribution for 150 MeV is shown. The dose-depth curve of the 150 MeV beam energy measurement is measured by Varian, see Section 3.1.4. Dose is normalized in order to compare the measurements with the simulations. The normalization factor is chosen such that the maximum of the dose-deposition curves is at 100. The relative error between the simulation and the measurement is given in Figure 29b.

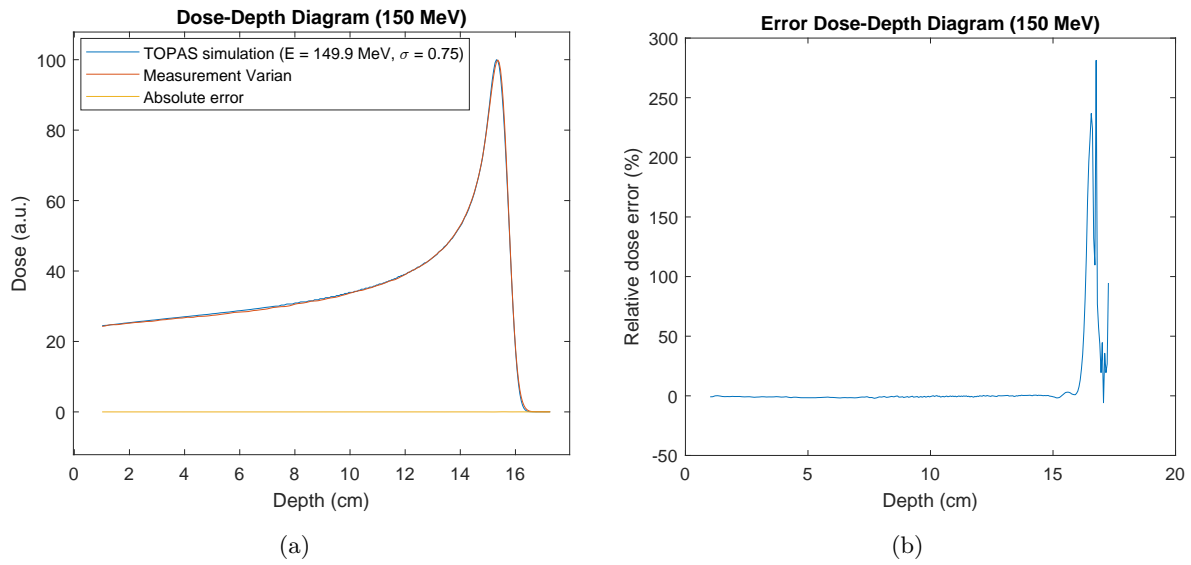


Figure 29: Comparison of a measured and simulated proton beam dose-depth distribution with a nominal energy of 150 MeV. In (a) the measured dose (red) and the simulated dose (blue) are given with the absolute error (yellow) over the depth of the phantom in cm. In (b) the relative error in % between the two dose-depth curves is shown over the depth of the phantom in cm. TOPAS simulation of the beam is done with an initial Gaussian energy distribution with a mean energy of 149.9 MeV and an energy spread of 0.75% of this value.

The absolute mean relative error for a depth smaller than 16.08 cm is 0.85%. At a depth of 16.08 cm, the measured dose-depth curve is at 10% of its maximum value.

For a nominal beam energy of 240 MeV, the results are shown in Figure 30.

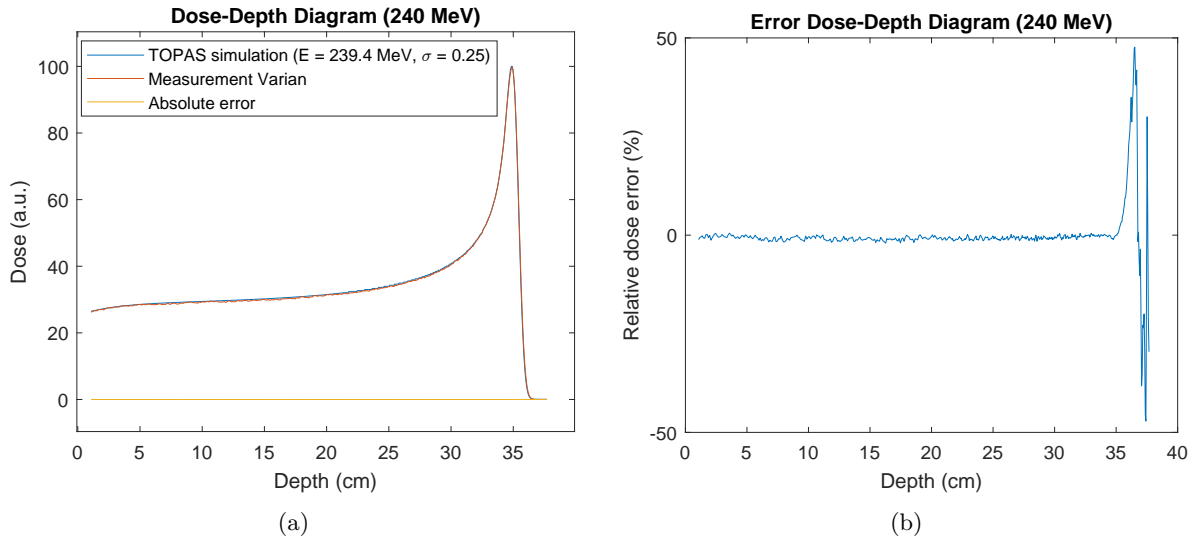


Figure 30: Comparison of a measured and simulated proton beam dose-depth distribution with a nominal energy of 240 MeV. In (a) the measured dose (red) and the simulated dose (blue) are given with the absolute error (yellow) over the depth of the phantom in cm. In (b) the relative error in % between the two dose-depth curves is shown over the depth of the phantom in cm. TOPAS simulation of the beam is done with an initial Gaussian energy distribution with a mean energy of 239.4 MeV and an energy spread of 0.25% of this value.

The absolute mean relative error for the depth up to 35.91 cm is 0.89%. At 35.91 cm, the measured dose-depth curve is at 10% of its maximum dose value.

#### 4.1.2 SOBP-simulations

Different SOBP-simulations have been done. First of all, to verify the position of the ridge filter. Besides that, also the energy spectrum of a typical ridge filter run is retrieved, for later use in spectrum optimizations. Finally, also the dose-depth curves of these simulations will be compared to measurements, executed by Ibrahim [49].

##### Position of ridge filter

The position of the ridge filter is not mentioned in the report describing the ridge filter measurements [49]. Therefore, first some simulations are done to validate that the exact position of the ridge filter does not affect the results significantly. In Figure 31, the results of these simulations are given. The curves in the graph are normalized such that the area under the curve is 1.

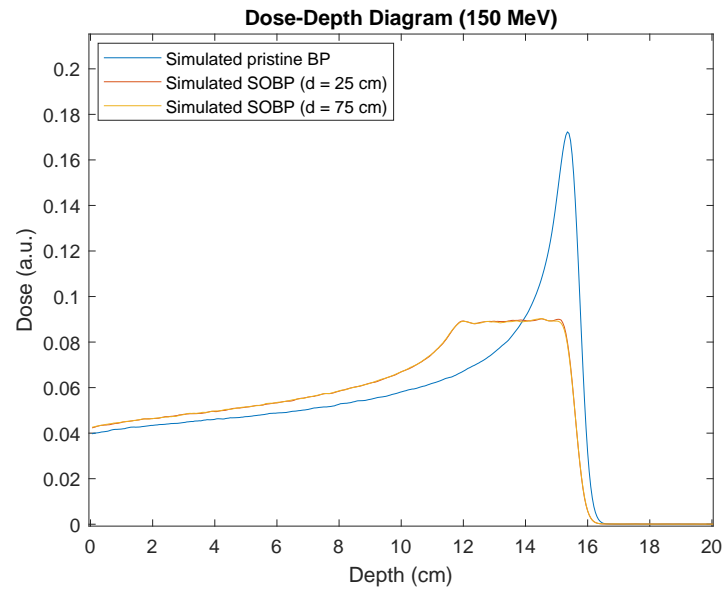


Figure 31: TOPAS simulations of a pristine Bragg peak and two TOPAS runs with a ridge filter. The blue curve shows the result of a simulation setup without a ridge filter, the red curve shows the result for a setup with a ridge filter at 24.7 cm from the exit window and the yellow curve shows the result for the ridge filter placed 74.7 cm from the exit window. All curves are normalized such that the area under the curve is 1. TOPAS simulation of the beam is done with an initial Gaussian energy distribution with a mean energy of 149.9 MeV and an energy spread of 0.75% of this value. The depth is given in cm.

The difference between the two curves with ridge filter is less than 1% for all depths. Thus, the difference is negligible and the ridge filter is placed 74.7 cm from the exit window.

### Energy spectra

The following energy spectrum before the ridge filter (9.7 cm from the exit window) and after the ridge filter (90.7 cm from the exit window) are generated.

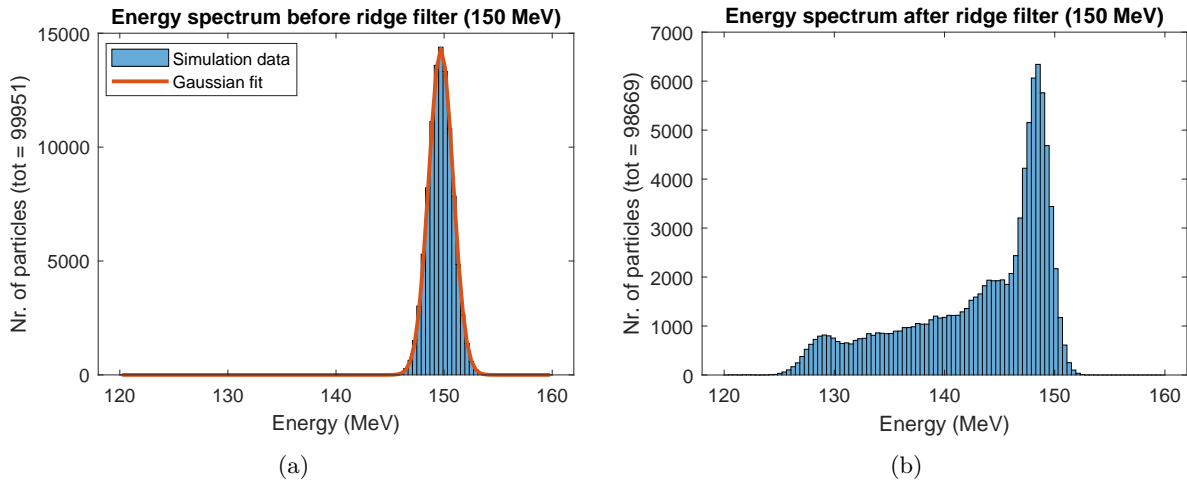


Figure 32: Energy spectra for a beam with a nominal mean energy of 149.9 MeV and an energy spread 0.75% of that value. In (a) the energy spectrum of the 150 MeV beam before the ridge filter with a Gaussian fit is shown and in (b) the energy spectrum after the ridge filter is shown.

It is visible in Figure 32a that the energy spectrum before the ridge filter indeed has a Gaussian distribution.

### Comparison with measurements

For several energies, the dose-depth profile of a proton beam going through a ridge filter is measured. Below the results for a nominal beam energy of 150 MeV is given.

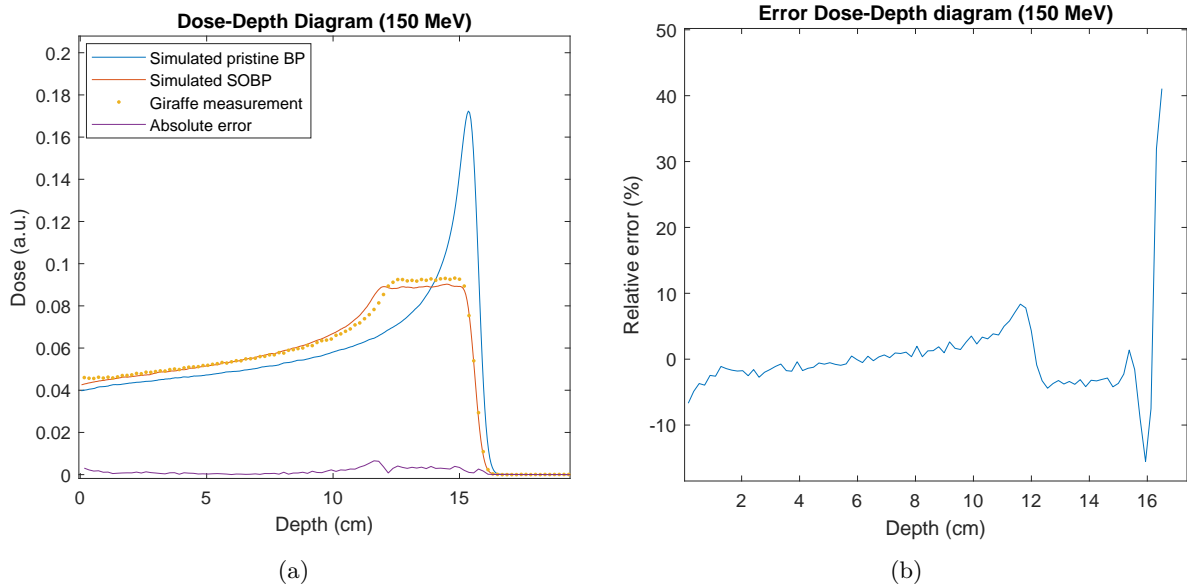


Figure 33: Comparison of measurements and simulations of a ridge filter beam. In (a) the dose-depth curves of a ridge filter beam with nominal energy of 150 MeV measured (yellow dots) and simulated (red) are given and the absolute error between them (purple). Also the pristine Bragg peak simulation is given (blue). In (b) the relative error of the SOBP simulation is given. The depth in both graphs is given in cm and the error in %.

The absolute mean relative error from 0.0 cm up to 10 cm is 1.6%, while from 10 cm depth to 15.97 cm (the depth where the measurement dose is 10% of its maximal value) the absolute mean relative error is 4.94%.

## 4.2 Validation of SOBP-database

In this section, the preparation for and generation of the SOBP-database are validated. In the preparations for the database generation the energy degradation and energy spread shift between the nominal and the phase plane are shown. Furthermore, SOBP-runs for several energies are shown. The validation of the database is done in two steps. First, dose-depth curves for a base energy implemented in a TOPAS simulation are verified. Secondly, the results for an interpolated energy will be analysed.

### 4.2.1 Preparation of the database generation

To approximate the phase space energy spectra after the ridge filter as sums of weighted Gaussians representing pencil beams, first the phase plane energies and energy spreads corresponding to the HollandPTC beam model need to be determined. For all the 19 base energies (every 10 MeV from 70 MeV up to 250 MeV) not only the energy spectrum of the SOBP-simulation is scored, but also the energy spectrum of a pristine Bragg peak simulation. Using these last energy spectra, the energy degradation and the evolution of the energy spread are determined for the base energies. The phase plane energies and spreads of the HollandPTC proton beams are then determined by interpolation.

#### Energy degradation

In Figure 34, the HollandPTC phase plane energies are validated using two different sets of simulations, one with  $10^5$  particles and the other with  $10^6$  particles.

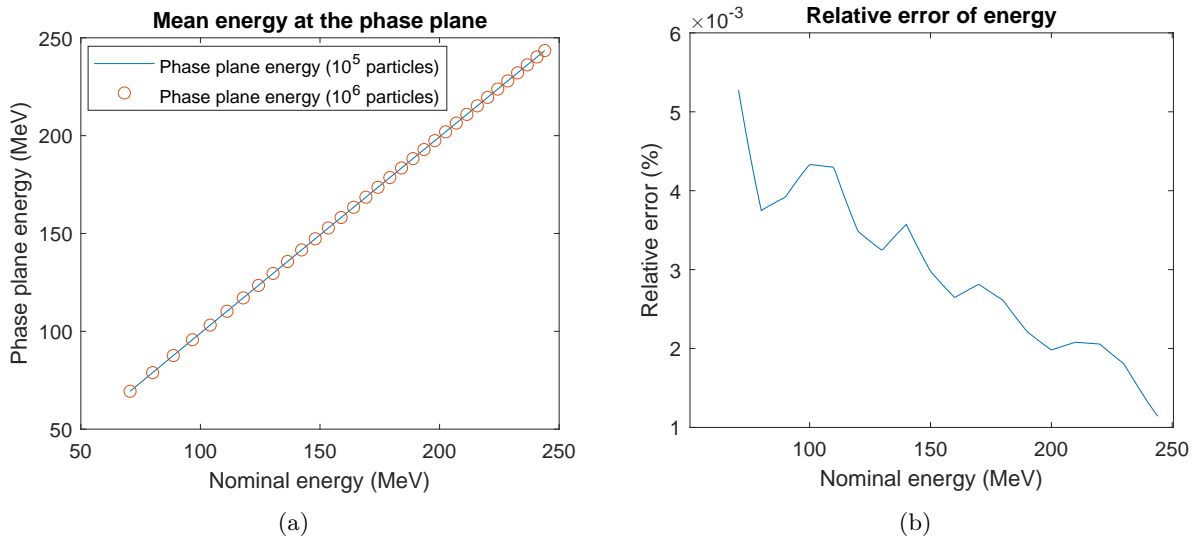


Figure 34: Validation of the HollandPTC phase plane energies. In (a), the HollandPTC phase plane energies derived from simulations with  $10^5$  particles (line) and simulations with  $10^6$  particles (circles) are shown. The relative error between these two line is given in (b). The energies are given in MeV and the relative errors in %.

The mean error in the phase plane energy between the run with  $10^5$  particles and  $10^6$  particles is 0.0027%. This error is negligible in the simulations.

### Energy spread change

The calculated phase plane energy spreads for the same simulation sets are given in Figure 35.

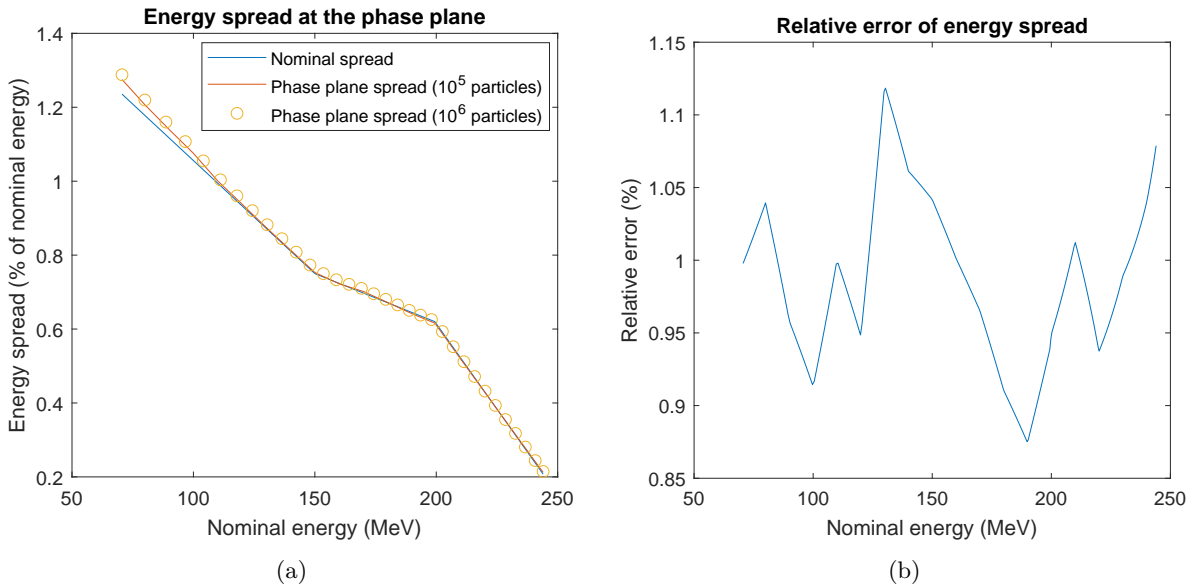


Figure 35: Validation of the HollandPTC phase plane energy spreads. In (a), the nominal HollandPTC energy spreads (blue line), the HollandPTC phase plane energy spreads derived from simulations with  $10^5$  particles (red line) and from simulations with  $10^6$  particles (circles) are shown. The relative error between the phase plane energy spread lines is given in (b). The energies are given in MeV, the spreads in % of the corresponding mean energy and the relative errors in %.

The mean error in the phase plane energy spread between the run with  $10^5$  particles and  $10^6$  particles is 0.98%. This difference is less than 1% and can therefore be neglected.

### SOBP-energy range

The SOBP-dose-depth profiles of some base energies are given in Figure 36.

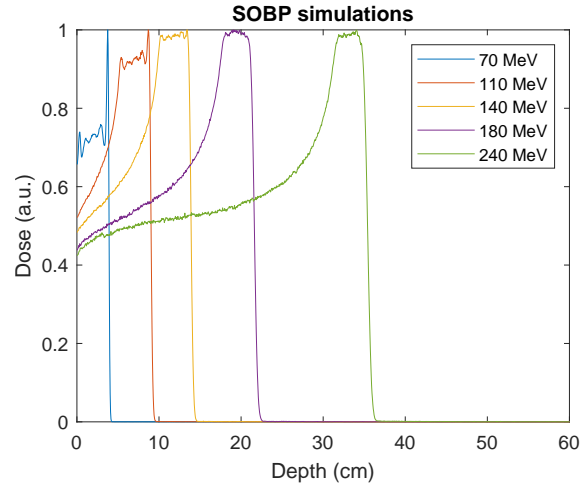


Figure 36: Integral dose-depth curves for TOPAS ridge filter simulations of a beam with a Gaussian energy distribution with different mean nominal energies and energy spreads. The ridge filter is implemented using the 3D CAD-file from GSI. The depth is given in cm.

As can be seen, for the lower energies the homogeneity of the SOBP decreases. In Figure 37, the energy spectrum for a ridge filter run with nominal energy of 100 MeV and of 110 MeV is shown.

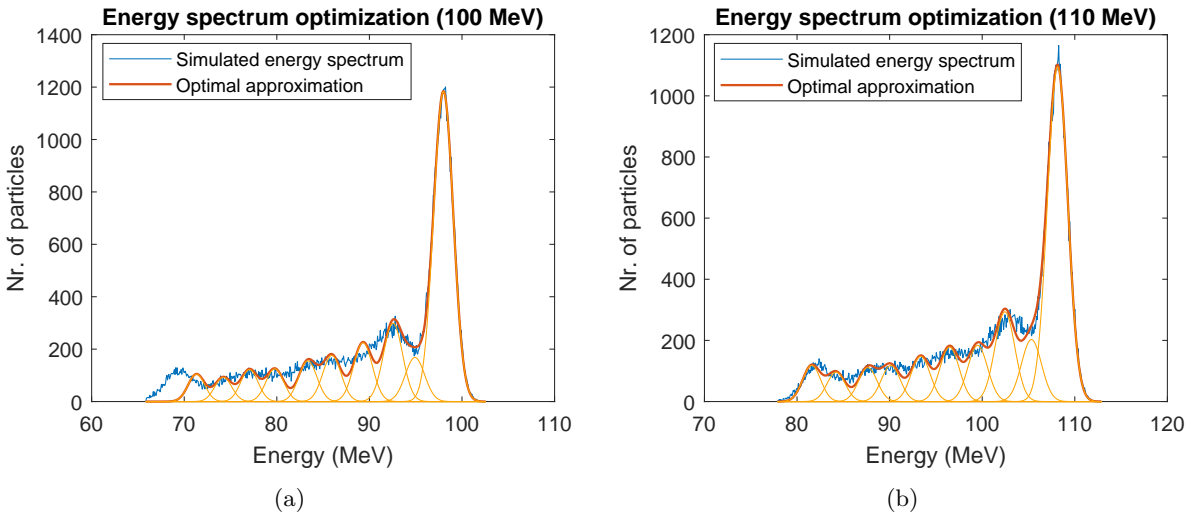


Figure 37: Energy spectra resulting from ridge filter proton beam simulations with their optimal energy spectrum approximation. (a) shows the results for a TOPAS simulation with a nominal energy of 100 MeV (blue) with the weighted superposition (red) of individual pencil beam energy distributions (yellow) is shown. In (b) the same results are shown for a simulation with a nominal energy of 110 MeV.

For the 100 MeV ridge filter run, the energy spectrum cannot be approximated well using the energies in the HollandPTC database. The pencil beams that would be needed are below the lowest HollandPTC energy. Therefore, the SOBP-database will only contain nominal SOBP-energies between 110 MeV and 244 MeV.

### 4.2.2 Validation of simulated data

To confirm that the Bragg peak energies and weights resulting from energy spectrum optimizations do represent the SOBP-beam well, the results for the 180 MeV simulations and optimization are given. 180 MeV is chosen as it is in the middle of the SOBP-database energy range.

In Figure 38, the scored energy spectrum of a TOPAS run with mean energy of 180 MeV is given with its optimal approximation.

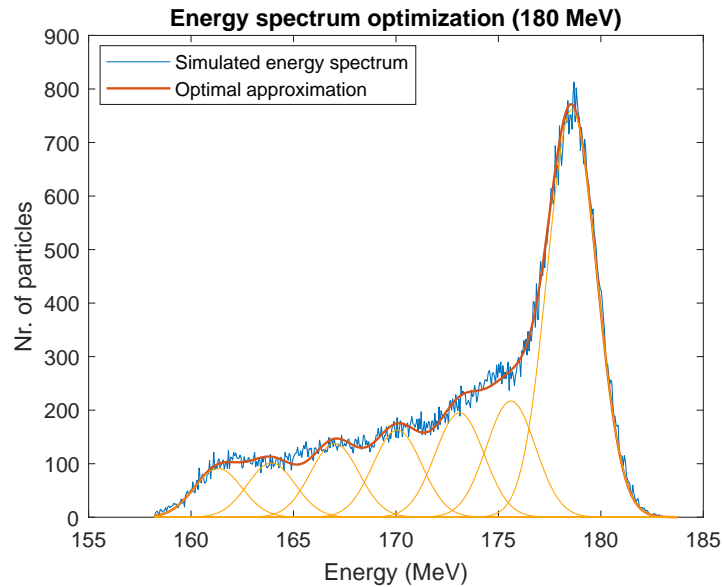


Figure 38: Energy spectrum resulting from a ridge filter proton beam simulation with its optimal energy spectrum approximation. The result for the TOPAS simulation with a nominal energy of 180 MeV is given (blue), with the weighted superposition (red) of individual pencil beam energy distributions (yellow).

The optimal mean beam energies from the optimization result shown above and their corresponding energy spreads are implemented in TOPAS. The resulting dose-depth curves are scored and summed up, taking the weight of each pencil beam into account. The resulting dose-depth curve with the directly scored ridge filter dose-depth curve are shown in Figure 39, with in Figure 39b the relative error between the curves.

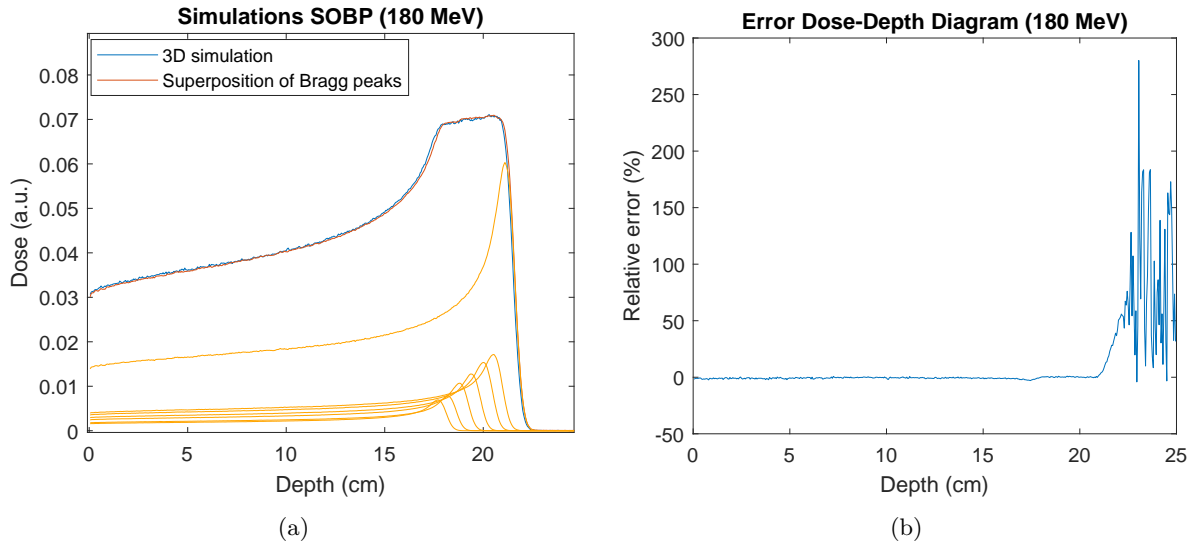


Figure 39: Dose-depth curve resulting from a direct ridge filter proton beam simulation with the superposition of the dose-depth curves from optimized beam energies and beam weights. In (a) the results for the direct TOPAS simulation, with a nominal energy of 180 MeV (blue) is given, with the weighted superposition (red) of individual Bragg peak dose-depth curves (yellow). (b) shows the relative error between the direct simulation result and the optimization result. The depth in both graphs is given in cm and the error in %.

The absolute mean relative error for the depth up to 21.94 cm is 1.59%. At 21.94 cm, the simulated SOBP dose-depth curve is at 10% of its maximum dose value.

#### 4.2.3 Validation of interpolated data

The validation for the interpolated data in the database is done in the same way as for the simulated base energies, but with an extra check. Not only the phase plane implementation of the optimal pencil beams is considered, but also the nominal plane implementation (with the from phase plane to nominal plane converted energies and energy spectra). The nominal ridge filter energy for which the interpolated data is validated is 186.98 MeV.

In Figure 40, the scored energy spectrum of a TOPAS run with mean energy of 180 MeV is given with its optimal approximation.

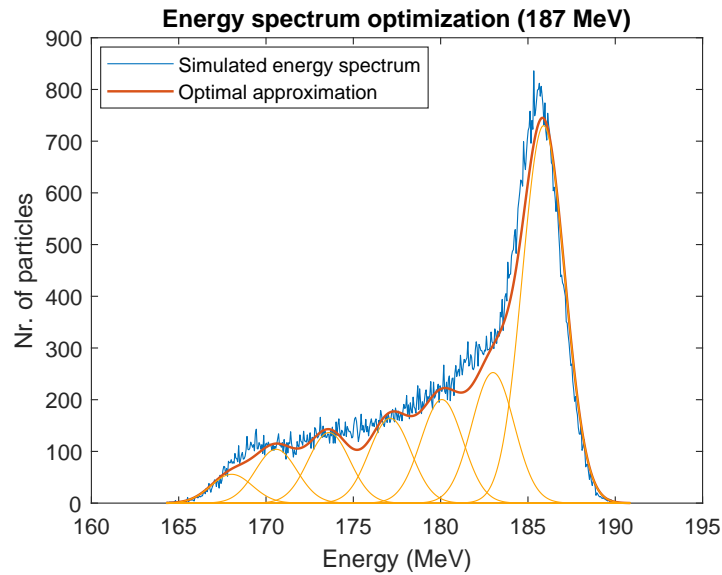


Figure 40: Energy spectrum resulting from a ridge filter proton beam simulation with its optimal energy spectrum approximation. The result for the TOPAS simulation with a nominal energy of 180 MeV is given (blue), with the weighted superposition (red) of individual pencil beam energy distributions (yellow).

The optimal mean beam energies from the optimization result shown above and their corresponding energy spreads are implemented in TOPAS. The resulting dose-depth curves are scored and summed up, taking the weight of each pencil beam into account. The resulting dose-depth curve with the directly scored ridge filter dose-depth curve are shown in Figure 41, with in Figure 41b the relative error between the curves.

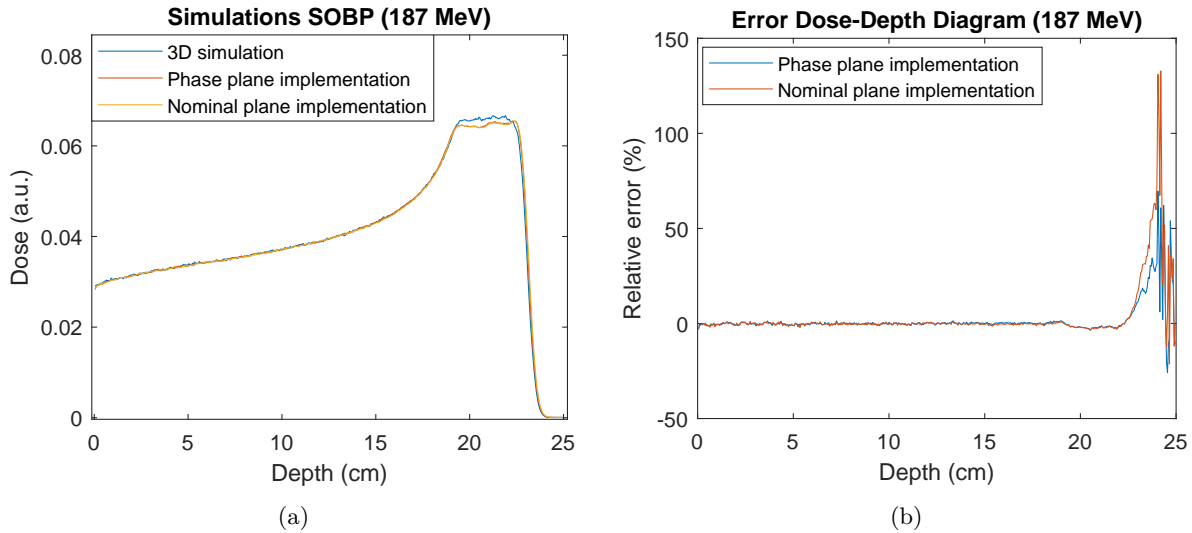


Figure 41: Dose-depth curve resulting from a direct ridge filter proton beam simulation with the superposition of the dose-depth curves from optimized beam energies and beam weights. In (a) the results for the direct TOPAS simulation, with a nominal energy of 180 MeV (blue) is given, with the weighted superposition (red) of individual Bragg peak dose-depth curves (yellow). (b) shows the relative error between the direct simulation result and the optimization result. The depth in both plots is given in cm and the error in %.

The absolute mean relative error for the depth up to 23.53 cm for the nominal and phase plane implementation are 1.53% and 1.15% respectively. At 23.53 cm, the simulated SOBP dose-depth curve is at 10% of its maximum dose value. The mean relative difference between the phase plane implementation and the nominal plane implementation for the depth up to 23.53 cm is 0.60%.

### 4.3 Erasmus-iCycle optimizations

The SOBP-database is implemented in iCycle to generate optimized treatment plans with SOBP-beams. The wishlist with the dose constraints and objectives that is used is given in Appendix A.2. Erasmus-iCycle treatment plans are generated for three patients with a brain tumour. In this chapter, the results of a conventional iCycle run, without the SOBP-database implementation, and SOBP-runs are given for the first patient. The results for the second and third patient can be found in Appendix A.5 and Appendix A.6.

#### 4.3.1 Conventional run

In the conventional iCycle runs, not SOBP-beams, but pristine Bragg peaks are commonly used in the dose optimization. For these runs the requirement of one beam per lateral position does not apply. Furthermore, the energy spacing between two consecutive spots with the same lateral position is 3 mm.

The optimal plan consists of 119 pencil beams in the first beam direction ( $240^\circ$ ) and 146 pencil beams in the second beam direction ( $300^\circ$ ). Figure 42 shows for both beam directions the lateral positions for which pristine Bragg peak beams would fall within the tumour (the spots in the original beamlist), and the lateral positions used in the optimized treatment plan.

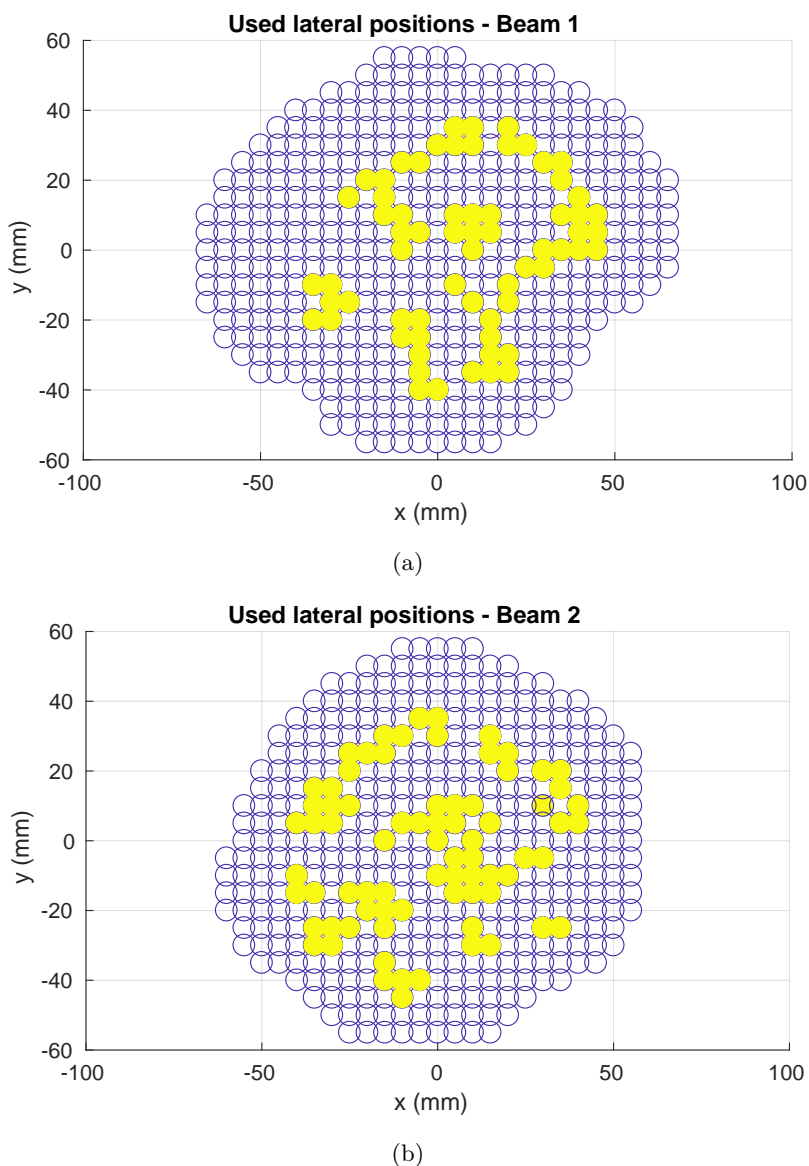


Figure 42: Lateral position of pencil beams used in the optimized treatment plan on a bixel grid. The open blue circles are the lateral positions of the spots in the original beamlist, the filled yellow circles are the used pencil beam positions in the conventional iCycle optimization.

The resulting dose distributions in the patient are shown in Figure 43. The results for the total dose and the doses of both beams separately are shown in the transverse planes that contain the isocenter, that is at a CT-offset of -6 mm.

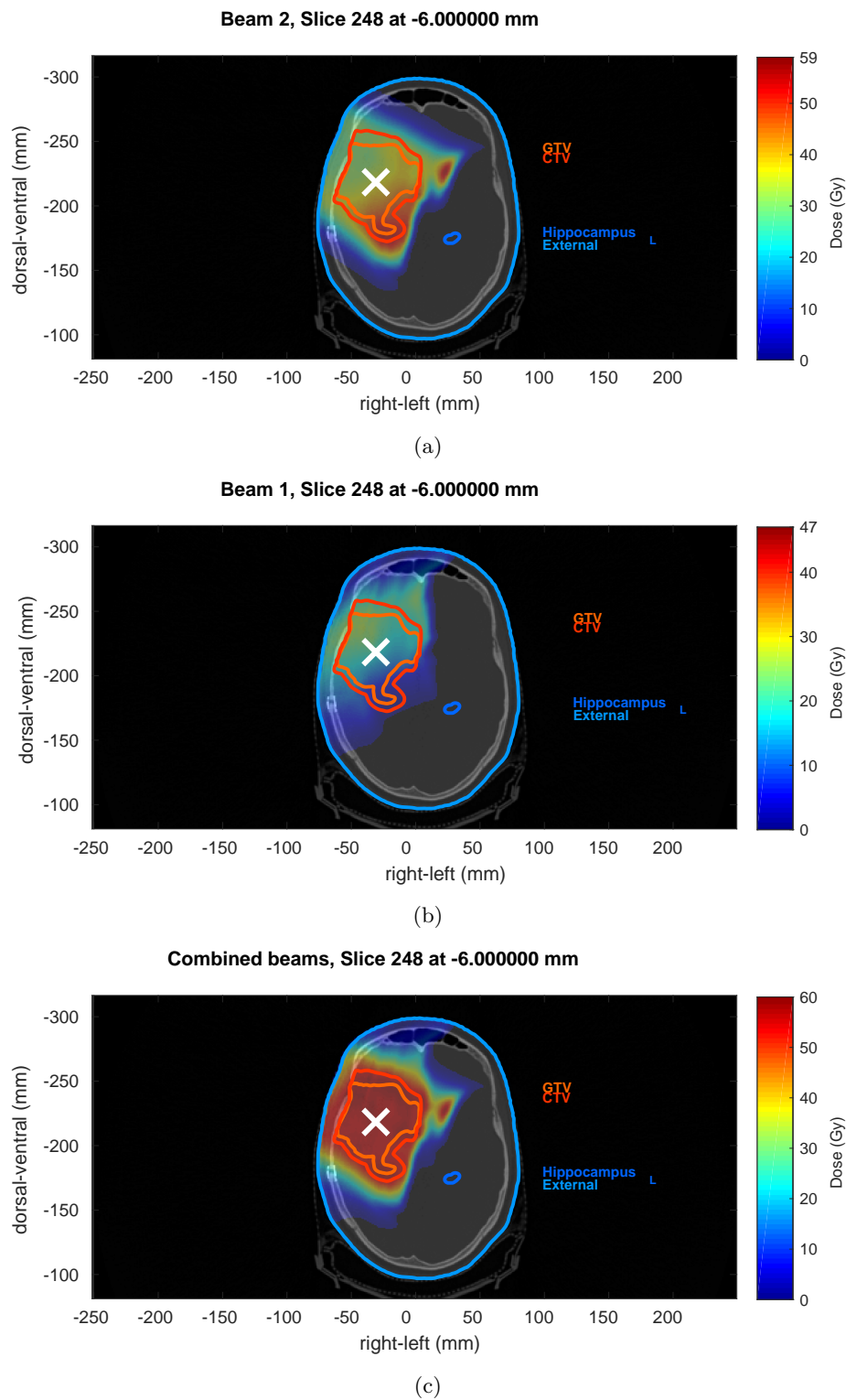


Figure 43: The dose distribution in Patient 1 for a conventional treatment plan optimization in iCycle using 2 beam directions ( $240^\circ$  and  $300^\circ$ ). In (a) the dose of both beams combined is given. In (b) and (c) the dose distributions of, respectively, beam 1, at  $240^\circ$ , and beam 2, at  $300^\circ$ , are given. The white 'x' denotes the position of the isocenter. The target structures (GTV and CTV), the organ at risk (hippocampus-left) and the external structure at this depth are indicated.

To quantify the treatment plan and give a measure for qualification, the dose-volume histograms of the optimization are given, see Figure 44. In these histograms, only two structures are considered, the CTV and the brain-CTV for the combined beams and both beams separately.

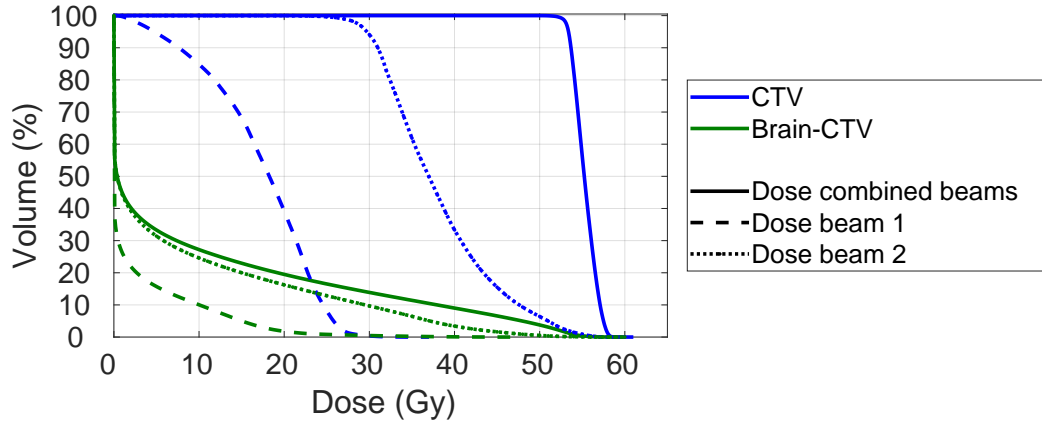


Figure 44: Dose-volume histogram showing the dose in the tumour (blue) and the dose in the healthy tissue (green) for the combined beams (continuous), the first beam, at  $240^\circ$  (dashed) and the second beam, at  $300^\circ$  (dotted).

Erasmus-iCycle took 384.58 minutes to optimize the treatment plan for this patient.

#### 4.3.2 Initial run

In the initial implementation of the code and SOBPs-database in iCycle, only SOBPs-beams with nominal energy higher than 130 MeV have been used. Furthermore, instead of an energy spacing of 3 mm, the energy spacing is set to 10 mm. The spread-out regions of the SOBPs in water are larger than 10 mm.

The optimal plan consists of 37 SOBPs pencil beams in the first beam direction ( $240^\circ$ ) and 48 SOBPs pencil beams in the second beam direction ( $300^\circ$ ). Figure 45 shows for both beam directions the lateral positions for which pristine Bragg peak beams would fall within the tumour (the spots in the original beamlist), and the optimal lateral SOBPs-locations with their nominal energy. No degrader has been used for this plan optimization.

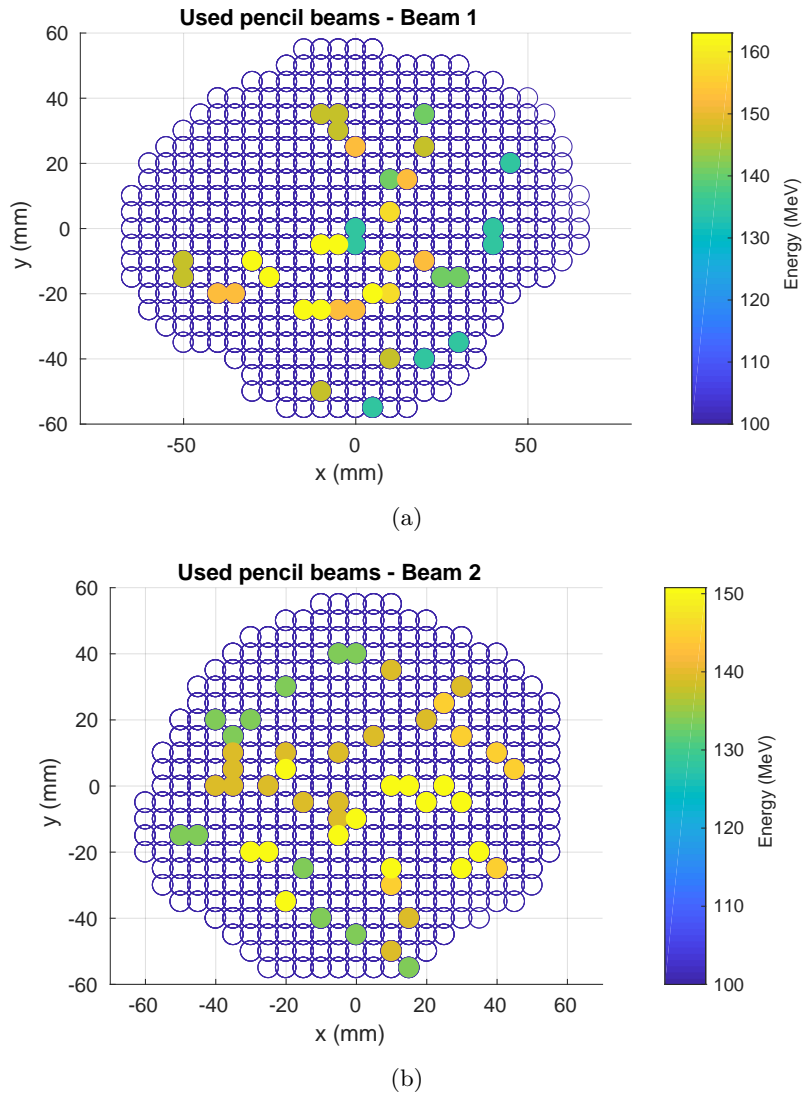


Figure 45: SOBP pencil beams used in the optimized treatment plan on a bixel grid. The open blue circles are the lateral positions of the spots in the original beamlist, the filled circles are the used pencil beams in the optimized SOBP-plan. The colour of the circles denotes the nominal energy of that pencil beam.

The resulting dose distributions in the patient are shown in Figure 46. The results for the total dose and the doses of both beams separately are shown in the transverse planes that contain the isocenter, that is at a CT-offset of -6 mm.

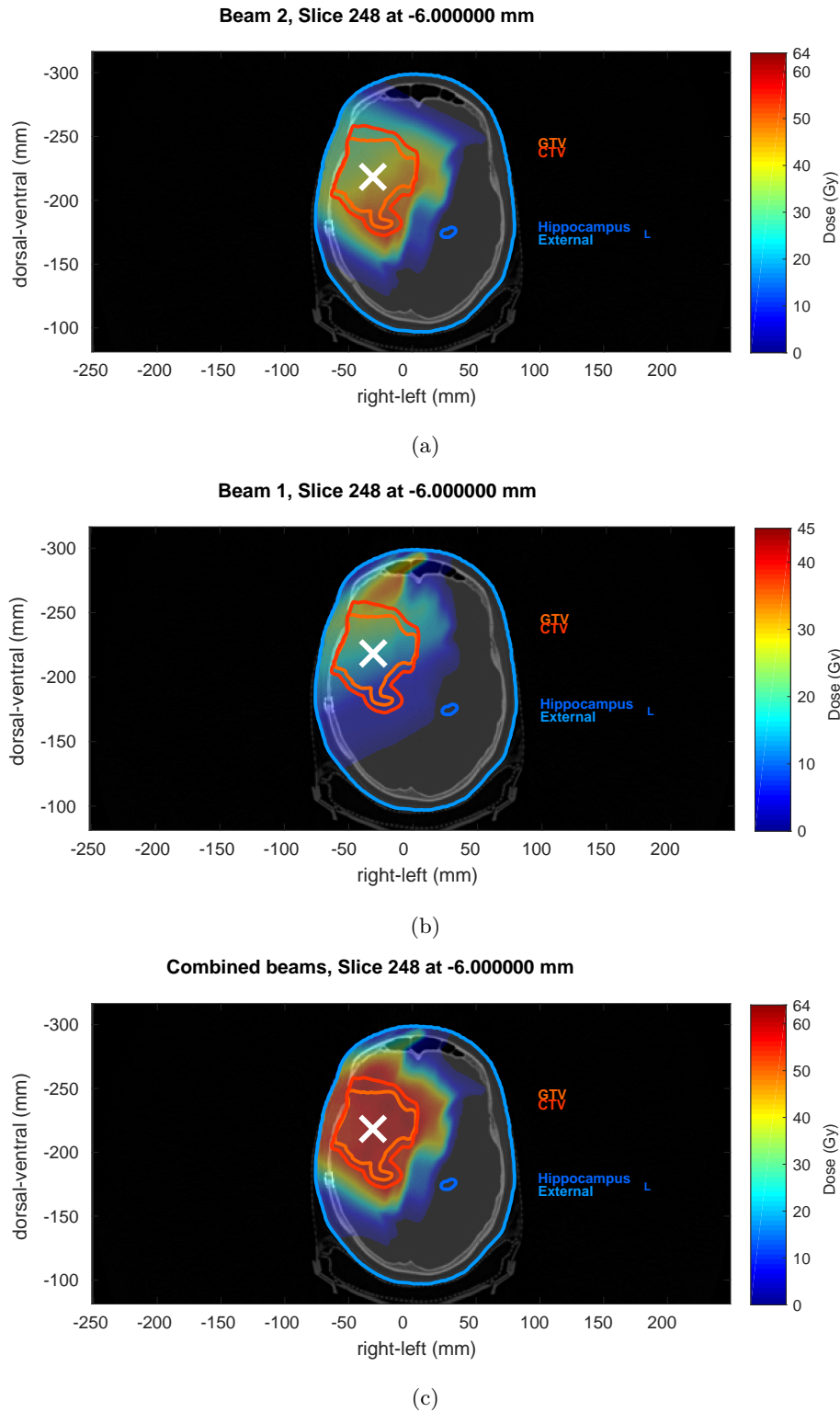


Figure 46: The dose distribution in Patient 1 for a treatment plan optimization in iCycle with SOBP-database using 2 beam directions ( $240^\circ$  and  $300^\circ$ ). In (a) the dose of both beams combined is given. In (b) and (c) the dose distributions of, respectively, beam 1, at  $240^\circ$ , and beam 2, at  $300^\circ$ , are given. The white 'x' denotes the position of the isocenter. The target structures (GTV and CTV), the organ at risk (hippocampus-left) and the external structure at this depth are indicated.

To quantify the treatment plan and provide a quality measure, the dose-volume histograms of the SOBP-optimization are given, see Figure 47. In these histograms, only two structures are considered, the CTV and the brain-CTV for the combined beams and both beams separately.

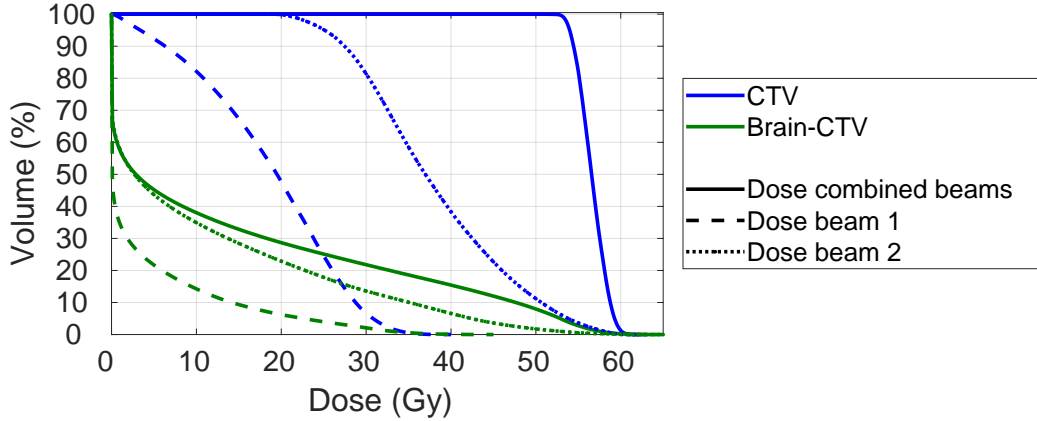


Figure 47: Dose-volume histogram showing the dose in the tumour (blue) and the dose in the healthy tissue (green) for the combined beams (continuous), the first beam, at  $240^\circ$  (dashed) and the second beam, at  $300^\circ$  (dotted).

Erasmus-iCycle took 10.98 minutes to optimize the treatment plan for this patient and in the optimized plan were no SOBP pencil beams with the same lateral position.

#### 4.3.3 Final runs

After a final calculation of the SOBP-database, with energies from 110 MeV and up, new results are calculated. In order to be able to compare these results to the previous results also a new database with energies from 130 MeV and up is used. Another variable that is taken into account is whether a static degrader is present or not.

For all patients, four optimizations are done:

- an optimization with a database upward of 110 MeV with a degrader;
- an optimization with a database upward of 110 MeV without a degrader;
- an optimization with a database upward of 130 MeV with a degrader, and
- an optimization with a database upward of 130 MeV without a degrader.

Again, the results for Patient 2 and 3 can be found in Appendix A.5 and Appendix A.6.

For Patient 1, the characteristics of the four runs are given in Table 5. Sometimes the optimizer did not converge to a feasible optimal plan, besides that also sometimes while optimizing an error occurred in the MU-objective optimization in the non-convex, non-linear optimizer. The exact cause of the error is still unclear. Other users of iCycle have also encountered this error [55].

Table 5: Characteristics of four final optimization runs for Patient 1. For each run the following information is given: the used database (first column); whether a degrader was used (second column); whether an error occurred in the optimization of the MU-objective (third column); whether the final plan was feasible (fourth column); how many SOBP pencil beams were deleted, in the case of lateral positions being used for multiple SOBP pencil beams (fifth column); the final number of SOBP pencil beams (sixth column), and the total optimization time,  $t_{opt}$ , in minutes (last column).

Run	Database	Degr.	MU error	Feasible	$N_{deleted}$	$N_{final}$	$t_{opt}$ (min)
1.	110 MeV	-	-	x	16	121	40.18
2.	110 MeV	x	-	x	65	213	38.88
3.	130 MeV	-	x	-	-	-	17.01
4.	130 MeV	x	-	x	27	179	20.50

To quantify the treatment plan and provide a quality measure, the dose-volume histograms of the SOBP-run are given, see Figure 48. In these histograms, only two structures, the CTV and the brain-CTV, are considered for the three plans with a feasible solution. Also a result for the infeasible run is shown. This is done by deleting all low-weight SOBP pencil beams from the final beamlist and calculating the dose for the resulting beamlist. A SOBP pencil beam is considered to low weight when the weight is lower than 0.0032 gigaprotons.

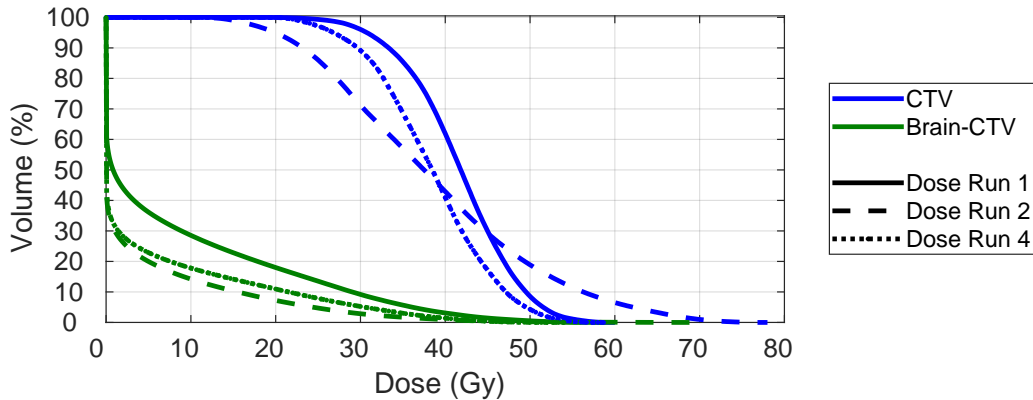


Figure 48: Dose-volume histogram showing the dose in the tumour (blue) and the dose in the healthy tissue (green) for Run 1 (continuous), Run 2 (dashed) and Run 4 (dotted) from Table 5.

For comparing treatment treatment plans, scaled dose-volume histograms are calculated. The histograms of all runs (the conventional run, the initial run and the final runs) are scaled such that 98% of the target volume (PTV or, when that structure is not present, CTV) receives at least 95% of the prescribed dose, see Figure 49. 95% of the prescribed dose of 54 Gy is 51.3 Gy.

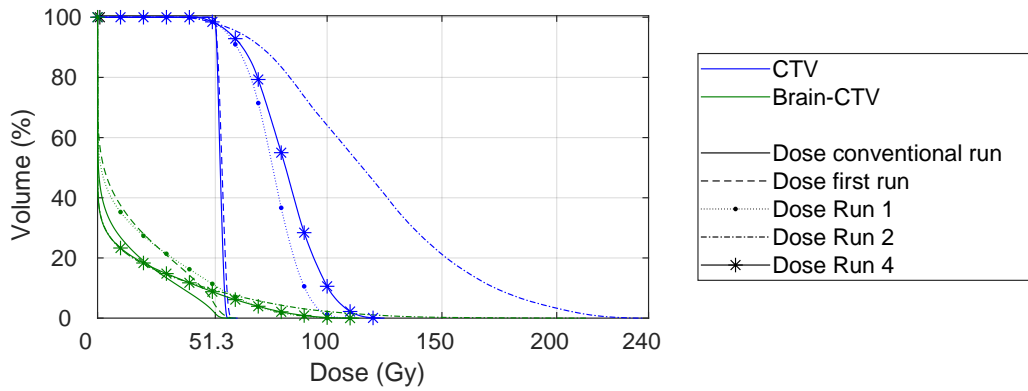


Figure 49: Dose-volume histogram showing the dose in the tumour (blue) and the dose in the healthy tissue (green) for Run 1 (continuous), Run 2 (dashed) and Run 4 (dotted) from Table 5.

The homogeneity indices, mean dose to healthy tissue and required FLASH enhancement ratio (FER) for the different runs are given in the table below.

Table 6: The homogeneity indices (HIs), mean doses,  $D_{mean}$ , to healthy tissue, and required FERs of the optimized treatment plans shown in Figure 49 are given. The HIs are calculated using Equation 10.

Optimization run	HI (%)	$D_{mean}$ healthy tissue (Gy)	Req. FER
Conventional	8.92	9.35	-
Initial	11.1	13.4	1.44
1.	86.2	14.9	1.60
2.	289	12.0	1.29
4.	110	10.6	1.14

## 5 Discussion

The results and their implications of this research are discussed in the chapter below. The chapter is divided in five main sections: the first regarding the TOPAS simulations; the second evaluating the energy spectrum optimization and SOBP-database generation; in the third the iCycle implementation and results are discussed; as fourth, the possible clinical significance and implementation of this research is considered, and finally, the implications and recommendations of this research for future research are elaborated.

### 5.1 Validation of TOPAS simulations

The SOBP-database that is implemented in iCycle is based on Monte Carlo simulations of the HollandPTC R&D beamline. To be able to validate the accuracy of the database, first the results of the TOPAS simulations need to be assessed. In this section the particle population of the TOPAS simulations, the beam modelling (using the Bragg peak results), and the ridge filter results are discussed. After that the setup of the TOPAS simulations is regarded, as is the physics of the simulations.

#### 5.1.1 Particle population

Accuracy of Monte Carlo particle transport simulations depends on several factors. The first to consider is the number of particles taken into account. Figures 27 and 28 as well as Figures 34 and 35 show that the chosen number of particles,  $10^5$ , is enough for the Monte Carlo simulations of the beam. In Figures 27 and 28, the mean relative difference between the curves of the  $10^5$  particles simulation and the  $10^6$  particles simulations is smaller than 1% for depths up to the  $d_{10}$ -value. The  $d_{10}$  is the depth at which the measurement has a dose value of 10% of its maximal dose value. Figures 34 and 35 show that the mean relative difference between the mean energies and energy spreads of the  $10^5$  particles simulation and the  $10^6$  particles simulation are also negligible. The difference between the energy spreads is slightly less than 1% and the difference between the mean energies is even as small as 0.0027%.

Because of the small difference in integral dose-depth curve result (the absolute relative error is less than 1%), the particle population is set to  $10^5$  particles. In view of the small difference between the simulations with  $10^5$  and  $10^6$  particles, it can be concluded that if there are obvious differences between TOPAS simulations and measurements, the particle population is probably not the main cause for those.

#### 5.1.2 Bragg peak results

The beam is modelled by specifying the beam parameters in TOPAS. The beam parameters used are given in Table 2 and 3 in Chapter 3.1.

To validate whether the base TOPAS implementation, without a ridge filter, correctly simulates the HollandPTC R&D beamline, it is important to consider the Bragg peak simulations. Figures 29 and 30 show that the results of the beam simulations resemble the Bragg peak measurements very well, both for the 150 MeV case as for the 240 MeV case. The absolute error is so small that, only regarding that, the conclusion could be drawn that this error is insignificant. Looking at the relative error for depths up to the  $d_{10}$ -depth it can be seen that indeed for these depths the error is smaller than 1% (150 MeV simulation: 0.85%, 240 MeV simulation: 0.89%) and is, therefore, negligible. For depths larger than the  $d_{10}$ -value, the error between simulations and measurements quickly rises. This is due to the fact that the measurement dose at these depths becomes very small. So, even if the absolute differences are small, the relative error might blow up. This is also the case for the Bragg peak simulations. Since in patient treatment planning the absolute dose of beams will be used, these large relative errors can

be disregarded.

It can be concluded that the values taken from the report of Rituerto [48] for the beam characteristics lead to good results for the integral dose-depth curves. Furthermore, what is important to keep in mind is that for the validation of the simulations, the integral dose-depth curves are used. Thus, the exact lateral profile of the dose is not verified.

### 5.1.3 Ridge filter results

When implementing the ridge filter, it is clear that the dose-depth curves generated do show a spreading of the Bragg peak compared to a pristine Bragg peak simulation, as can be seen in Figure 31. The same figure shows that within a certain range, the precise position of the ridge filter has little influence on the results. The difference between the result for a TOPAS simulation with a ridge filter 24.7 cm from the exit window or 74.7 cm from the exit window is less than 1%. To check whether the results are correct, a simulation is compared to a measurement, Figure 33. In the entrance area, from a depth of 1.5 cm up to 10 cm the SOBP-simulation and -measurement seem to be in good agreement, with small relative errors, Figure 33b. Also the range of the simulation and the measurement coincides. There are, however, some clear differences for depths lower than 1.5 cm and around the spread-out region. Partially, the error may be due to the way in which the simulations and the measurement are normalized. All curves are scaled such that the area under the curve is 1.0. Changing the scaling, however, will not solve the difference.

In the following two sections on the physics of the simulations and the simulation setup some possible reasons for these differences will be visited. Though the results from the SOBP-simulations are not in complete agreement with the measurement data, they are used in the generation of the SOBP-database. The reason for this is that the simulated SOBP-dose-depth profile is coherent with what an SOBP-dose-depth curve is expected to look like. Furthermore, only a limited number of SOBP-measurements were available. Therefore, simulated data was used.

### 5.1.4 Simulation setup

In the simulations, only a few elements are taken into account: the exit window, the water phantom/scorer and possibly the ridge filter, see Figure 18.

The **exit window** is taken from the research of Rituerto [48] and is assumed to be modelled correctly.

The **water phantom** is implemented as a cube of water with a scoring element. In the actual Bragg peak measurements, the MP3-M water tank is not merely a cube of water, it has PMMA sides and a Bragg peak chamber and X-ray therapy monitor chamber are implemented. In the data analysis of the TOPAS simulations, these elements are taken into account by implementing the water equivalent thicknesses of the materials. However, there is some uncertainty in WETs of the materials. These values are energy dependent and their exact WETs at each beam energy are not documented clearly. Therefore this energy dependence is not taken into account for energies other than 150 MeV and 240 MeV and for those energies there is also some uncertainty in the exact values.

Besides this, in the SOBP-simulations, the water phantom is also used, while in the SOBP-measurements the Giraffe detector is used. The Giraffe detector's main purpose is to determine the range of a proton beam in water and not the acquisition of dose-depth curves [52]. Some differences between the simulations and the measurements may be due to that fact. But this cannot explain the large difference between the SOBP-measurements and SOBP-simulations. An explanation for these large differences may be that the Giraffe detector was probably not aligned correctly with the proton beam [56]. Instead of the beam falling on the detector with an angle of 90° angle, the angle might have been slightly off.

Also, though the range is compensated using the WETs, build up in the entrance area of the dose-depth curves due to scatter or electron build-up in the measurement materials (the detectors and/or the PMMA wall of the water tank) is not taken into account. The Monte Carlo code does not simulate this scatter, since the materials are not implemented. This may be an explanation for the small difference between the SOBP-simulation and -measurement in Figure 33.

The **scorers** in the simulations are implemented as virtual, cylindrical elements in the water tank. These scoring elements can score the dose-depth curve or the phase space without physically interacting with the simulation. The dimensions, and especially the radius, of these scorers influence the resulting dose-depth curve. If the radius of the scorer is taken too large, more scattered secondaries are detected and thus a dose build-up occurs in the entrance area. On the other hand, if the radius is too small, you lose secondaries in the entrance area. In the simulations, the radii of the detectors used in the experiments are used (for the Bragg peak measurements: the TM34070 Bragg Peak Chamber, and for the SOBP-measurements: the Giraffe detector). An increase or decrease of a few millimetres in the radius does already impact the dose-depth curve. This might also be a contributing factor in the differences between the SOBP-simulations and the SOBP-measurements.

For the SOBP-measurements TOPAS has taken into account the energy degradation and scattering due to the **ridge filter**. Small deficiencies may occur because the 3D-file that is used in TOPAS has very small structures. This is taken into account by lowering the step size in this element. However, in the TOPAS-runs with the ridge filter, though a relatively small portion, more histories are interrupted than in the Bragg peak simulations. A history is interrupted when a rare Geant4 error occurs. The impact of these interrupted histories is minor since less than 50 of the 100.000 particle histories are interrupted.

### 5.1.5 Physics of the simulations

The TOPAS simulations take into account many physical processes, as discussed in Chapter 3.1. Inaccuracies in the simulations may be caused by TOPAS using default values for material properties and physical properties such as the ionization potentials of the materials in the simulations. Besides this, TOPAS does take into account the physical processes involving the generated secondaries (the halo of the proton beam), high-energy nuclear reactions and range straggling.

## 5.2 SOBP-database generation

Using SOBP-simulations from TOPAS, the SOBP-database is generated.

### 5.2.1 Phase plane properties

Before calculating the database, first some beam properties, the mean energy in the phase plane and the energy spread in the phase plane, are explored. In Figure 34, the simulated mean energy in the phase plane is given. The curve of phase plane energies seems to be linear. This is, however, not exactly the case. Energy degradation is energy dependent, so for beams with different nominal energies a different amount of energy is transferred when travelling the same distance. Since the differences in energy transfer are so small, this is not visible in Figure 34.

Besides the mean energy, also the simulated phase plane energy spread is considered. Figure 35 shows the nominal energy spread for different nominal energies and the phase plane energy spread for these nominal energies. Here, the difference between phase plane spreads for low energies and for high energies is more clear. For lower energies, the energy spread increases more over distance. The kinks in the graphs are due to the fact that the nominal spreads used for the simulations have been interpolated from the results for four energies (70, 150, 200 and 240 MeV) of Rituerto [48].

### 5.2.2 SOBP-database range

The range of the SOBP-database is determined from Figures 36 and 37 as is explained in Section 4.2. For the lower energy, 70 and 110 MeV, SOBP-simulations, Figure 36 shows that the spread-out region is less homogeneous than for the higher energy simulations. This might be due to the fact that the ridge filter is manufactured for use at a certain energy. For another energy, to obtain the same spread-out region, another filter should be manufactured. The simulations imply that this filter can generate a reasonable SOBP for different, but not for all energies. It is also visible in the figure that the spread-out region is smaller for higher energies. This is mainly caused by the energy dependence of the energy transfer. The spreading of the energy in the ridge filter for higher energy beams is lower. It is clear from Figure 37 that the range of the nominal beam energies for which the approximation energies and weights are optimized starts from 110 MeV. The ridge filter energy spectrum of nominal beam energies lower than 110 MeV cannot be approximated by a weighted superposition of available Gaussians. The energies needed for those superpositions are lower than the HollandPTC database allows.

### 5.2.3 Energy spectrum optimization

The problem of approximating the dose-depth curve of a ridge filter simulation with a weighted superposition of Bragg peaks can be addressed in two ways. One way is to directly approximate the ridge filter dose-depth curve with the pencil beam dose-depth curves. Another is to retrieve the energy spectrum of the beam after the ridge filter and approximate this spectrum with Gaussians. In this research the latter option is chosen. Reasons for this are mainly practical. In iCycle, the beamlist that is generated, and where the Bragg peak pencil beams are added, uses the energy of the beam. Thus, it felt natural to use the energy for optimization. Furthermore, information available about the phase plane mean energy and energy spread of the pencil beams is interpolated easier than a dose-depth curve. Ideally, both ways of optimizing would give the same result. However, for these optimizations this is not the case, as can be seen in Appendix A.4. The difference is mainly due to the difference between the simulated energy spectrum and the approximated spectrum. Besides this, the dose-depth curve optimization also tries to minimize the error in the entrance area. Since all beams deposit energy in the entrance area, a lower weight of one Bragg curve can be compensated by a higher weight to another.

In the energy spectrum optimization a distinction is made between lower energies and higher energies. For nominal beam energies from 200 MeV upwards, there is a 2 MeV discretization between the Gaussian mean energies in the optimization, while for the lower energies a 3 MeV discretization is used. Again, as mentioned in the previous paragraphs, this has to do with the energy dependent energy transfer. Using a 3 MeV spacing in the optimization of energy spectra from high energies does not give a good spectrum approximation, see Appendix A.4.

### 5.2.4 Database generation

The validity of the database is checked by considering one simulated nominal energy and one interpolated nominal energy.

For the simulated energy, the optimal phase plane energies are implemented in a TOPAS simulation to obtain their dose-depth curve. The weighted superpositions of these Bragg peaks are compared with the direct simulation of the ridge filter dose-depth curve in Figure 39. The profiles are in good agreement, they almost coincide. For a SOBP-approximation, an absolute mean relative error of 1.59% is acceptable since it allows proof of concept results. With this it is concluded that the database of simulated energies contains adequate beam energies and weights.

The results for an interpolated part of the database are shown in Figures 40 and 41. Figure 40 shows that the largest energy peak in the optimal approximation does not fully cover the peak in the

simulated spectrum. From 180 MeV up till 187 MeV, the approximated curve lies below the simulation. Also for the lower energies there are some areas where the approximation does not resemble the simulation accurately. Looking at the dose-depth curve results of the direct simulation and the optimized Bragg peak implementations, Figure 41, the resulting difference is clear. In the entrance area, the curves nearly coincide, however, at the top of the spread-out region, the direct simulation obviously has higher dose than the approximations. This difference is caused by two factors: 1. the energy discretization of 3 MeV, and 2. the interpolation of the optimal energies. This ‘interpolation’ is done by just shifting the optimal energies of the nearest base energy (every 10 MeV there is a base energy for which the simulations and optimizations are done). This method does not accurately take into account the energy dependence of the energy spectrum. The energy spectrum after the ridge filter is not the same, an energy shift disregarded, for all energies. Improving these interpolated results can be done by 1. refining the energy discretization in the optimization of the spectrum to lower than 3 MeV, or 2. by doing simulations not only every 10 MeV, but every  $x$  MeV, with  $x < 10$ . Due to (computation) time limitations and the fact that the error in the SOBP-region is just around 3%, this is not further implemented in this research. Furthermore, in the dose calculation, iCycle also uses pencil beam data that are interpolated from data of every 10 MeV.

If for a ridge filter energy spectrum the optimal phase plane energies are found, these energies are converted to nominal energies. Since the information for both is available, in Figure 41, the results from nominal plane TOPAS simulations and phase plane TOPAS simulations are given. These different curves are in good agreement with each other. Figure 41b shows that only on the distal edge of the SOBP-curve the error of the phase plane implementation error is less than that of the nominal plane implementation. Differences can be explained by the uncertainty and rounding of the phase plane to nominal plane conversion of the energies, see Section 3.2.3. Since the main differences are only present at depths where the absolute dose is near 0, these differences can be ignored. Thus, the conversion from phase plane to nominal plane is valid.

It can be concluded that the database that is generated does give the energies and weights for relatively good SOBP-approximations. For a proof of concept research, this is sufficient, since the difference in dose-depth curve are relatively small.

### 5.3 Erasmus-iCycle optimizations

In this section, the resulting optimized treatment plans of iCycle are discussed. Chapter 4 only shows the results for Patient 1. Patient 2 and 3 are also taken into consideration in this analysis, their results can be found in Appendix A.5 and Appendix A.6.

It is clear from the results of the iCycle optimizations, the dose-volume histograms, that the implemented extensions and adjustments nearly always imply a degradation of the treatment plan compared to the conventional treatment plan. This is, of course, to be expected, since implementing spread-out Bragg peak beams decreases the flexibility of the optimizer. Instead of being able to set a specific weight, and thus tweak the dose, every 5mm, the weights of different positions are correlated.

#### 5.3.1 Number of pencil beams

Before diving deeper into the dose distribution, it is interesting to look into the number of pencil beams used in the conventional and the SOBP-plans. The hypothesis is that when using SOBP-plans, less SOBP pencil beams are required for covering the tumour than when considering pristine Bragg peak pencil beams. SOBP pencil beams deliver dose to a larger region than Bragg peak pencil beams. When looking at the results for the three patients, it can be observed that for all patients this is the case, all SOBP-plans have less beams than the conventional plan. The amount of decrease is very different. For Patient 1, the initial run has 85 SOBP-beams, much less than the final runs. In con-

trast to that, for Patient 2, the final runs have less beams than the initial run, though the difference is not very large. In Patient 3, one final SOBP-run has significant more beams than the other SOBP-runs.

When looking at which SOBP-runs have more pencil beams, it seems the feasible treatment plans with a static degrader tend to have more SOBP-pencil beams. This might be caused because when a degrader is added the range in which Bragg peaks can end up is increased. For example, for shallow tumours, the peak of a 110 MeV (the lowest energy beam in the SOBP-database) beam may already end up behind the tumour and therefore be left out of the optimization. This can be remedied by adding a degrader.

### 5.3.2 Dose homogeneity

For dose delivered to a tumour, it is desirable that the dose is homogeneous, otherwise one part of the tumour may be over-irradiated, while another part is under-dosed. Therefore, generally, radiotherapy is more efficient when the tumour dose is homogeneous.

Since the optimization of the SOBP-runs is more correlated than the conventional runs, one would probably expect the conventional dose to be the most homogeneous. The results are, as to the homogeneity in the tumour, rather puzzling. In Patient 1 and 2, the conventional run is indeed one of the most homogeneous runs (Figures 49 and 63 and Tables 6 and 8). However, in Patient 3, only 1 of the 4 SOBP-plans has a worse homogeneity than the conventional plan. It is difficult to track this difference back to its roots with the results given in this report. There is no factor for which the homogeneity consistently becomes worse.

Realizable treatment plans should aim for a homogeneity index between 0 and 50% [45]. In that respect, there are SOBP-treatment plans in this report that qualify. Of course, before concluding plans are positively realizable, there are a number of other aspects that need to be taken into account.

### 5.3.3 Dose conformity

One of those aspects is the dose conformity to the tumour. In this research, lateral scatter coming from the ridge filter is not intentionally taken into account. However, in iCycle, the lateral penumbra of the SOBP-beams with a certain energy do have a less steep fall-off than the Bragg peak beams with that energy. This stems from the fact that lower energy Bragg peak beams have a wider lateral penumbra than higher energy beams. The SOBP-beams are interpreted as sums of lower energy Bragg peak beams, and thus some lateral dose spread is taken into account.

Besides this, when looking at the dose-distributions in the patients (Figures 46, 60 and 68) resulting from the initial SOBP-runs, for Patient 1 (Figure 46) and Patient 3 (Figure 68) it is clear that the dose conformity in the patient has decreased and more healthy tissue is being irradiated. This can also be concluded from their dose-volume histograms (Figure 49 and Figure 71). The green dashed lines (initial run) start at a higher volume percentage than the continuous green lines (conventional run).

In Patient 1, one of the reasons for this may be the site at which the tumour is located. The tumour is located close to the skin. The effect this has on the dose distribution can be seen in Figure 46. This initial run for Patient 1 did not include a degrader. The effect of the lack of a degrader, described in Section 5.3.1, can be seen in the dose distributions per beam (Figure 46b and 46a): the overshoot of high dose to healthy tissue (beam 1) or to the distal edge of the tumour (beam 2), to obtain a higher minimum dose in the tumour.

For Patient 3, the shape of the tumour has a large influence on the dose deposition to the surrounding healthy tissue. In Figure 68, the effect of the ridge filter (the spreading-out of the Bragg peak) is clearly

visible in the dose distributions per beam. When a tumour has a shape with (small) protrusions, the spread-out dose-deposit region of the SOBPs can already cause over- or under-shooting of the tumour (so, dose may be deposited behind or before the tumour).

In contrast to the other patients, for Patient 2, the conventional run is, in general, less conformal. So, in terms of dose conformity and dose to healthy tissue, some SOBPs-plans from Patient 2 seem to be favourable over the conventional plan.

Besides this, another trend is that in the SOBP-runs with a degrader, a smaller healthy tissue volume receives dose. An explanation for this could be, as previously described in Section 5.3.1, that with the degrader, Bragg peaks that would fall behind the tumour now end up within the tumour. Without the degrader, in order to meet the minimum dose constraint in the tumour, higher energy beams, that fall behind the tumour, could have been given higher weights in order to deliver a higher dose with their entrance areas. Using a degrader, this is probably not necessary anymore.

### 5.3.4 Difference between initial and final runs

Since only one initial run has been done for every patient, it is difficult to draw definite conclusions on the significance of the differences between the initial and the final runs. In Patient 1, it is obvious that, in term of dose homogeneity and dose delivery to the tumour, the first run is far more favourable than the later runs. There is a price, since more healthy tissue is irradiated, Figure 49. However, compared to the final runs, the healthy tissue that is irradiated, in general, receives less dose. Also in Patient 2 and 3, the initially optimized treatment plan is often favourable over the other SOBP-plans.

One of the reasons for this difference is that the SOBP-database has been updated between the first and final runs. However, this should not make a lot of difference, since the generation of the database was done in a similar way. The only aspects that had changed in the database generation are: 1. energies from 110 MeV onward had been included instead of from 130 MeV onward, and 2. some small TOPAS simulation settings had been set more precisely then before. That the differences caused by the changing of the database are small can be seen in Figure 50.

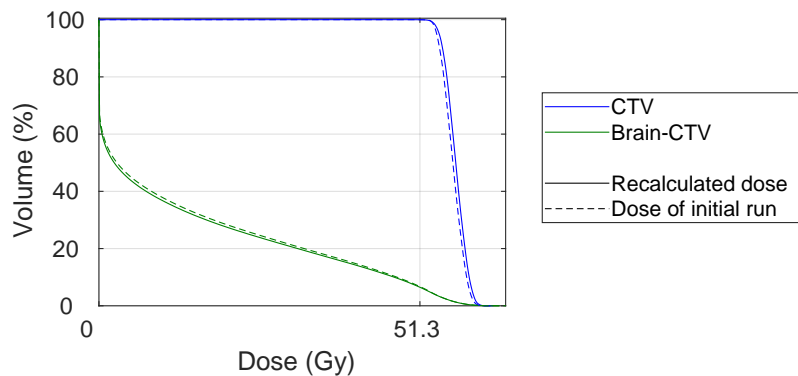


Figure 50: Dose-volume histograms for different dose calculations of the initial optimized SOBP treatment plan of Patient 1. The continuous lines represent the dose calculated with the newer SOBP-database, while the dashed lines show the dose calculated with the old database. In the dose-volume histograms, the CTV (blue) and Brain-CTV (green) structures are considered.

Another possibility is that some other optimization specifications were set for the iCycle optimizations. Some differences have been tracked. When the initial runs were done, there was a bug in the program that set all the optimization specs regarding the degrader. That is also why the initial

plans of Patient 1 and 3 do not use a degrader, while the initial plan for Patient 2 does. From the results discussed earlier, it can be concluded that using a degrader has influence on the optimized plan.

Besides this, the cause of the differences is still unclear. It may be that something in the implemented code has changed. From Figure 50 it can be concluded that the initial runs are feasible runs and there was no error in the final dose calculation.

### 5.3.5 Computation time

Though the SOBP-plans may be less homogeneous or conformal, there is one thing they all have in common: their relatively small computation time. While a conventional, non-robust treatment plan optimization can take 6 hours to run, for the same patient, Patient 1, the SOBP-runs can be calculated in less than an hour and the initial run even as fast as 11 minutes. Also for Patient 2 and 3 the SOBP-optimizations take less time than the conventional runs. The initial run is always one of the fastest optimizations (130 MeV database), while the 110 MeV database run without a degrader always takes the longest of the SOBP-runs.

The computation time depends on many factors, such as the volume of the tumour, the energy spacing and the lateral spacing of the spots. In the SOBP-runs, instead of using an energy spacing of 3 mm, an energy spacing of 10 mm is used. Therefore, the initial beamlist is smaller and thus the initial optimization problem is smaller, causing a shorter computation time. The SOBP-run that takes the longest is still a factor 2.6 faster than the conventional run. However, when allowing for more degrees of freedom the computation time will, of course, increase.

## 5.4 Clinical implementation

In the Chapter 1, we started with describing the clinical context of this research. In this section, we will come back to this by looking at the advantages and disadvantages and general remarks on the possible use of ridge filters in clinical (FLASH) proton therapy.

### 5.4.1 FLASH proton therapy

As mentioned earlier, irradiating a tumour with FLASH proton beams does come with its challenges. The three conditions for FLASH: dose  $> 8$  Gy, dose rate  $> 40$  Gy/s and treatment times  $< 0.1$  s, have all kinds of practical implications.

#### Treatment planning

In terms of treatment planning these conditions have been reduced to: 1. no two pencil beams, with different energies, may have the same lateral position, and 2. as in conventional treatment plans, the dose of one fraction, so one beam direction, to the tumour should be as homogeneous as possible.

In this research, the first requirement has been implemented successfully. This can be seen in the Figures 45, 59 and 67. There, the energy of the beams lies between 130 and 180 MeV. There are no SOBP-beams with an energy lower than 130 MeV here, since these figures show the pencil beams for the first SOBP-runs where a SOBP-database is used with energies larger than 130 MeV. The energies of these beams are lower than the 244 MeV that would be used for irradiation with ultra-high dose rate beams. For the 244 MeV beam to end up with the energies in the optimization, the ridge filter and a patient specific range modulator are used.

The second condition has not been actively implemented or optimized. It is clear that without implementing any optimizations on that requirement, the dose distributions of each beam in the tumour are not necessarily very homogeneous, see Figures 46, 60 and 68 and the dose-volume histograms in Figures 47, 61 and 69. For Patient 1 and 3 the homogeneity of the dose delivered by one beam is

really low. For Patient 2, it is still not optimal, but it is an improvement compared to the other patients.

Looking at the treatment plans resulting from the SOBP-runs, some of the treatment plans seem promising. SOBP tumour dose distributions with a similar or better homogeneity than the conventional run are:

- for Patient 1: the initial run;
- for Patient 2: run 3, and
- for Patient 3: the initial run, run 2 and run 3.

For these runs some more healthy tissue may be irradiated. With a FLASH-enhancement ratio between 1.4 and 2.1, this disadvantage may be turned away, as can be seen in Tables 6, 8 and 10. The ratios are based on the mean doses to the healthy tissue and are therefore not the only metric that should be taken into account when determining FLASH-compatibility. The dose distributions in the healthy tissue may be very unwanted for treatment. To determine the FLASH-compatibility more accurately, the ratios and final FLASH doses for each organ at risk should be considered. For now, not enough research has been done into FLASH treatment planning, the effect of fractionation and re-irradiation, and the feasibility of even higher FLASH-enhancement ratios to conclude that these plans would indeed be beneficial. However, some results do look promising.

A disadvantage of the current implementation of the SOBP-database in iCycle is that stably generating results has proven challenging. Sometimes errors occur in the optimization, or no feasible plan is found with a 110 MeV database run, while the smaller 130 MeV database run does find a feasible plan. Also, it is very hard to predict when the SOBP-plans from the optimizations will make sense or be much worse than the conventional run. A lot of factors influence the plan quality: the tumour site, the shape of the tumour and its size as well as the optimization specifications of using a degrader and probably more.

FLASH irradiation may improve the prognosis for high grade brain tumours, such as a glioblastoma. Re-irradiation of a recurrent glioblastoma is a palliative treatment where dose to organs at risk is critical. Therefore, for the primary irradiation of a glioblastoma, where high doses are used in the irradiation fractions, FLASH may prove to be useful.

### Ridge filters in the clinic

Besides these notes on FLASH irradiation, there are also the physical, practical consequences of using a ridge filter.

In this research, a non-patient specific ridge filter is used. As proposed before, aligning and conforming the proton beam to the tumour would be done by using a patient specific range modulator and, if necessary, a collimator. When making treatment plans with a spacing of 5 mm between two consecutive spots, this is assumed to be possible. A consequence of only using static objects in the FLASH dose delivery is that for each beam direction a different range compensator should be used. So, the more beam directions there would be used, the more range compensators would be needed.

## 5.5 Future research

In the previous sections, some limitations of this research have already been described. In this section, some more will be mentioned and several ideas for future research will be given.

- Consider which factors in the iCycle optimization have a large influence on the ridge filter beam treatment plan optimization for a given clinical application. Investigate why the optimization is not always stably converging to a feasible, optimal treatment plan.

- Proton range uncertainties have not been taken into account in this research. Using transmission beams these drawbacks may have less influence. It would be interesting to consider both techniques and investigate in which cases and for which tumour sites which one would be favourable.
- The relative biological effectiveness (RBE) has not been taken into consideration in this research. Further research could also be conducted to determine whether the RBE in FLASH radiotherapy is similar to the RBE in conventional radiotherapy.
- As mentioned before, FLASH proton therapy has 3 requirements: dose  $> 8$  Gy, dose rate  $> 40$  Gy/s and treatment times  $< 0.1$  s. For final FLASH treatment plan optimizations, by all means, also dose rate optimizations (for example by implementing objectives and constraints for the pencil beam scanning dose rate or the dose-averaged dose rate) and checks whether the dose and dose rate are FLASH-compatible need to be implemented.
- For a more exact implementation of a SOBP-database in iCycle, dose-depth curve measurements with the ridge filter need to be done to verify/improve the TOPAS simulations. In that way, also the lateral scatter can be taken into account more accurately.
- In the iCycle optimization, a SOBP-database is implemented for one ridge filter and one degrader. More ridge filter databases and degraders can be implemented in iCycle. For different fractions, different ridge filters may be used.
- Single-fraction FLASH irradiation experiments have given positive results. In this research treatment plans are optimized using 2 beams, so at least 2 FLASH fractions. Fractionation of FLASH beams, re-irradiation of the tumour and the total delivery time may all be important for the FLASH effect, but their exact impact is still to be determined.
- A last interesting direction of research would be to investigate how a tumour responds to a combined FLASH/non-FLASH treatment. One of the possibilities is to consider an intra-fractionation combination of FLASH and non-FLASH. Irradiate a tumour with one beam direction and, if the dose delivered in the tumour is not homogeneous enough, irradiate the under-dosed regions with conventional proton therapy. Another possibility is to study inter-fractionation combinations of FLASH and non-FLASH. So, deliver some fractions with FLASH and others without FLASH and check the behaviour of the tumour.

## 6 Conclusion

This study set out to investigate to what extent FLASH compatible treatment plans optimized using spread-out Bragg peak (SOBP) beams are clinically acceptable. The results have shown that it is indeed possible to optimize treatment plans in Erasmus-iCycle using SOBP-beams. However, the clinical acceptability of the plans remains to be seen. In some cases, overall less healthy tissue is irradiated using SOBP-beams, but the homogeneity of the dose in the tumour has decreased, or vice versa. In other cases both the homogeneity and the conformity of the treatment plan have decreased. Without calculating and taking into account the FLASH effect, a conclusion on the acceptability of the treatment plans cannot be made. In some treatment plans, a FLASH enhancement ratio of between 1.4 and 2.1 would be enough to eliminate the extra dose to healthy tissue.

The quality of the SOBP-beam optimized treatment plans mainly depends on five main factors:

- the shape of the tumour,
- the position of the tumour,
- the involved organs at risk,
- the used beam directions, and
- whether a static degrader is added in the optimization.

A main limitation of this study is that configuration of the treatment plan optimizer is challenging. Furthermore, only three patients are considered. Therefore, no unambiguous generalisations can be done for the five factors. Besides this, the simulations used for the generation of the SOBP-database are not in complete agreement with the measurements. Therefore, the SOBP-beams used in the iCycle optimizations might not be completely accurate, thus also accounting for some inaccuracies in the final treatment plans.

The implementation of the SOBP-beam optimization in iCycle is not fundamentally different from the conventional treatment plan optimization. Therefore, further work needs to be done to establish the stability of the iCycle optimization using SOBP-beams. Besides this, a more experimentally verified SOBP-database should be implemented for more accurate dose calculations.

An expansion of this research would be to not only implement one ridge filter and one static degrader in the iCycle optimizations, but implement more. In that way, there are more degrees of freedom in the optimization. This might slow down the optimizer, but will improve the resulting treatment plans.

If the debate on clinically acceptable FLASH treatment plans is to be moved forward, the other requirements for FLASH, the minimal dose and dose rate, also need to be implemented in iCycle to find the FLASH-compatible regions. This can be done by implementing a dose rate metric (for example the pencil beam scanning dose rate or the dose-averaged dose rate) that can be optimized in a similar fashion as the dose. Additionally, research into the RBE and the biological character of FLASH will increase the understanding of the FLASH effect overall. With an improved understanding of the effect comes a more efficient and more accurate implementation of FLASH. Another important point for further research is the influence of fractionation of ultra-high dose rate beams on the FLASH effect. This information is essential for bringing FLASH to the clinic, as all treatment plans for patients are fractionated. Furthermore, it would be interesting to investigate combined FLASH and non-FLASH treatment. Then some regions of the tumour can be irradiated with ultra-high dose rate beams, while underdosed regions can be irradiated with conventional IMPT.

## References

- [1] World Health Organization. (2020). Cancer, [Online]. Available: <https://www.who.int/health-topics/cancer>.
- [2] National Cancer Institute. (2020). Types of cancer treatment, [Online]. Available: <https://www.cancer.gov/about-cancer/treatment/types>.
- [3] Shinohara, E. and Whaley, J.T. (Mar. 2020). Radiation therapy: Which type is right for me?, [Online]. Available: <https://www.oncolink.org/cancer-treatment/radiation/introduction-to-radiation-therapy/radiation-therapy-which-type-is-right-for-me>.
- [4] A. Kaiser, J. G. Eley, N. E. Onyeuku, S. R. Rice, C. C. Wright, N. E. McGovern, M. Sank, M. Zhu, Z. Vujaskovic, C. B. Simone 2nd, *et al.*, “Proton therapy delivery and its clinical application in select solid tumor malignancies”, *JoVE (Journal of Visualized Experiments)*, no. 144, e58372, 2019.
- [5] Holland PTC. (2020). Wat zijn de voordelen van protontherapie?, [Online]. Available: <https://www.hollandptc.nl/faqs/>.
- [6] D. Indelicato, T. Merchant, N. Laperriere, Y. Lassen, S. Vennarini, S. Wolden, W. Hartsell, M. Pankuch, P. Brandal, C.-C. Law, R. Taylor, S. Laskar, M. Okcu, E. Bouffet, H. Mandeville, T. Björk-Eriksson, K. Nilsson, H. Nyström, L. Constine, and R.-D. Kortmann, “Consensus report from the stockholm pediatric proton therapy conference”, *International journal of radiation oncology, biology, physics*, vol. 96, pp. 387–392, Oct. 2016. DOI: 10.1016/j.ijrobp.2016.06.2446.
- [7] H. Paganetti, *Proton therapy physics*. CRC press, 2018.
- [8] H. Paganetti, “Nuclear interactions in proton therapy: Dose and relative biological effect distributions originating from primary and secondary particles”, *Physics in Medicine and Biology*, vol. 47, no. 5, pp. 747–764, Feb. 2002. DOI: 10.1088/0031-9155/47/5/305. [Online]. Available: <https://doi.org/10.1088/0031-9155/47/5/305>.
- [9] X. R. Zhu, Y. Li, D. Mackin, H. Li, F. Poenisch, A. K. Lee, A. Mahajan, S. J. Frank, M. T. Gillin, N. Sahoo, *et al.*, “Towards effective and efficient patient-specific quality assurance for spot scanning proton therapy”, *Cancers*, vol. 7, no. 2, pp. 631–647, 2015.
- [10] H. Liu and J. Y. Chang, “Proton therapy in clinical practice”, *Chinese journal of cancer*, vol. 30, no. 5, p. 315, 2011.
- [11] M. Durante, “Proton beam therapy in europe: More centres need more research”, *British Journal of Cancer*, vol. 120, no. 8, p. 777, 2019.
- [12] V. Favaudon, L. Caplier, V. Monceau, F. Pouzoulet, M. Sayarath, C. Fouillade, M.-F. Poupon, I. Brito, P. Hupé, J. Bourhis, *et al.*, “Ultrahigh dose-rate flash irradiation increases the differential response between normal and tumor tissue in mice”, *Science translational medicine*, vol. 6, no. 245, 245ra93–245ra93, 2014.
- [13] Y. Simeonov, U. Weber, P. Penchev, T. P. Ringbæk, C. Schuy, S. Brons, R. Engenhardt-Cabillic, J. Bliedtner, and K. Zink, “3d range-modulator for scanned particle therapy: Development, monte carlo simulations and experimental evaluation”, *Physics in Medicine & Biology*, vol. 62, no. 17, p. 7075, 2017.
- [14] M.-C. Vozenin, J. H. Hendry, and C. Limoli, “Biological benefits of ultra-high dose rate flash radiotherapy: Sleeping beauty awoken”, *Clinical oncology*, vol. 31, no. 7, pp. 407–415, 2019.
- [15] M.-C. Vozenin, M. Baumann, R. P. Coppes, and J. Bourhis, “Flash radiotherapy international workshop”, *Radiotherapy and Oncology*, vol. 139, pp. 1–3, 2019.
- [16] J. Groen, “Flash optimisation in clinical impt treatment planning”, Master’s thesis, Delft University of Technology, Jul. 2020.

- [17] M.-C. Vozenin, “Can flash-rt change the way we treat cancer? (what we think we know and what we don’t know)”, Radiotherapy Research Round Erasmus MC, 2021.
- [18] M. Durante, E. Bräuer-Krisch, and M. Hill, “Faster and safer? flash ultra-high dose rate in radiotherapy”, *The British journal of radiology*, vol. 91, no. 1082, p. 20170628, 2018.
- [19] C. Fouillade, S. Curras-Alonso, L. Giuranno, E. Queleynec, S. Heinrich, S. Bonnet-Boissinot, A. Beddok, S. Leboucher, H. U. Karakurt, M. Bohec, *et al.*, “Flash irradiation spares lung progenitor cells and limits the incidence of radio-induced senescence”, *Clinical Cancer Research*, vol. 26, no. 6, pp. 1497–1506, 2020.
- [20] M. Buonanno, V. Grilj, and D. J. Brenner, “Biological effects in normal cells exposed to flash dose rate protons”, *Radiotherapy and Oncology*, vol. 139, pp. 51–55, 2019.
- [21] J. Bourhis, W. J. Sozzi, P. G. Jorge, O. Gaide, C. Bailat, F. Duclos, D. Patin, M. Ozsahin, F. Bochud, J.-F. Germond, *et al.*, “Treatment of a first patient with flash-radiotherapy”, *Radiotherapy and oncology*, vol. 139, pp. 18–22, 2019.
- [22] Mar. 2019. [Online]. Available: [https://iba-worldwide.com/sites/protontherapy/files/media\\_document/20190308\\_flash\\_groningen\\_final.pdf](https://iba-worldwide.com/sites/protontherapy/files/media_document/20190308_flash_groningen_final.pdf).
- [23] F. Stichelbaut and Y. Jongen, “Properties of an energy degrader for light ions”, *Progress in Nuclear Science and Technology*, vol. 4, pp. 272–275, 2014.
- [24] P. van Marlen, M. Dachele, M. Folkerts, E. Abel, B. J. Slotman, and W. F. Verbakel, “Bringing flash to the clinic: Treatment planning considerations for ultrahigh dose-rate proton beams”, *International Journal of Radiation Oncology\* Biology\* Physics*, vol. 106, no. 3, pp. 621–629, 2020.
- [25] A. Patriarca, C. Fouillade, M. Auger, F. Martin, F. Pouzoulet, C. Nauraye, S. Heinrich, V. Favaudon, S. Meyroneinc, R. Dendale, *et al.*, “Experimental set-up for flash proton irradiation of small animals using a clinical system”, *International Journal of Radiation Oncology\* Biology\* Physics*, vol. 102, no. 3, pp. 619–626, 2018.
- [26] T. Sakae, A. Nohtomi, A. Maruhashi, M. Sato, K. Hosono, T. Terunuma, R. Kohno, Y. Akine, and Y. Hayakawa, “Three-dimensional conformal irradiation with a multilayer energy filter for proton therapy”, *Review of scientific instruments*, vol. 72, no. 1, pp. 234–236, 2001.
- [27] HollandPTC. (Sep. 2018). 1e patiënt succesvol bestraald. hollandptc open voor patiëntenzorg en onderzoek, [Online]. Available: <https://www.hollandptc.nl/1e-patient-succesvol-bestraald-hollandptc-open-voor-patientenzorg-en-onderzoek/>.
- [28] L. L. Carter and E. D. Cashwell, “Particle-transport simulation with the monte carlo method”, Los Alamos Scientific Lab., N. Mex.(USA), Tech. Rep., 1975.
- [29] J. Seco and F. Verhaegen, *Monte Carlo techniques in radiation therapy*. CRC press, 2013.
- [30] S. Agostinelli, J. Allison, K. a. Amako, J. Apostolakis, H. Araujo, P. Arce, M. Asai, D. Axen, S. Banerjee, G. 2. Barrant, *et al.*, “Geant4—a simulation toolkit”, *Nuclear instruments and methods in physics research section A: Accelerators, Spectrometers, Detectors and Associated Equipment*, vol. 506, no. 3, pp. 250–303, 2003.
- [31] J. Perl, J. Shin, J. Schuemann, J. Ramos, D. Hall, A. Biegun, and F. Guan, *Topas documentation - release 3.1*, TOPAS MC Inc., Mar. 2021.
- [32] R. Capote, R. Jeraj, C. Ma, D. W. Rogers, F. Sánchez-Doblado, J. Sempau, J. Seuntjens, and J. Siebers, “Phase-space database for external beam radiotherapy. summary report of a consultants’ meeting”, 2006.
- [33] S. Breedveld, P. R. Storchi, P. W. Voet, and B. J. Heijmen, “Icycle: Integrated, multicriterial beam angle, and profile optimization for generation of coplanar and noncoplanar imrt plans”, *Medical physics*, vol. 39, no. 2, pp. 951–963, 2012.

- [34] S. Breedveld, P. R. Storchi, M. Keijzer, A. W. Heemink, and B. J. Heijmen, “A novel approach to multi-criteria inverse planning for imrt”, *Physics in Medicine & Biology*, vol. 52, no. 20, p. 6339, 2007.
- [35] Taschetta-Millane, M. (Jul. 2016). Treatment planning systems overview, [Online]. Available: <https://www.itnonline.com/article/treatment-planning-systems-overview>.
- [36] S. Breedveld, P. R. Storchi, and B. J. Heijmen, “The equivalence of multi-criteria methods for radiotherapy plan optimization”, *Physics in Medicine & Biology*, vol. 54, no. 23, p. 7199, 2009.
- [37] S. van de Water, I. van Dam, D. R. Schaart, A. Al-Mamgani, B. J. Heijmen, and M. S. Hoogeman, “The price of robustness; impact of worst-case optimization on organ-at-risk dose and complication probability in intensity-modulated proton therapy for oropharyngeal cancer patients”, *Radiotherapy and Oncology*, vol. 120, no. 1, pp. 56–62, 2016.
- [38] H. M. Kooy, B. M. Clasié, H.-M. Lu, T. M. Madden, H. Bentefour, N. Depauw, J. A. Adams, A. V. Trofimov, D. Demaret, T. F. Delaney, *et al.*, “A case study in proton pencil-beam scanning delivery”, *International Journal of Radiation Oncology\* Biology\* Physics*, vol. 76, no. 2, pp. 624–630, 2010.
- [39] N. Hodapp, “The icru report 83: Prescribing, recording and reporting photon-beam intensity-modulated radiation therapy (imrt)”, *Strahlentherapie und Onkologie: Organ der Deutschen Röntgengesellschaft...[et al]*, vol. 188, no. 1, pp. 97–99, 2012.
- [40] J. Alfonso, M. A. Herrero, and L. Nunez, “A dose-volume histogram based decision-support system for dosimetric comparison of radiotherapy treatment plans”, *Radiation Oncology*, vol. 10, no. 1, pp. 1–9, 2015.
- [41] M. Mrozowska and P. Kukołowicz, “Relationships between various indices of doses distribution homogeneity”, *Reports of Practical Oncology & Radiotherapy*, vol. 20, no. 4, pp. 278–283, 2015.
- [42] C. t. Haar, “Robustness recipes for proton therapy: Polynomial chaos expansion as a tool to construct robustness recipes for proton therapy”, Master’s thesis, Delft University of Technology, Feb. 2018.
- [43] P. C. Park, X. R. Zhu, A. K. Lee, N. Sahoo, A. D. Melancon, L. Zhang, and L. Dong, “A beam-specific planning target volume (ptv) design for proton therapy to account for setup and range uncertainties”, *International Journal of Radiation Oncology\* Biology\* Physics*, vol. 82, no. 2, e329–e336, 2012.
- [44] M. Hoogeman, personal meeting, Jun. 2021.
- [45] L. Yan, Y. Xu, X. Chen, X. Xie, B. Liang, and J. Dai, “A new homogeneity index definition for evaluation of radiotherapy plans”, *Journal of applied clinical medical physics*, vol. 20, no. 11, pp. 50–56, 2019.
- [46] J. Perl, J. Shin, J. Schumann, B. Faddegon, and H. Paganetti, “TOPAS: An innovative proton Monte Carlo platform for research and clinical applications”, *Medical Physics*, vol. 39, p. 6818, 2012. DOI: 10.1118/1.4758060.
- [47] CERN, *Geant4 user guide for application developers*, Dec. 2020.
- [48] M. Rituerto Prieto, “Passive beam field characterization for application in radiobiology”, Master’s thesis, Delft University of Technology, Sep. 2020.
- [49] A. Ibrahim, “Characterization of the proton beam line in the experimental room of hollandptc”, Master’s thesis, Delft University of Technology, Dec. 2020.
- [50] M. Rovituso, email correspondence, Dec. 2020.
- [51] Y. Simeonov, email correspondence, Dec. 2020.
- [52] C. Bäumer, B. Koska, J. Lambert, B. Timmermann, T. Mertens, and P. T. Talla, “Evaluation of detectors for acquisition of pristine depth-dose curves in pencil beam scanning”, *Journal of applied clinical medical physics*, vol. 16, no. 6, pp. 151–163, 2015.

- 
- [53] *Particle therapy qa tools*, PTW Dosimetry, Apr. 2019. [Online]. Available: <https://www.ptwdosimetry.com/en/products/mp3-ppl/?type=3451&downloadfile=951&cHash=9f153c45fea1ac05ba289c2fb>
- [54] Micheau, Antoine and Hoa, Denis. (Mar. 2020). Ct scan of head and neck, [Online]. Available: <https://www.imaios.com/en/e-Anatomy/Head-and-Neck/Head-and-neck-CT>.
- [55] M. Oud, email conversation, Jun. 2021.
- [56] C. Groenendijk, personal meeting, Jun. 2021.

## A Appendix

### A.1 TOPAS scripts

#### A.1.1 Physics settings

```

1 s:Ph/ListOfNames = "Default"
2
3 b:Ph/ListOfProcesses = "False" # Set true to dump list of active physics
  processes to console
4 s:Ph/Default/Type = "Geant4_Modular"
5 sv:Ph/Default/Modules = 6 "g4em-standard_opt4" "g4h-phy_QGSP_BIC_HP" "
  g4decay" "g4ion-binarycascade" "g4h-elastic_HP" "g4stopping" #
  Default in TOPAS
6
7 b:Ph/Default/Fluorescence = "True"
8 b:Ph/Default/PIXE = "True"
9 b:Ph/Default/AugerCascade = "True"

```

#### A.1.2 Beam characteristics

```

1 s:Ge/World/Material = "Air"
2 d:Ge/World/HLX = 5.0 m
3 d:Ge/World/HLY = 5.0 m
4 d:Ge/World/HLZ = 5.0 m
5 b:Ge/World/Invisible = "True"
6
7 s:Ge/BeamPosition/Parent = "World"
8 s:Ge/BeamPosition/Type = "Group"
9 d:Ge/BeamPosition/TransX = 0. m
10 d:Ge/BeamPosition/TransY = 0. m
11 d:Ge/BeamPosition/TransZ = Ge/World/HLZ m #to the left of the z-axis,
  so 5 m from the center of the world in the z-direction
12 d:Ge/BeamPosition/RotX = 180. deg
13 d:Ge/BeamPosition/RotY = 0. deg
14 d:Ge/BeamPosition/RotZ = 0. deg
15
16 s:So/Example/Type = "Beam"
17 s:So/Example/Component = "BeamPosition"
18 s:So/Example/BeamParticle = "proton"
19 d:So/Example/BeamEnergy = 239.5 MeV
20 u:So/Example/BeamEnergySpread = 0.25
21 s:So/Example/BeamPositionDistribution = "Gaussian"
22 s:So/Example/BeamPositionCutoffShape = "Ellipse"
23 d:So/Example/BeamPositionCutoffX = 10. cm
24 d:So/Example/BeamPositionCutoffY = 10. cm
25 d:So/Example/BeamPositionSpreadX = 0.24 cm
26 d:So/Example/BeamPositionSpreadY = 0.18 cm
27 s:So/Example/BeamAngularDistribution = "Gaussian"
28 d:So/Example/BeamAngularCutoffX = 90. deg
29 d:So/Example/BeamAngularCutoffY = 90. deg

```

```

30 d:So/Example/BeamAngularSpreadX      = 0.0032 rad
31 d:So/Example/BeamAngularSpreadY      = 0.0034 rad
32 i:So/Example/NumberOfHistoriesInRun  = 100000

```

### A.1.3 Pristine Bragg peak simulations

```

1 #####
2 # Kapton Exit Window
3 #####
4 s:Ge/ExitWindow/Parent      = "World"
5 s:Ge/ExitWindow/Type        = "TsCylinder"
6 s:Ge/ExitWindow/Material    = "Kapton"
7 d:Ge/ExitWindow/RMin        = 0.0 mm
8 d:Ge/ExitWindow/RMax        = 50.0 mm
9 d:Ge/ExitWindow/HL          = 0.125 mm
10 d:Ge/ExitWindow/SPhi        = 0.0 deg
11 d:Ge/ExitWindow/DPhi        = 360.0 deg
12 d:Ge/ExitWindow/TransX      = 0.0 mm
13 d:Ge/ExitWindow/TransY      = 0.0 mm
14 d:Ge/ExitWindow/TransZ      = 499.8 cm
15 d:Ge/ExitWindow/RotX        = 0.0 deg
16 d:Ge/ExitWindow/RotY        = 0.0 deg
17 d:Ge/ExitWindow/RotZ        = 0.0 deg
18 b:Ge/ExitWindow/Include     = "TRUE"
19 s:Ge/ExitWindow/DrawingStyle = "Solid"
20
21 #####
22 # Water phantom
23 #####
24 s:Ge/WaterPhantom/Type      = "TsBox"
25 s:Ge/WaterPhantom/Parent    = "World"
26 s:Ge/WaterPhantom/Material  = "G4_WATER"
27 d:Ge/WaterPhantom/HLX       = 15. cm
28 d:Ge/WaterPhantom/HLY       = 15. cm
29 d:Ge/WaterPhantom/HLZ       = 30.0 cm
30 d:Ge/WaterPhantom/TransZ     = 378.675 cm #I place it 91 cm away (
    entrance of BM1)
31 s:Ge/WaterPhantom/Color     = "blue"
32 i:Ge/WaterPhantom/Xbins     = 1
33 i:Ge/WaterPhantom/Ybins     = 1
34 i:Ge/WaterPhantom/Zbins     = 1
35 d:Ge/WaterPhantom/MaxStepSize = .1 mm
36
37 #####
38 # Scorer
39 #####
40 s:Ge/Detector/Type          = "TsCylinder"
41 s:Ge/Detector/Parent        = "World"
42 d:Ge/Detector/RMin          = 0. cm
43 d:Ge/Detector/RMax          = 4.08 cm
44 d:Ge/Detector/HL            = 30.0 cm

```

```

45 d:Ge/Detector/SPhi      = 0. deg
46 d:Ge/Detector/DPhi     = 360. deg
47 d:Ge/Detector/TransZ   = 378.675 cm #I place it 91 cm away (entrance
    of BM1)
48 s:Ge/Detector/Color    = "blue"
49 s:Ge/Detector/Message  = "Constructing Detector"
50 i:Ge/Detector/RBins    = 1
51 i:Ge/Detector/PhiBins  = 1
52 i:Ge/Detector/ZBins    = 1200
53 b:Ge/Detector/IsParallel = "True"
54
55
56 s:Sc/BinScorer/Quantity      = "DoseToMedium"
57 s:Sc/BinScorer/Component     = "Detector"
58 b:Sc/BinScorer/OutputToConsole = "False"
59 s:Sc/BinScorer/OutputType    = "csv"
60 s:Sc/BinScorer/IfOutputFileAlreadyExists = "Overwrite"
61 s:Sc/BinScorer/OutputFile    = "[name file]"
62 sv:Sc/BinScorer/Report = 2 "Mean" "Standard_Deviation"

```

#### A.1.4 Spread-out Bragg peak simulations

```

1 #####
2 # Kapton Exit Window
3 #####
4 s:Ge/ExitWindow/Parent      = "World"
5 s:Ge/ExitWindow/Type       = "TsCylinder"
6 s:Ge/ExitWindow/Material   = "Kapton"
7 d:Ge/ExitWindow/RMin      = 0.0 mm
8 d:Ge/ExitWindow/RMax      = 50.0 mm
9 d:Ge/ExitWindow/HL        = 0.125 mm
10 d:Ge/ExitWindow/SPhi      = 0.0 deg
11 d:Ge/ExitWindow/DPhi      = 360.0 deg
12 d:Ge/ExitWindow/TransX    = 0.0 mm
13 d:Ge/ExitWindow/TransY    = 0.0 mm
14 d:Ge/ExitWindow/TransZ    = 499.8 cm
15 d:Ge/ExitWindow/RotX      = 0.0 deg
16 d:Ge/ExitWindow/RotY      = 0.0 deg
17 d:Ge/ExitWindow/RotZ      = 0.0 deg
18 b:Ge/ExitWindow/Include   = "TRUE"
19 s:Ge/ExitWindow/DrawingStyle = "Solid"
20
21
22 #####
23 # Ridge Filter
24 #####
25 sv:Ma/Plastic/Components = 3 "Hydrogen" "Carbon" "Oxygen"
26 uv:Ma/Plastic/Fractions = 3 0.071062 0.740938 0.188000
27 d:Ma/Plastic/Density = 1.4 g/cm3
28 sc:Ma/Plastic/DefaultColor = "yellow"
29

```

```
30 s:Ge/RidgeFilterfromSTL/Type = "TsCAD"
31 s:Ge/RidgeFilterfromSTL/Parent = "World"
32 s:Ge/RidgeFilterfromSTL/Material = "Plastic"
33 d:Ge/RidgeFilterfromSTL/TransX = 0.0 cm
34 d:Ge/RidgeFilterfromSTL/TransY = 0.0 cm
35 d:Ge/RidgeFilterfromSTL/TransZ = 425. cm
36 d:Ge/RidgeFilterfromSTL/RotX = 0.0 deg
37 d:Ge/RidgeFilterfromSTL/RotY = 0.0 deg
38 d:Ge/RidgeFilterfromSTL/RotZ = 0.0 deg
39 s:Ge/RidgeFilterfromSTL/DrawingStyle = "Wireframe"
40
41 s:Ge/RidgeFilterfromSTL/InputFile = "p_154MeV_D0.015
    _3cm_Edge_3mm_TRENT0_33x33Pins"
42 s:Ge/RidgeFilterfromSTL/FileFormat = "stl"
43 d:Ge/RidgeFilterfromSTL/Units = 1.0 mm
44 d:Ge/RidgeFilterfromSTL/MaxStepSize = 0.1 mm
45
46 #####
47 # Water phantom
48 #####
49
50 s:Ge/WaterPhantom/Type = "TsBox"
51 s:Ge/WaterPhantom/Parent = "World"
52 s:Ge/WaterPhantom/Material = "G4_WATER"
53 d:Ge/WaterPhantom/HLX = 15. cm
54 d:Ge/WaterPhantom/HLY = 15. cm
55 d:Ge/WaterPhantom/HLZ = 30.0 cm
56 d:Ge/WaterPhantom/TransZ = 378.675 cm #I place it 91 cm away (
    entrance of BM1)
57 s:Ge/WaterPhantom/Color = "blue"
58 i:Ge/WaterPhantom/Xbins = 1
59 i:Ge/WaterPhantom/Ybins = 1
60 i:Ge/WaterPhantom/Zbins = 1
61 d:Ge/WaterPhantom/MaxStepSize = .1 mm
62
63 #####
64 # Scorers
65 #####
66 s:Ge/PhaseSpaceScorerBox2/Type = "TsBox"
67 s:Ge/PhaseSpaceScorerBox2/Parent = "World"
68 s:Ge/PhaseSpaceScorerBox2/Material = "Air"
69 d:Ge/PhaseSpaceScorerBox2/HLX = 10. cm
70 d:Ge/PhaseSpaceScorerBox2/HLY = 10. cm
71 d:Ge/PhaseSpaceScorerBox2/HLZ = 0.01 cm
72 d:Ge/PhaseSpaceScorerBox2/TransX = 0. cm
73 d:Ge/PhaseSpaceScorerBox2/TransY = 0. cm
74 d:Ge/PhaseSpaceScorerBox2/TransZ = 409. cm
75 d:Ge/PhaseSpaceScorerBox2/MaxStepSize = 0.02 mm
76
77 s:Sc/PhaseSpaceScorer2/Quantity = "PhaseSpace"
78 s:Sc/PhaseSpaceScorer2/Surface = "PhaseSpaceScorerBox2/ZPlusSurface"
79 b:Sc/PhaseSpaceScorer2/OutputToConsole = "False"
```

```
80 s:Sc/PhaseSpaceScorer2/OutputType = "ASCII"
81 sv:Sc/PhaseSpaceScorer2/OnlyIncludeParticlesNamed = 1 "proton"
82 s:Sc/PhaseSpaceScorer2/OnlyIncludeParticlesOfGeneration = "Primary"
83 s:Sc/PhaseSpaceScorer2/IfOutputFileAlreadyExists = "Overwrite" # Exit,
    Overwrite or Increment
84 s:Sc/PhaseSpaceScorer2/OutputFile = "Results_report/
    PhaseSpace_070_124_after_GSI_stl_7"
85
86 s:Ge/Detector/Type = "TsCylinder"
87 s:Ge/Detector/Parent = "World"
88 d:Ge/Detector/RMin = 0. cm
89 d:Ge/Detector/RMax = 6. cm
90 d:Ge/Detector/HL = 30.0 cm
91 d:Ge/Detector/SPhi = 0. deg
92 d:Ge/Detector/DPhi = 360. deg
93 d:Ge/Detector/TransZ = 378.675 cm #I place it 91 cm away (entrance
    of BM1)
94 s:Ge/Detector/Color = "blue"
95 s:Ge/Detector/Message = "Constructing Detector"
96 i:Ge/Detector/RBins = 1
97 i:Ge/Detector/PhiBins = 1
98 i:Ge/Detector/ZBins = 1200
99 b:Ge/Detector/IsParallel = "True"
100
101 s:Sc/BinScorer/Quantity = "DoseToMedium"
102 s:Sc/BinScorer/Component = "Detector"
103 b:Sc/BinScorer/OutputToConsole = "False"
104 s:Sc/BinScorer/OutputType = "csv"
105 s:Sc/BinScorer/IfOutputFileAlreadyExists = "Overwrite"
106 s:Sc/BinScorer/OutputFile = "[name file]"
107 sv:Sc/BinScorer/Report = 2 "Mean" "Standard_Deviation"
```

## A.2 Wishlist

	Structure	Min/Max	Type	Goal	Limit	Sufficient	Priority	Weight	Parameters	Active	LRPM	Robust
1	GTV	Maximize (minimum) ↑	linear	$A * 0.95$			Constraint	1		Yes	0	No
2	CTV_5040	Maximize (minimum) ↑	linear	$A * 0.98$			Constraint	1		Yes	0	No
3	OpticNrv_L	Minimize (maximum) ↓	linear	55			Constraint	1		Yes	0	No
4	OpticNrv_R	Minimize (maximum) ↓	linear	55			Constraint	1		Yes	0	No
5	OpticChiasm	Minimize (maximum) ↓	linear	55			Constraint	1		Yes	0	No
6	GTV	Minimize (maximum) ↓	linear	$A * 1.12$			1	1		Yes	0	No
7	CTV_5040	Minimize (maximum) ↓	linear	$A * 1.07$			1	1		Yes	0	No
8	Hippocampus_L	Minimize (maximum) ↓	mean	1			2	1		Yes	0	No
9	Brainstem	Minimize (maximum) ↓	linear	55			3	1		Yes	0	No
10	Cochlea_R	Minimize (maximum) ↓	mean	45			4	1		Yes	0	No
11	Cochlea_L	Minimize (maximum) ↓	mean	45			4	1		Yes	0	No
12	Retina_L	Minimize (maximum) ↓	linear	20			5	1		Yes	0	No
13	Retina_R	Minimize (maximum) ↓	linear	20			5	1		Yes	0	No
14	GlnD_Lacrimal_R	Minimize (maximum) ↓	mean	26			7	1		Yes	0	No
15	MU	Minimize (maximum) ↓	linear	1			8	1		Yes	0	No

Figure 51: Example of a wish-list for a neuro-oncological tumour, with  $A$  the desired dose at the tumour. In this case,  $A$  is 54 Gy.

### A.3 Structure iCycle

The bold, italic, orange MATLAB-files are adjusted because code is implemented, or because another adjusted file is called in the file. Not *all* functions of iCycle are shown here, only the ones relevant for this research.

#### *icycle\_protons.m*

(runs the entire optimization)

⇒ **import\_patient\_data.m**

(input: Lucy-file; output: Patient, constraints, data, metadata)

⇒ **proton\_settings.m**

(‘upgrades’ Patient, data, constraints, metadata and ResampData with new info)

⇒ **setup\_beams.m**

(input: metadata, ‘MC’, Patient; output: Beams. Beams contains angles, energies, algorithm, etc. Beams.BeamList is initialized)

⇒ *optimization\_protons.m*

⇒ *do\_resampling\_optimization\_protons.m*

⇒ *resampling\_protons.m*

⇒ **select\_candidate\_beams\_protons.m** (if resampling is used)

⇒ *generate\_beam\_list\_protons.m* (else)

Finds all x,y-coordinates for the pencil beams that fall within the tumour. Makes a list with tumor voxel characteristics: x, y, WER\_min, WER\_max. Gets desired ranges in RangeList (= EnergyRangeList(:,2) – RangeShifter(1)).

BeamList exists of the energies from EnergyRangeList, every energy multiple times (for different x,y-values).

Added: BeamList is extended with for every pencil beam with energy > 110 MeV in the original beamlist  $x$  pencil beams with the same lateral position but with an energy shift (to modulate SOBP beams) coming from the SOBP-database. The pencil beams with energy < 110 MeV are deleted (they fall outside the HollandPTC data and the SOBP-database).

The initial beamlist is saved as Beams.Beams.InitialBeamList and the initial beamlist without the pencil beams < 110 MeV is saved as Beams.Beams.ShortBeamList. In Beams.Beams.ShortBeamList a column with the index of that beam in the initial beamlist is added and a column with for every pencil beam the number of pencil beams that are needed to make it a SOBP-beam. In Beams.Beams.BeamList (the extended beamlist), a column with the index of the ‘base’ pencil beam is added and a column with for every pencil beam in the extended list the weight of that pencil beam.

⇒ *combine\_beams.m*

⇒ **generate\_beams.m**

⇒ **compute\_dose.m**

⇒ **compute\_dose\_protons.m**

⇒ **protodose\_Boston.m**

Returns dose-deposition matrix for all voxels and pencil beams in the BeamList. Duplicate beams are not calculated twice, but the result is implemented for both of them at once.

(cont. `compute_dose_protons.m`)

Matrix from `protondose_Boston.m` is divided into matrices for the different structures in the patient. If the mean dose is needed in the optimization, it is calculated.

⇒ **`combine_beams_int.m`**

In `datain` are the optimization matrix and vectors for every structure in the patient. `Dataout` is the updated `datain`.

(cont. `combine_beams.m`)

Added: After the initial dose-deposition matrix is calculated (this is done for the extended beamlist), the columns of the pencil beams that make up each SOBPs beam are summed up (taking the weights per pencil beam into account).

⇒ *`combine_sampled_beams_protons.m`*

Added: `Beams.Index/Plan.Beams.Index = length of the ShortBeamList` instead of `BeamList`.

⇒ *`reduce_optimization_voxels_protons.m`*

Reduces voxels in patient, excludes superfluous voxels (that fall outside a margin/outside External).

Added: `OriginalData.ShortBeamList = Beams.Beams.ShortBeamList`

⇒ *`reduce_optimization_beams_protons.m`*

Subtracts beams that do not contribute to the dose. Subtract them from the beamlist and from the dose deposition matrix.

Added: conversions from the short beamlist to the extended beamlist.

⇒ **`mcopt.m`**

Does the optimization with the `x0`-vector and the `dataopt`-matrix.

⇒ *`remove_spots_from_optimization_protons.m`*

Subtracts beams with weight < `minMU` per fraction. Subtract them from the beamlist and from the dose deposition matrix.

Added: conversions from the short beamlist to the extended beamlist.

⇒ *`reset_dataopt_protons.m`*

Added: conversions from the short beamlist to the extended beamlist.

(cont. `optimization_protons.m`)

Added: convert `xopt`, which has the size of the number of combined SOBPs-beams used (the short beamlist) to a size of the number of individual pencil beams (the extended beamlist) using the weight for each individual pencil beam.

⇒ **`compute_accurate_dose_protons.m`**

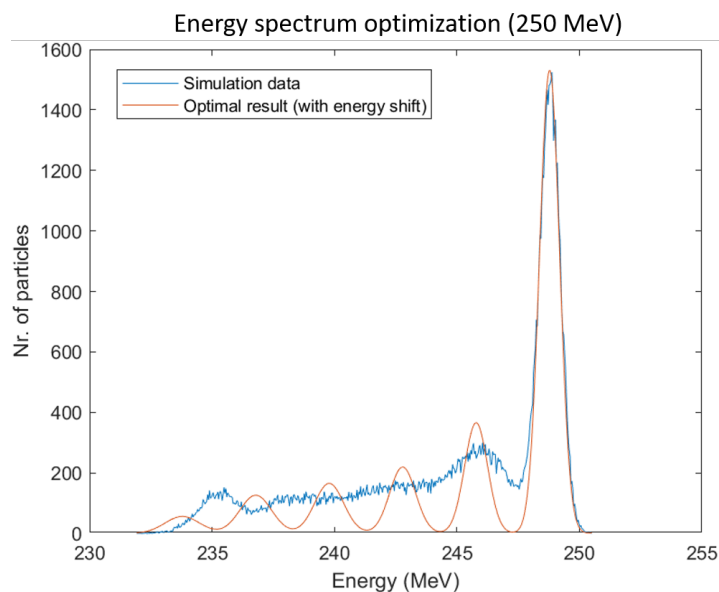
Compute the final dose in the patient using the extended (non-combined) dose-depth matrix with all used pencil beams.

⇒ **`proton_Boston.m`**

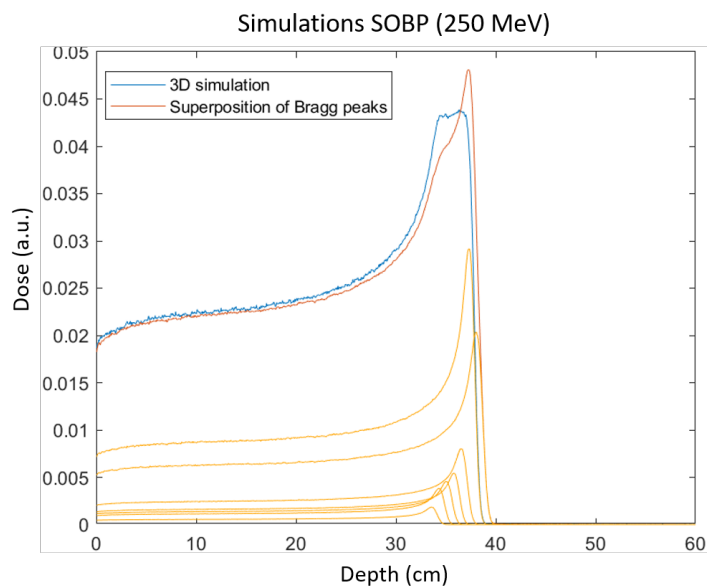
## A.4 Additional results of the energy spectrum optimization

### Energy discretization for high energies

In Figure 52, it is shown that an energy optimization using an energy discretization of 3 MeV does not generate a neat homogeneous SOBPs.



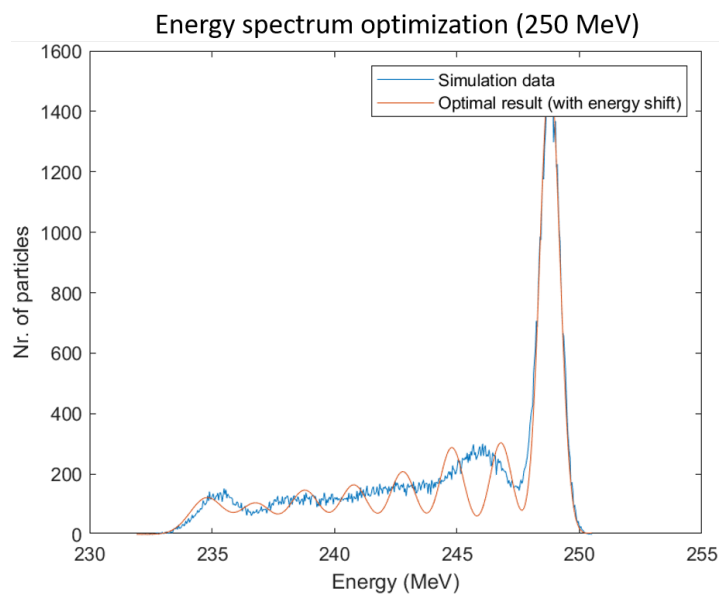
(a)



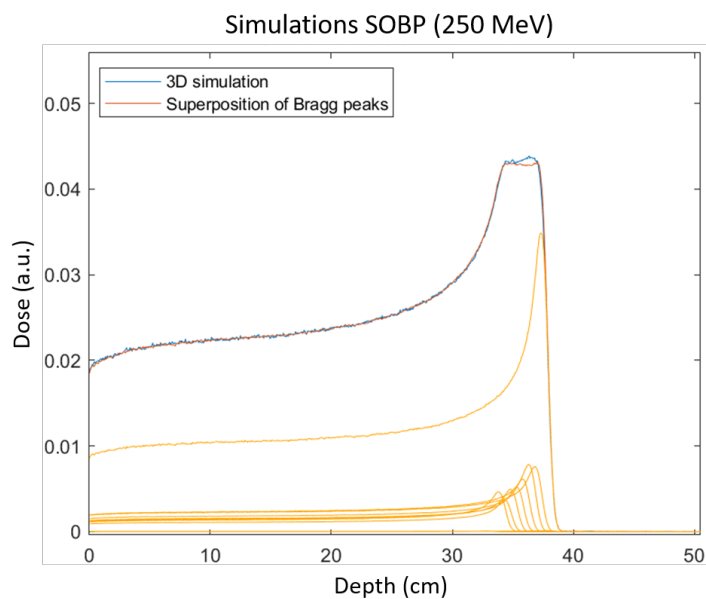
(b)

Figure 52: Ridge filter energy spectrum optimization for a phase plane energy spectrum of a 250 MeV nominal beam. In (a) the optimal spectrum approximation with an energy discretization of 3 MeV, and in (b) the resulting dose-depth curve.

The following figures show that using a 2 MeV energy discretization, the results have already improved a lot.



(a)



(b)

Figure 53: Ridge filter energy spectrum optimization for a phase plane energy spectrum of a 250 MeV nominal beam. In (a) the optimal spectrum approximation with an energy discretization of 2 MeV, and in (b) the resulting dose-depth curve.

### Difference between energy spectrum optimization and dose-depth curve optimization

Figure 54 shows for the 180 MeV base energy the energy spectrum optimization result with its resulting dose-depth curve.

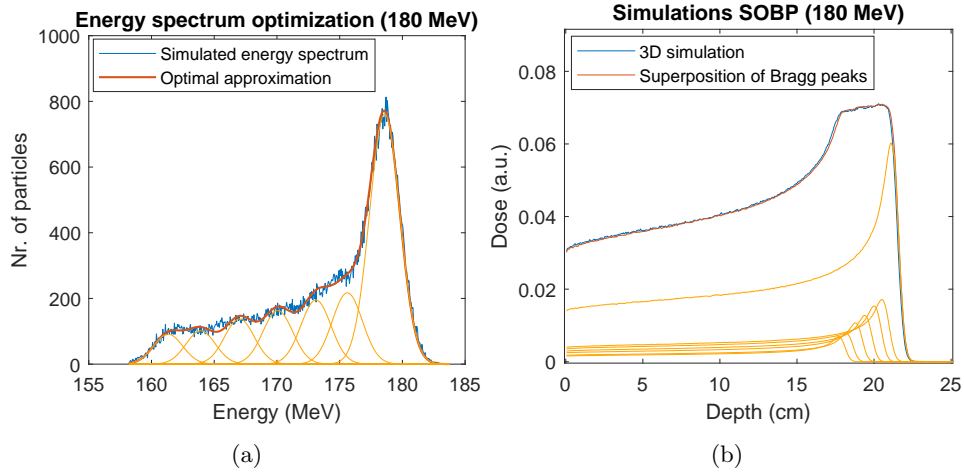


Figure 54: a) Energy spectrum resulting from a ridge filter proton beam simulation with its optimal energy spectrum approximation. The result for the TOPAS simulation with a nominal energy of 180 MeV is given (blue), with the weighted superposition (red) of individual pencil beam energy distributions (yellow). b) Dose-depth curve resulting from a direct ridge filter proton beam simulation with the superposition of the dose-depth curves from optimized beam energies and beam weights. The result for the direct TOPAS simulation, with a nominal energy of 180 MeV (blue) are given, with the weighted superposition (red) of individual Bragg peak dose-depth curves (yellow).

Optimizing the dose-depth curve instead of the energy spectrum gives the following resulting dose-depth curve and corresponding energy spectrum.

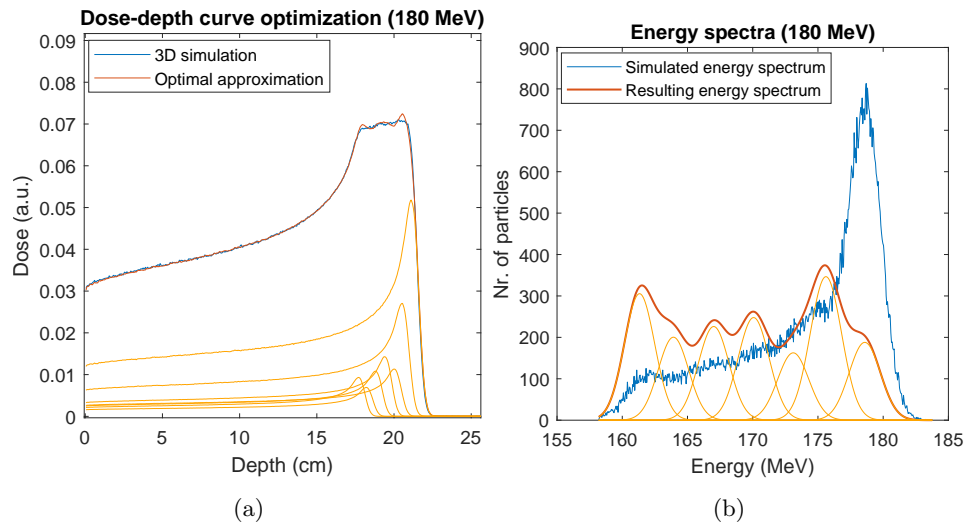


Figure 55: a) Dose-depth curve resulting from a direct ridge filter proton beam simulation (blue) with its optimal superposition (red) of the dose-depth curves (yellow). The nominal beam energy of the ridge filter simulation was 180 MeV. b) Energy spectrum resulting from a ridge filter proton beam simulation (blue) with the weighted superposition (red) of the pencil beam energy spectra (yellow) resulting from the dose-depth curve optimization.

## A.5 Erasmus-iCycle results - Patient 2

### A.5.1 Conventional plan

The optimal plan consists of 42 pencil beams in the first beam direction ( $240^\circ$ ) and 42 pencil beams in the second beam direction ( $300^\circ$ ). Figure 56 shows for both beam directions the lateral positions for which pristine Bragg peak beams would fall within the tumour (the spots in the original beamlist), and the lateral positions used in the optimized treatment plan.

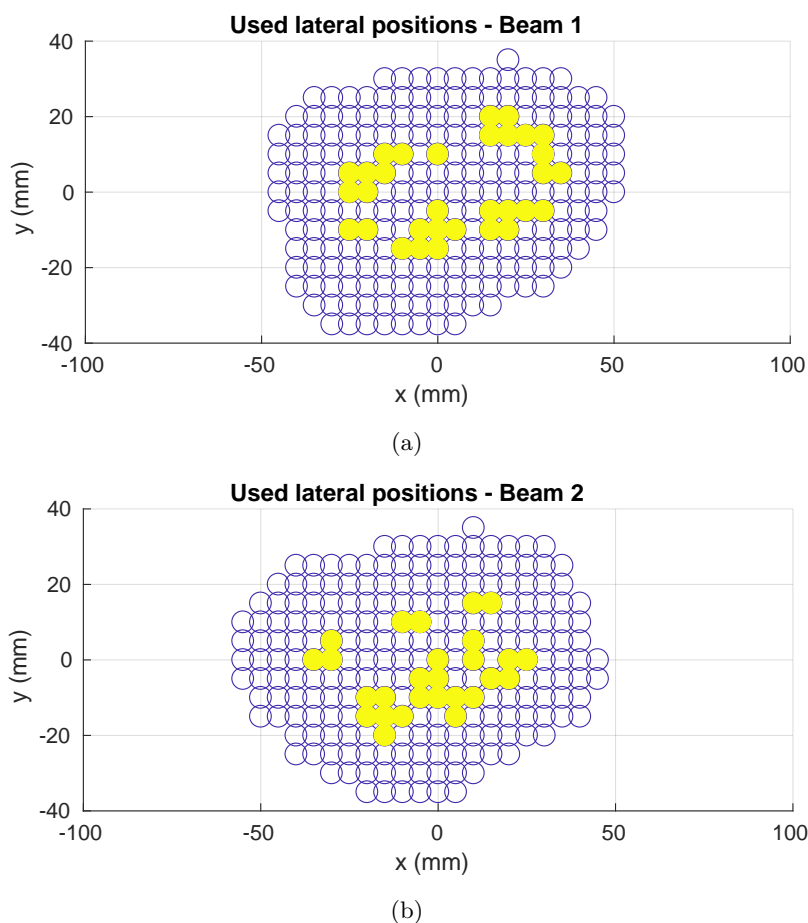


Figure 56: Lateral position of pencil beams used in the optimized treatment plan on a bixel grid. The open blue circles are the lateral positions of the spots in the original beamlist, the filled yellow circles are the used pencil beam positions in the conventional iCycle optimization.

The resulting dose distributions in the patient are shown in Figure 57. The results for the total dose and the doses of both beams separately are shown in the transverse planes near isocenter, that is at a CT-offset of -147 mm.

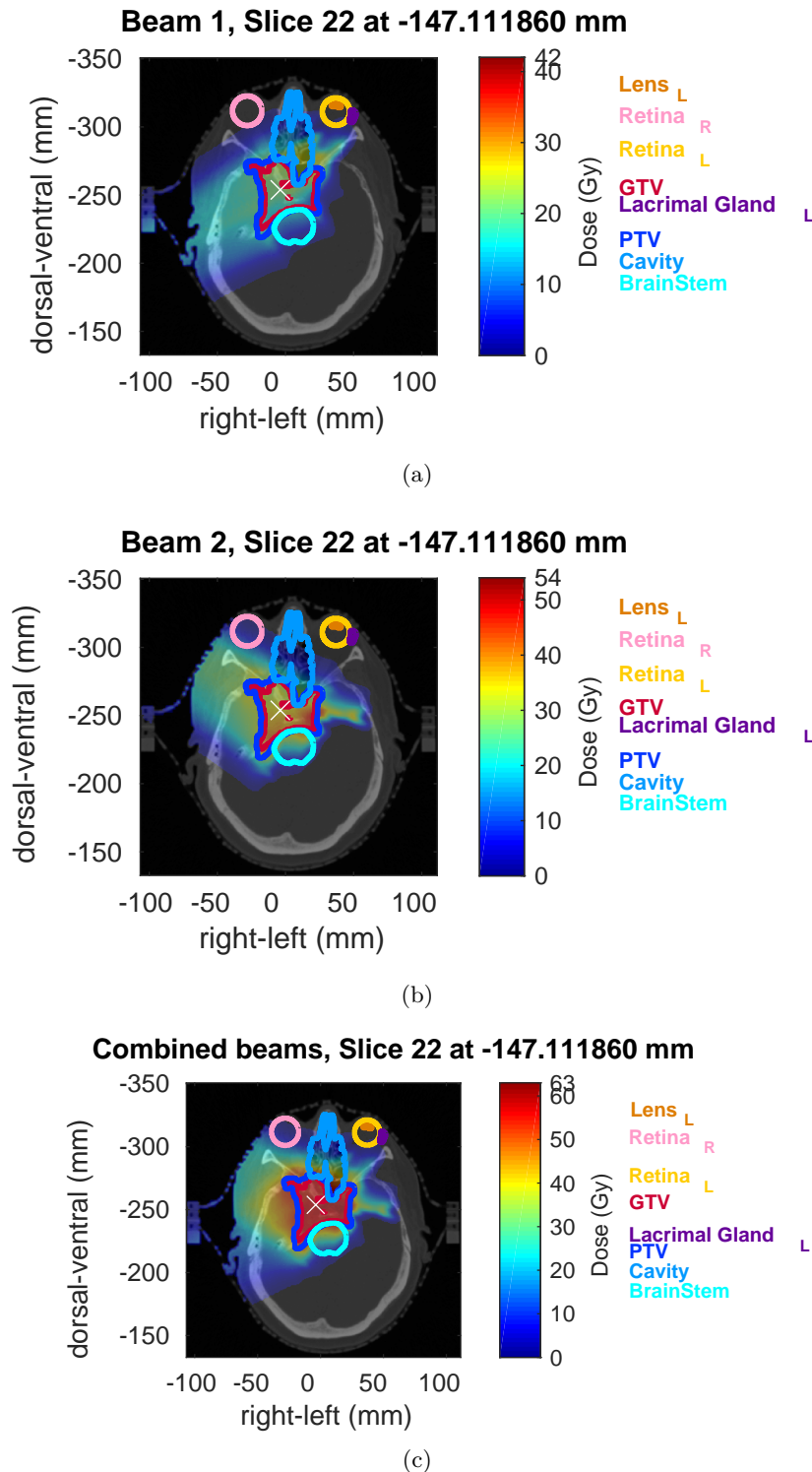


Figure 57: The dose distribution in Patient 2 for a conventional treatment plan optimization in iCycle using 2 beam directions ( $240^\circ$  and  $300^\circ$ ). In (a) the dose of both beams combined is given. In (b) and (c) the dose distributions of, respectively, beam 1, at  $240^\circ$ , and beam 2, at  $300^\circ$ , are given. The white 'x' denotes the position of the isocenter. The target structures (GTV and PTV) and the organs at risk (the two retinas, one lens, the cavity, the brain stem and the lacrimal gland on the left) at this depth are indicated.

To quantify the treatment plan and give a measure for qualification, the dose-volume histograms of the optimization are given, see Figure 58. In these histograms, only two structures are considered, the PTV and the brain-PTV for the combined beams and both beams separately.

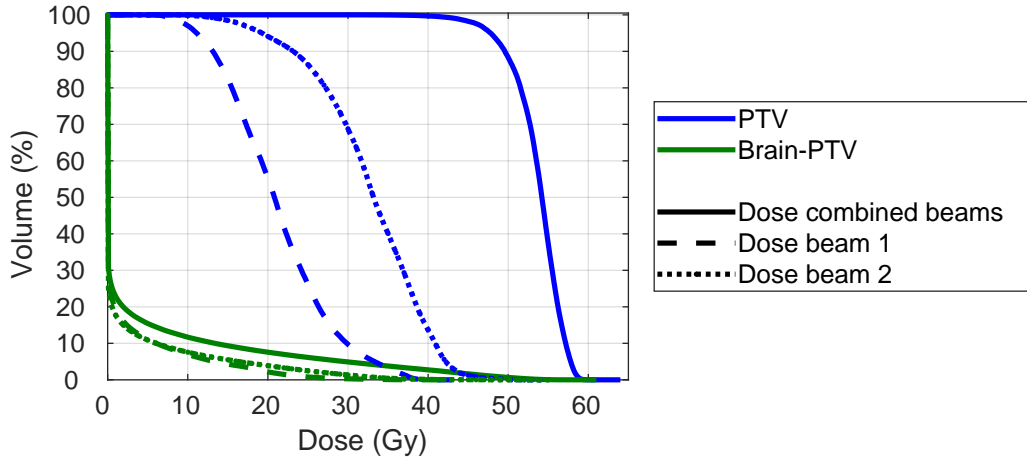


Figure 58: Dose-volume histogram showing the dose in the tumour (blue) and the dose in the healthy tissue (green) for the combined beams (continuous), the first beam, at  $240^\circ$  (dashed) and the second beam, at  $300^\circ$  (dotted).

The treatment planner took 108.36 minutes to optimize the treatment plan for this patient.

### A.5.2 Initial run

The optimal plan consists of 38 SOBPs pencil beams in the first beam direction ( $240^\circ$ ) and 37 SOBPs pencil beams in the second beam direction ( $300^\circ$ ). Figure 59 shows for both beam directions the lateral positions for which pristine Bragg peak beams would fall within the tumour (the spots in the original beamlist), and the optimal lateral SOBPs-locations with their nominal energy. In this optimization, a static degrader has been taken into account.

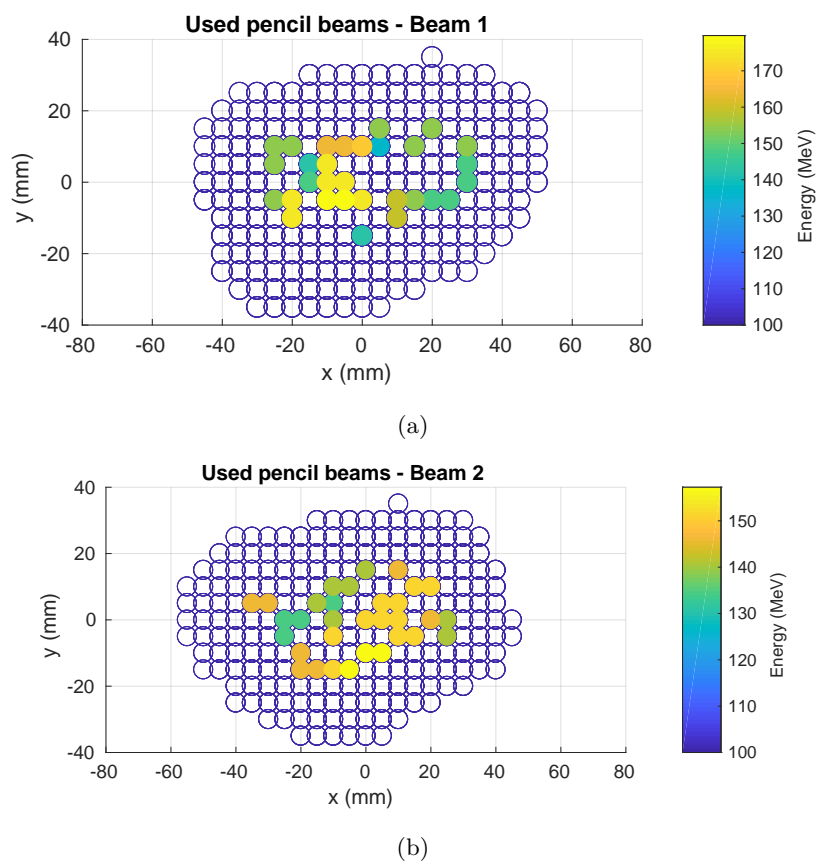


Figure 59: SOBP pencil beams used in the optimized treatment plan on a bixel grid. The open blue circles are the lateral positions of the spots in the original beamlist, the filled circles are the used pencil beams in the optimized SOBP-plan. The colour of the circles denotes the nominal energy of that pencil beam.

The resulting dose distributions in the patient are shown in Figure 60. The results for the total dose and the doses of both beams separately are shown in the transverse planes near isocenter, that is at a CT-offset of -147 mm.

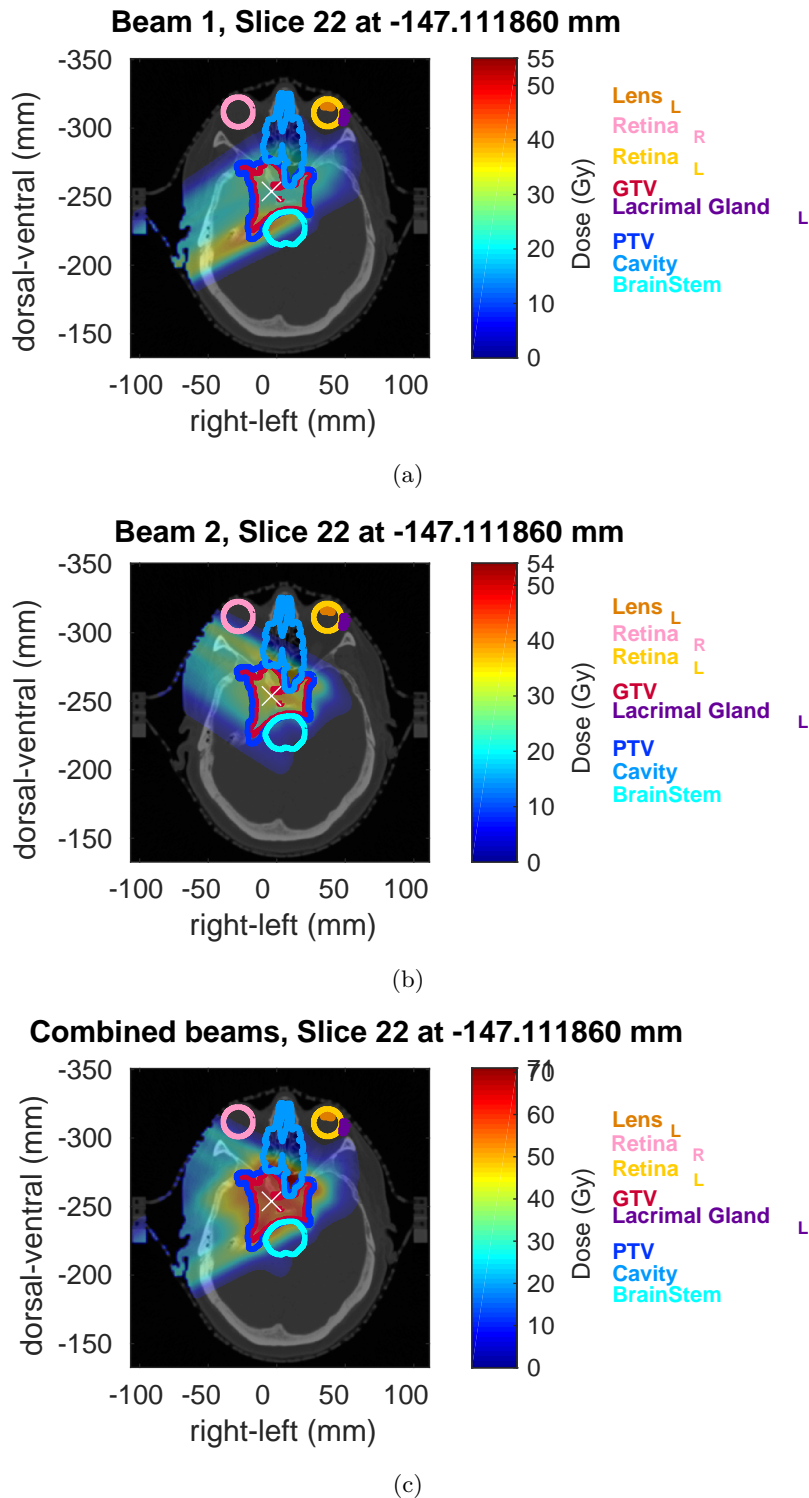


Figure 60: The dose distribution in Patient 2 for a treatment plan optimization in iCycle with SOBP-database using 2 beam directions ( $240^\circ$  and  $300^\circ$ ). In (a) the dose of both beams combined is given. In (b) and (c) the dose distributions of, respectively, beam 1, at  $240^\circ$ , and beam 2, at  $300^\circ$ , are given. The white 'x' denotes the position of the isocenter. The target structures (GTV and PTV) and the organs at risk (the two retinas, one lens, the cavity, the brain stem and the lacrimal gland on the left) at this depth are indicated.

To quantify the treatment plan and give a measure for qualification, the dose-volume histograms of the SOBP-optimization are given, see Figure 61. In these histograms, only two structures are considered, the PTV and the brain-PTV for the combined beams and both beams separately.

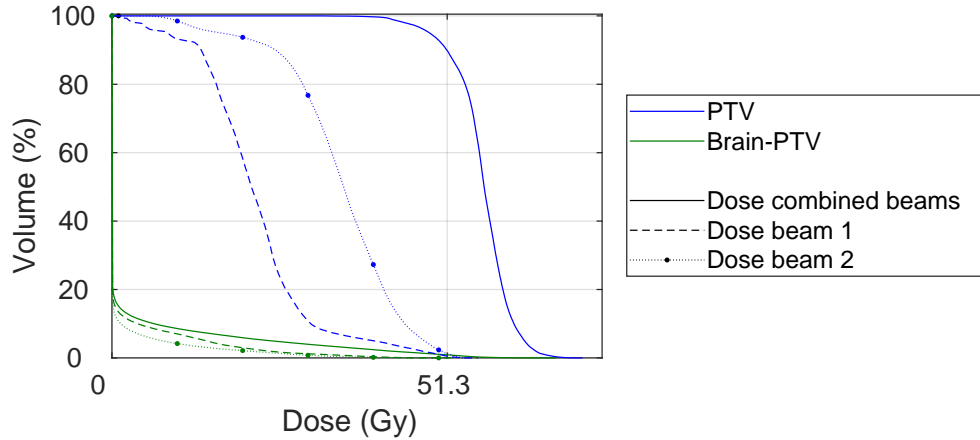


Figure 61: Dose-volume histogram showing the dose in the tumour (blue) and the dose in the healthy tissue (green) for the combined beams (continuous), the first beam, at  $240^\circ$  (dashed) and the second beam, at  $300^\circ$  (dotted).

The treatment planner took 10.62 minutes to optimize the treatment plan for this patient and in the optimized plan were initially 13 lateral positions that occurred more than once.

### A.5.3 Final runs

For Patient 2, the characteristics of the four runs are given in Table 7. Sometimes the optimizer did not converge to a feasible optimal plan, besides that also sometimes while optimizing an error occurred in the MU-objective optimization in the non-convex, non-linear optimizer. The exact cause of the error is still unclear. Other users of iCycle have seen the same error before [55].

Table 7: Characteristics of four final optimization runs for Patient 1. For each run the following information is given: the used database (first column); whether a degrader was used (second column); whether an error occurred in the optimization of the MU-objective (third column); whether the final plan was feasible (fourth column); how many SOBP pencil beams were deleted, in the case of lateral positions being used for multiple SOBP pencil beams (fifth column); the final number of SOBP pencil beams (sixth column), and the total optimization time,  $t_{opt}$ , in minutes (last column).

Run	Database	Degr.	MU error	Feasible	$N_{deleted}$	$N_{final}$	$t_{opt}$ (min)
1.	110 MeV	-	x	-	-	-	20.38
2.	110 MeV	x	-	x	12	72	16.78
3.	130 MeV	-	x	x	2	61	10.30
4.	130 MeV	x	-	x	16	74	12.54

To quantify the treatment plan and give a measure for qualification, the dose-volume histograms of the SOBP-run are given, see Figure 62. In these histograms, only two structures, the PTV and the brain-PTV, are considered for the three plans with a feasible solution. Also a result for the infeasible run is shown. This is done by deleting all low-weight SOBP pencil beams from the final beamlist and calculating the dose for the resulting beamlist. A SOBP pencil beam has a low weight when the weight is lower than 0.0032 gigaprotons.

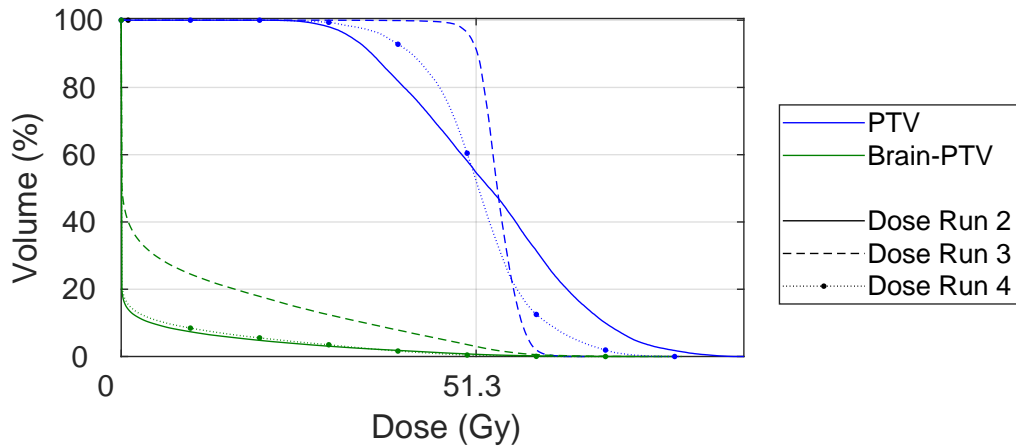


Figure 62: Dose-volume histogram showing the dose in the tumour (blue) and the dose in the healthy tissue (green) for Run 2 (continuous), Run 3 (dashed) and Run 4 (dotted) from Table 7.

For comparing treatment treatment plans, scaled dose-volume histograms are calculated. The histograms of all runs (the conventional run, the initial run and the final runs) are scaled such that 98% of the target volume (PTV or, when that structure is not present, CTV) receives at least 95% of the prescribed dose, see Figure 63. 95% of the prescribed dose of 54 Gy is 51.3 Gy.

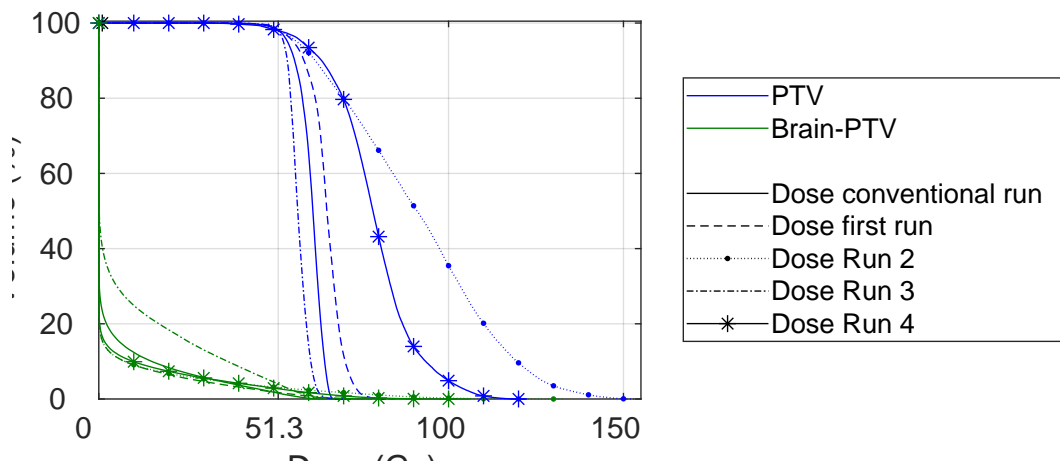


Figure 63: Dose-volume histogram showing the dose in the tumour (blue) and the dose in the healthy tissue (green) for Run 2 (continuous), Run 3 (dashed) and Run 4 (dotted) from Table 7.

The homogeneity indices, mean dose to healthy tissue and required FLASH enhancement ratio (FER) for the different runs are given in the table below.

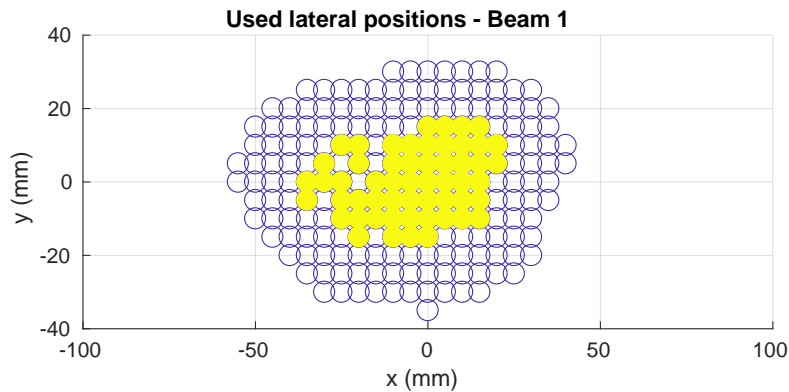
Table 8: The homogeneity indices (HIs), mean doses to healthy tissue, and required FERs of the optimized treatment plans shown in Figure 63 are given. The HIs are calculated using Equation 10.

<b>Optimization run</b>	<b>Homogeneity index (%)</b>	$D_{mean}$ <b>healthy tissue (Gy)</b>	<b>Req. FER</b>
Conventional	26.9	4.26	-
Initial	42.5	3.30	-
2.	156	4.15	-
3.	21.1	8.91	2.09
4.	101	4.03	-

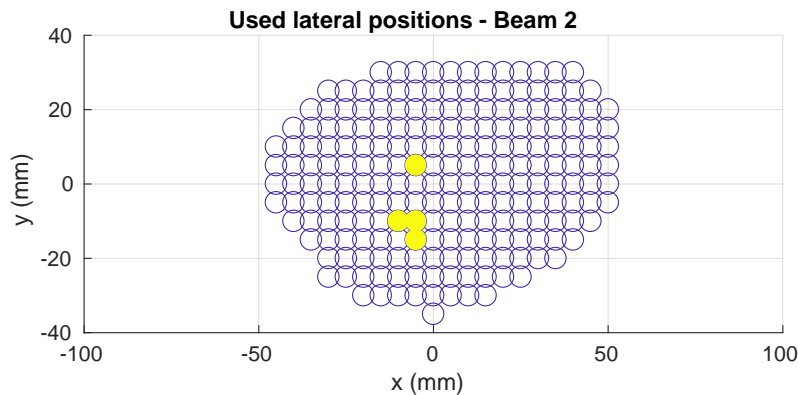
## A.6 Erasmus-iCycle results - Patient 3

### A.6.1 Conventional run

The optimal plan consists of 110 pencil beams in the first beam direction ( $240^\circ$ ) and 4 pencil beams in the second beam direction ( $300^\circ$ ). Figure 64 shows for both beam directions the lateral positions for which pristine Bragg peak beams would fall within the tumour (the spots in the original beamlist), and the lateral positions used in the optimized treatment plan.



(a)



(b)

Figure 64: Lateral position of pencil beams used in the optimized treatment plan on a bixel grid. The open blue circles are the lateral positions of the spots in the original beamlist, the filled yellow circles are the used pencil beam positions in the conventional iCycle optimization.

The resulting dose distributions in the patient are shown in Figure 65. The results for the total dose and the doses of both beams separately are shown in the transverse planes near isocenter, that is at a CT-offset of +64.5 mm.

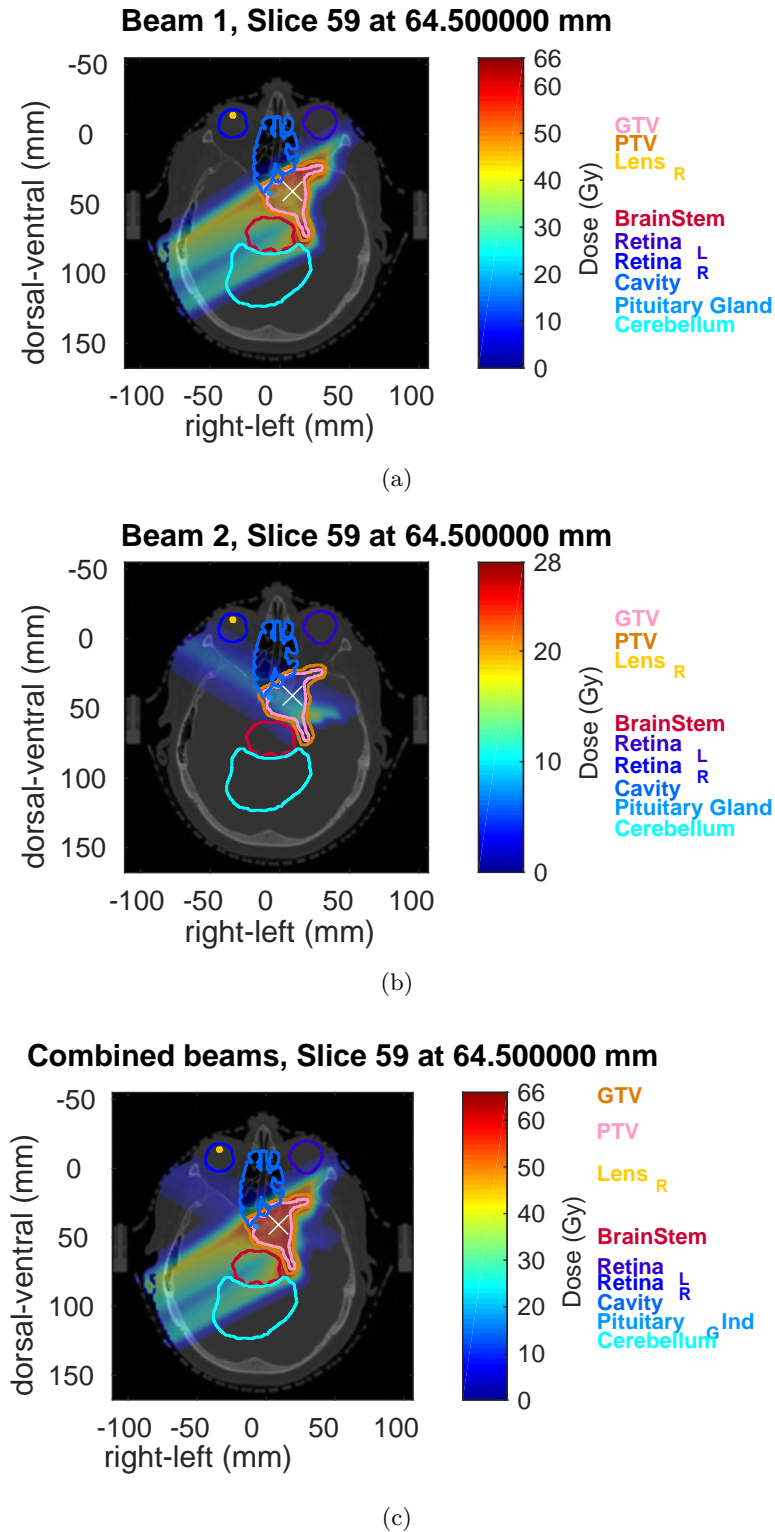


Figure 65: The dose distribution in Patient 3 for a conventional treatment plan optimization in iCycle using 2 beam directions ( $240^\circ$  and  $300^\circ$ ). In (a) the dose of both beams combined is given. In (b) and (c) the dose distributions of, respectively, beam 1, at  $240^\circ$ , and beam 2, at  $300^\circ$ , are given. The white 'x' denotes the position of the isocenter. The target structures (GTV and PTV) and the organs at risk (the two retinas, one lens, the cavity, the brain stem, the pituitary gland and cerebellum) at this depth are indicated.

To quantify the treatment plan and give a measure for qualification, the dose-volume histograms of the optimization are given, see Figure 66. In these histograms, only two structures are considered, the PTV and the brain-PTV for the combined beams and both beams separately.

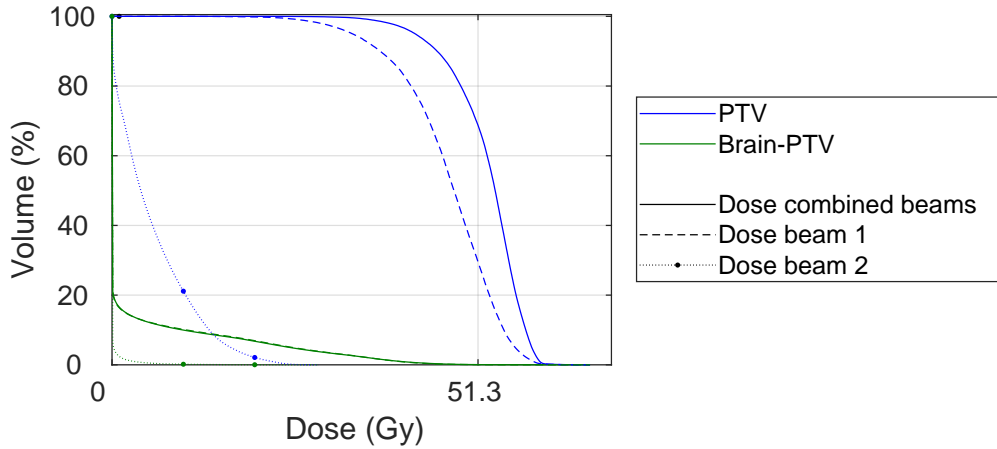


Figure 66: Dose-volume histogram showing the dose in the tumour (blue) and the dose in the healthy tissue (green) for the combined beams (continuous), the first beam, at  $240^\circ$  (dashed) and the second beam, at  $300^\circ$  (dotted).

The treatment planner took 50.36 minutes to optimize the treatment plan for this patient.

### A.6.2 Initial run

The optimal plan consists of 31 SOBPs pencil beams in the first beam direction ( $240^\circ$ ) and 20 SOBPs pencil beams in the second beam direction ( $300^\circ$ ). Figure 67 shows for both beam directions the lateral positions for which pristine Bragg peak beams would fall within the tumour (the spots in the original beamlist), and the optimal lateral SOBPs-locations with their nominal energy. In this optimization, no static degrader has been used.

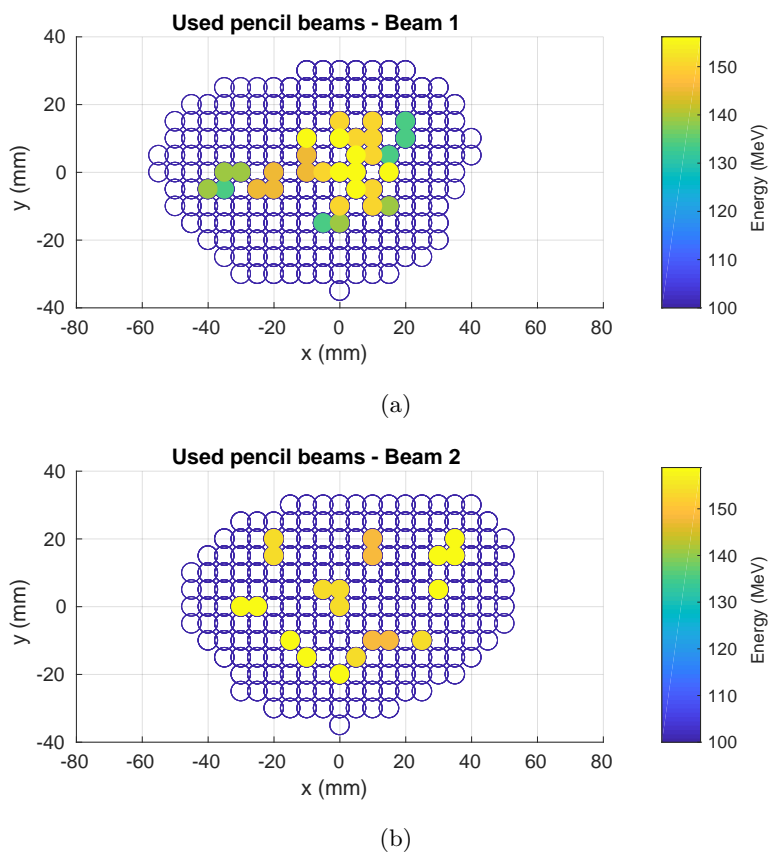
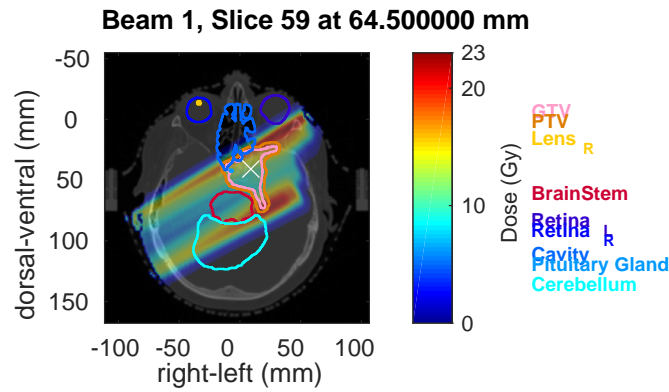
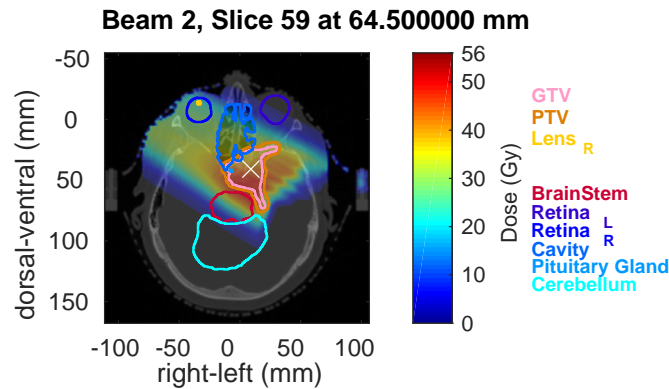


Figure 67: SOBP pencil beams used in the optimized treatment plan on a bixel grid. The open blue circles are the lateral positions of the spots in the original beamlist, the filled circles are the used pencil beams in the optimized SOBP-plan. The colour of the circles denotes the nominal energy of that pencil beam.

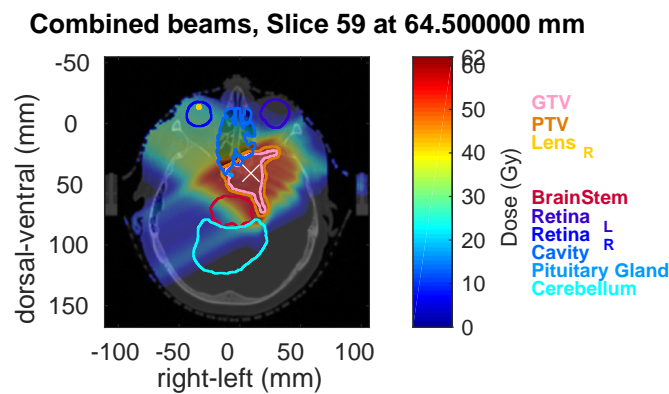
The resulting dose distributions in the patient are shown in Figure 68. The results for the total dose and the doses of both beams separately are shown in the transverse planes near isocenter, that is at a CT-offset of +64.5 mm.



(a)



(b)



(c)

Figure 68: The dose distribution in Patient 2 for a treatment plan optimization in iCycle with SOBP-database using 2 beam directions ( $240^\circ$  and  $300^\circ$ ). In (a) the dose of both beams combined is given. In (b) and (c) the dose distributions of, respectively, beam 1, at  $240^\circ$ , and beam 2, at  $300^\circ$ , are given. The white 'x' denotes the position of the isocenter. The target structures (GTV and PTV) and the organs at risk (the two retinas, one lens, the cavity, the brain stem, the pituitary gland and cerebellum) at this depth are indicated.

To quantify the treatment plan and give a measure for qualification, the dose-volume histograms of the SOBP-optimization are given, see Figure 69. In these histograms, only two structures are considered, the PTV and the brain-PTV for the combined beams and both beams separately.

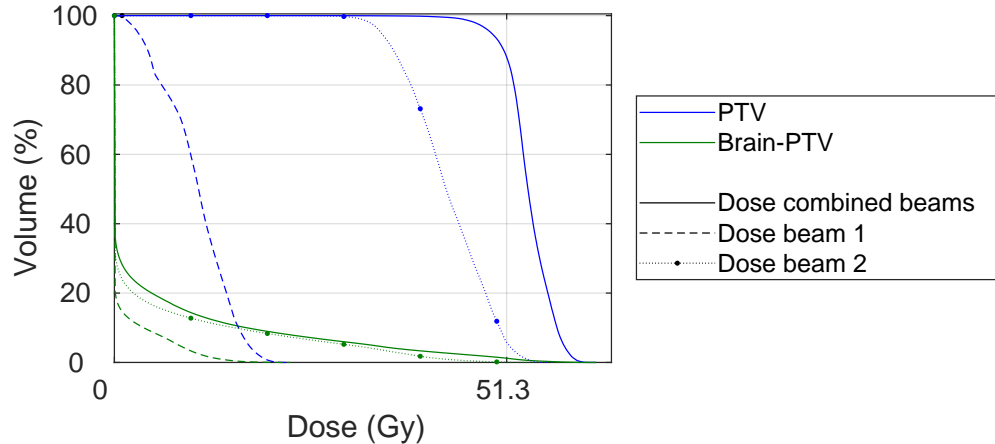


Figure 69: Dose-volume histogram showing the dose in the tumour (blue) and the dose in the healthy tissue (green) for the combined beams (continuous), the first beam, at  $240^\circ$  (dashed) and the second beam, at  $300^\circ$  (dotted).

The treatment planner took 7.77 minutes to optimize the treatment plan for this patient and in the optimized plan were initially 3 lateral positions that occurred more than once.

### A.6.3 Final runs

For Patient 3, the characteristics of the four runs are given in Table 9. Sometimes the optimizer did not converge to a feasible optimal plan, besides that also sometimes while optimizing an error occurred in the MU-objective optimization in the non-convex, non-linear optimizer. The exact cause of the error is still unclear. Other users of iCycle have seen the same error before [55].

Table 9: Characteristics of four final optimization runs for Patient 1. For each run the following information is given: the used database (first column); whether a degrader was used (second column); whether an error occurred in the optimization of the MU-objective (third column); whether the final plan was feasible (fourth column); how many SOBP pencil beams were deleted, in the case of lateral positions being used for multiple SOBP pencil beams (fifth column); the final number of SOBP pencil beams (sixth column), and the total optimization time,  $t_{opt}$ , in minutes (last column).

Run	Database	Degr.	MU error	Feasible	$N_{deleted}$	$N_{final}$	$t_{opt}$ (min)
1.	110 MeV	-	-	x	13	57	18.87
2.	110 MeV	x	x	-	5	72	16.09
3.	130 MeV	-	-	x	2	52	8.99
4.	130 MeV	x	x	-	-	-	17.65

To quantify the treatment plan and give a measure for qualification, the dose-volume histograms of the SOBP-run are given, see Figure 70. In these histograms, only two structures, the PTV and the brain-PTV, are considered for the three plans with a feasible solution. Also a result for the infeasible run is shown. This is done by deleting all low-weight SOBP pencil beams from the final beamlist and

calculating the dose for the resulting beamlist. A SOBP pencil beam has a low weight when the weight is lower than 0.0032 gigaprotons.

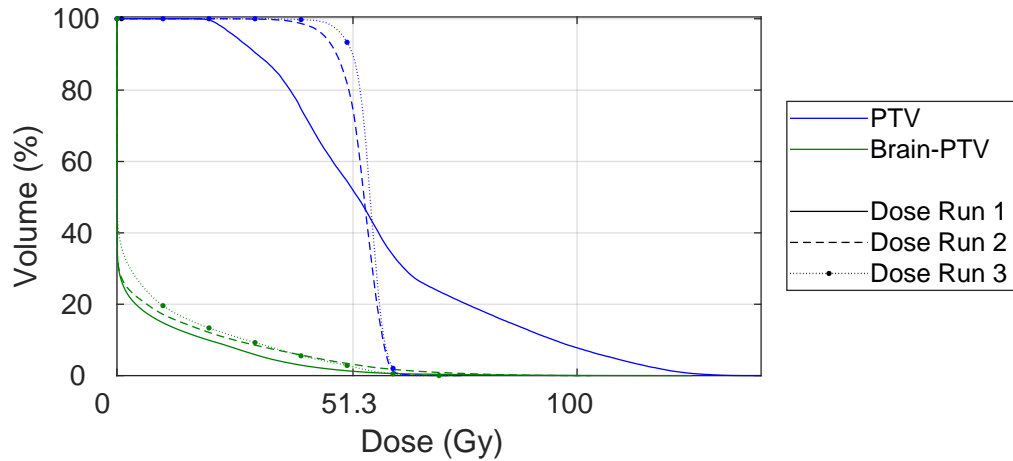


Figure 70: Dose-volume histogram showing the dose in the tumour (blue) and the dose in the healthy tissue (green) for Run 1 (continuous), Run 2 (dashed) and Run 3 (dotted) from Table 7.

For comparing treatment treatment plans, scaled dose-volume histograms are calculated. The histograms of all runs (the conventional run, the initial run and the final runs) are scaled such that 98% of the target volume (PTV or, when that structure is not present, CTV) receives at least 95% of the prescribed dose, see Figure 63. 95% of the prescribed dose of 54 Gy is 51.3 Gy.

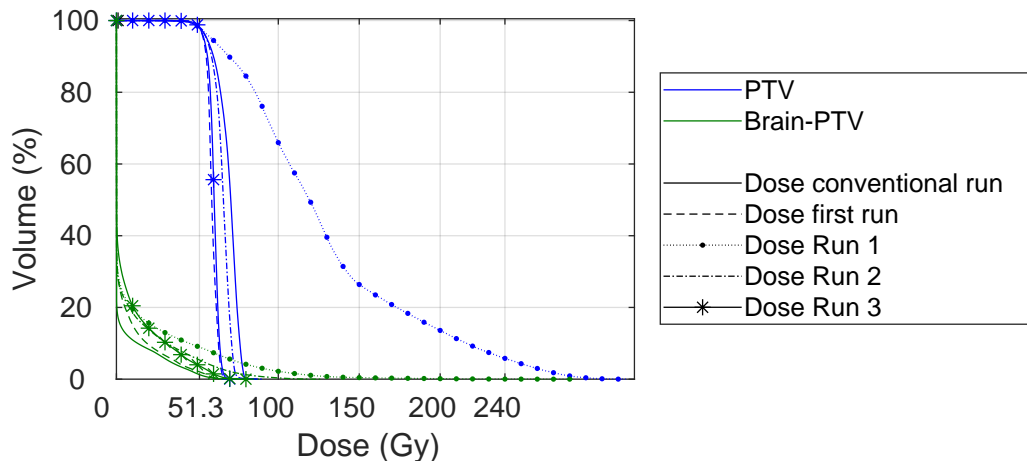


Figure 71: Dose-volume histogram showing the dose in the tumour (blue) and the dose in the healthy tissue (green) for Run 1 (continuous), Run 2 (dashed) and Run 3 (dotted) from Table 9.

The homogeneity indices, mean dose to healthy tissue and required FLASH enhancement ratio (FER) for the different runs are given in the table below.

Table 10: The homogeneity indices (HIs), mean doses to healthy tissue, and required FERs of the optimized treatment plans shown in Figure 71 are given. The HIs are calculated using Equation 10.

<b>Optimization run</b>	<b>Homogeneity index (%)</b>	$D_{mean}$ <b>healthy tissue (Gy)</b>	<b>Req. FER</b>
Conventional	52.8	3.82	-
Initial	25.3	5.12	1.34
1.	40.2	11.0	2.88
2.	40.7	7.75	2.03
3.	27.0	7.42	1.94